Optical control of primary rat cortical neural activity *in vitro*

Von der Fakultät für Mathematik, Informatik und Naturwissenschaften der RWTH Aachen University zur Erlangung des akademischen Grades eines Doktors der Naturwissenschaften genehmigte Dissertation

vorgelegt von

Master of Science in Biology

Lei Jin

aus Hubei, China

Berichter: Universitätsprofessor Dr. rer. nat. Andreas Offenhäusser

Universitätsprofessor Dr. rer. nat. Marc Spehr

Tag der mündlichen Prüfung: 19. Juli 2016

For my dearly beloved family members!

献给我深爱的家人！

Contents

Lists of Figures

Figures in the text

Supplementary figures

List of Tables

1 Introduction

This chapter presents the background of my work, including the basic knowledge of optogenetics and its application in patterned neurons. Also, recombinant adeno-associated viruses (rAAVs) as a potential tool for the expression of optogenetic tools is presented. Finally, the motivation of this work is detailed. In one word, the outcomes of my work will facilitate and expand the optical control of neural activity.

1.1 Optogenetics

Nowadays optogenetics plays a very important role in neuroscience. Optogenetic approaches have promoted *in vitro* and *in vivo* experiments investigating cellular signaling and neuronal network activity with high temporal and spatial resolution (Arenkiel et al., 2007); (Madisen et al., 2012); (Avermann et al., 2012); (Huber et al., 2008); (Desai et al., 2011); (Lin et al., 2013);(Dawydow et al., 2014). Beyond modulating and monitoring neuronal network properties, optogenetic methods have been applied to control signaling in sperm (Jansen et al., 2015) and to stimulate gene expression (Tabor et al., 2009, 2011) (Konermann et al., 2013). Optogenetic experiments, however, require efficient introduction and expression of light-sensitive proteins in cells or tissue.

The blue light-gated cation channel Channelrhodopsin-2 (ChR2) is an intensely studied optogenetic tool (Nagel et al., 2003a);(Nagel et al., 2005a); (Boyden et al., 2005); (Li et al., 2005); (Petreanu et al., 2007); (Ishizuka et al., 2006); (Dawydow et al., 2014). The heterologous expression of ChR2 in electrogenic cells such as neurons can be utilized to depolarize the cell's membrane potential, thereby evoking action potentials (Zhang et al., 2006); (Wang et al., 2007). Since its discovery, numerous ChR2 variants have been engineered to improve properties, such as expression level, closing dynamics (Dawydow et al., 2014) (Gunaydin et al., 2010), and stable photo-switching (Berndt et al., 2009). In addition to triggering action potentials, ChR2 can be employed to silence neuronal activity by changing its ion selectivity to anions (Wietek et al., 2014); (Berndt et al., 2014). Fluorescent tags such as mKate and YFP fused to ChR2 have been used to identify cells expressing ChR2 and to assess its subcellular distribution (Shcherbo et al., 2007); (Nagel et al., 2005b), as light-induced manipulation of neuronal electrical activity depends on the expression level of ChR2 in the cell membrane (Lin et al., 2013).

1.1.1 The history of optogenetics

Optogenetics refers to the combination of optics and genetics to achieve the activation or inhibition of neural activity (Nagel et al., 2005b) (Boyden et al., 2005) (Zhang et al., 2006) (Deisseroth et al., 2006) (Boyden, 2011). The original of the conceptual inspiration for optogenetics can be traced back to the 1970s. In 1979 Francis Crick (see: **Figure 1.1-1A**), who was awarded the Nobel Prize in Physiology or Medicine 1962, published one paper (Crick, 1979) in the book of *Scientific American* (**Figure 1.1-1B**). In this paper he proposed that a major challenge in the neuroscience field was the lack of a method to precisely control neural activity in one cell type while leaving the others unaltered (**Figure 1.1-1C**). In 1999, Crick inferred in lectures that light might be a relevant control tool, but without a detailed concept for how this could be achieved (Yizhar et al., 2011a).

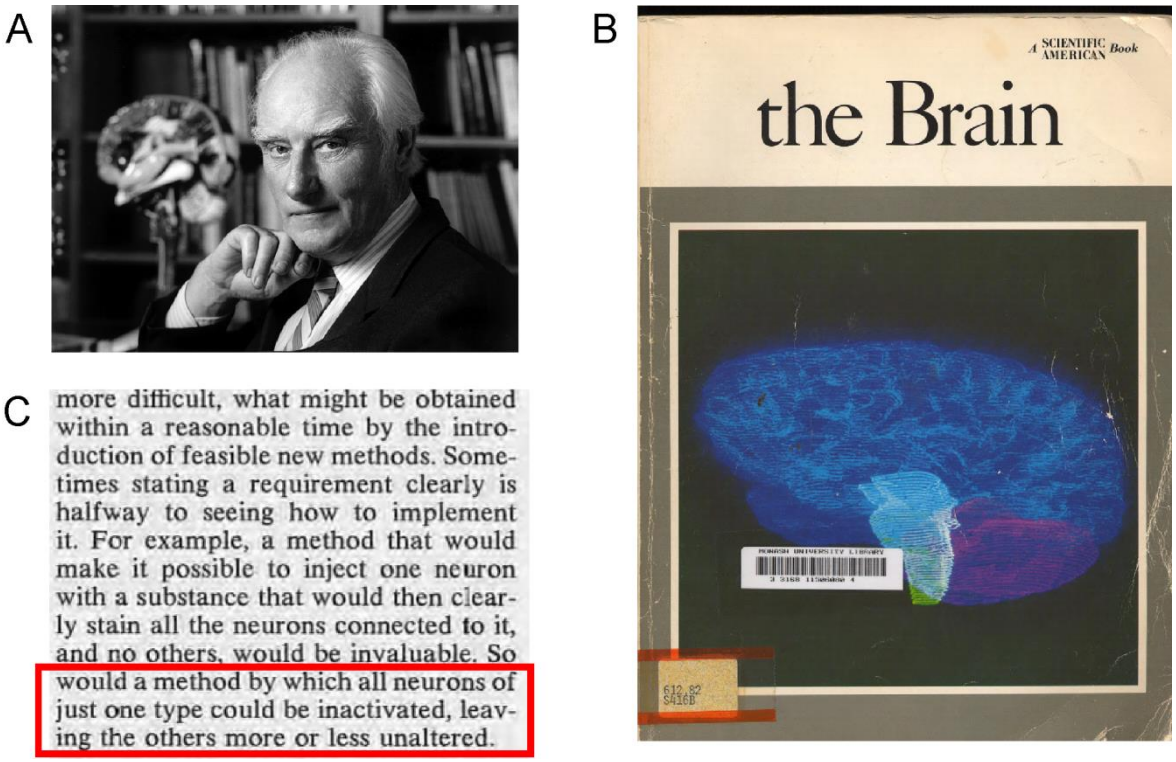

Figure 1.1-1 The original of the conceptual inspiration for optogenetics

A) Francis Crick was in his office. Behind him is a model of the human brain that he inherited from Jacob Bronowski. The figure is adapted from (Siegel and Callaway, 2004). B) The cover of the book of *Scientific American* (1979) in which Francis Crick noted the original of the conceptual inspiration for optogenetics. C) The original notes by Francis Crick in the book of *Scientific American.* The words highlighted with red color inspired optogenetics. This notes is snipped from (Crick, 1979).

Francis Crick's idea was achieved in 2005 by combining light and the light-gated ion channel named Channelrhodopsin-2 (see: **Figure 1.1-2**) (Boyden et al., 2005) (Li et al., 2005). From then on, optogenetics came into the world. In 2010, optogenetics was named Method of the Year 2010 across all fields of life sciences and chemistry by the leading journal *Nature Methods*, and 'Breakthrough of the Decade' by the journal *Science*. Its roots were in Europe: German and Austrian scientists discovered light-sensitive ion channels capable of changing the activity of cells in response to light, and developed methods to use such molecules to exercise selective control over particular classes of neurons (Zemelman et al., 2002)(Nagel et al., 2002)(Nagel et al., 2003a)(Nagel et al., 2005a).

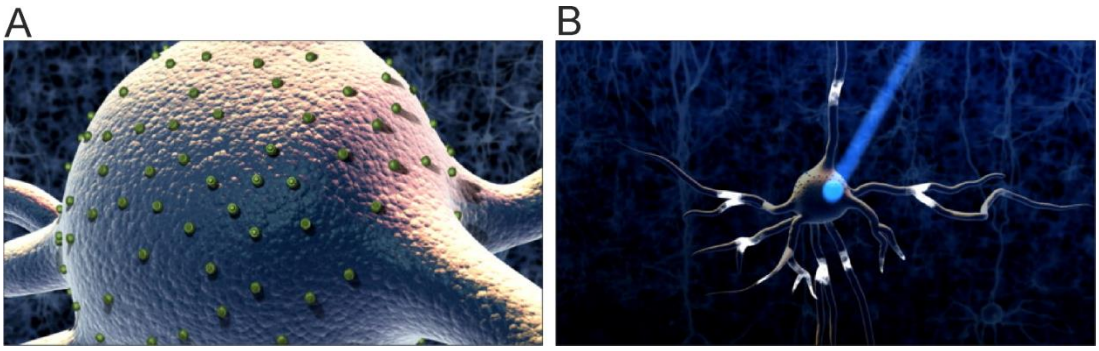

Figure 1.1-2 The schematic of optogenetics

A) Light-gated ion channels – Channelrhodopsin-2, expressed on neural membrane. B) Neural activity induced by light stimulation. Figures are adapted with permissions from (Holmes, 2012).

Over the last 11 years, optogenetics has become a very promising technology in the field of neuroscience for the study of how different types of neuron contribute to brain function and neural diseases. Many studies using optogenetics were done including *in vitro* and *in vivo* (Govorunova et al., 2015; Lange et al., 2014; Liewald et al., 2008; Lim et al., 2013; Nagel et al., 2003b; Ramirez et al., 2013; Sandoz and Levitz, 2013; Yizhar et al., 2011b). The very important roles of optogenetics as a type of technology and a therapy approach have emerged.

1.1.2 Channelrhodopsin-2

The discovery of Channelrhodopsins (ChRs) could be traced back to at least 140 years ago. Many scientists have investigated the swimming behavior and light responses of motile microalgae over these years (**Figure 1.1-3A**). However, the big progress of ChRs happened in 2001, when researchers in the Hegemann's group identified novel DNA

sequences encoding for large microbial-type rhodopsins in a cDNA data bank from *Chlamydomonas*. In order to investigate their function, their fascinating collaboration started when Prof. Dr. Georg Nagel heterologously expressed the two rhodopsins in the membrane of an animal cell, the oocyte of *Xenopus* laevis. They first indicated that both DNAs encode directly light-gated cation channels, and named these new genes channelrhodopsin-1 (ChR1) and channelrhodopsin-2 (ChR2, **Figure 1.1-3B**) (Nagel et al., 2002) (Nagel et al., 2003a). They also heterologously expressed ChR2 in human kidney (HEK293) and baby hamster kidney (BHK) cells, where they showed large light-induced membrane depolarization when the cells were illuminated by blue light, and suggested that ChR2 may be used in other cells to depolarize them with light (Nagel et al., 2003a). Therefore, optogenetics has emerged after these works.

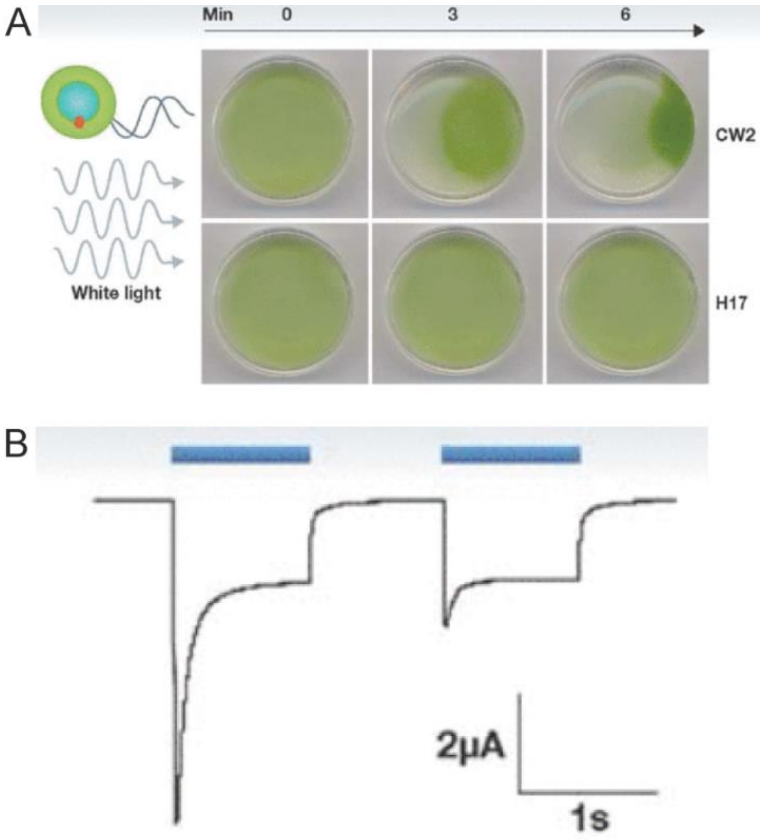

Figure 1.1-3 The discovery of channelrhodopsins

A) Phototaxis of the *Chlamydomonas* wild type strain CW2 and the channelrhodopsin-defective mutant H17 showing the swimming behavior and light responses of motile microalgae is associated with channelrhodopsin; B) Photocurrent of channelrhodopsin-2 (ChR2) in *Xenopus* oocytes (two illuminations for 1 s, blue bars)

at −100 mV. Figures are reproduced from (Hegemann and Nagel, 2013).

ChR2 is a seven transmembrane protein that is a directly light-gated cation-selective membrane channel (Nagel et al., 2003a). Moreover, it is retinal-binding membrane protein. Retinal is a bound chromophore that absorbs photons, resulting in its conformation change from all-trans retinal to 13-cis retinal that opens the channels (**Figure 1.1-4A**). Consequently, ion influx could happen across the plasma membrane through ChR2. When ChR2 is heterologously expressed in the membrane of neurons, it can be used to control neuronal activity with millisecond precision by light stimulation (**Figure 1.1-4B**) (Boyden et al., 2005).

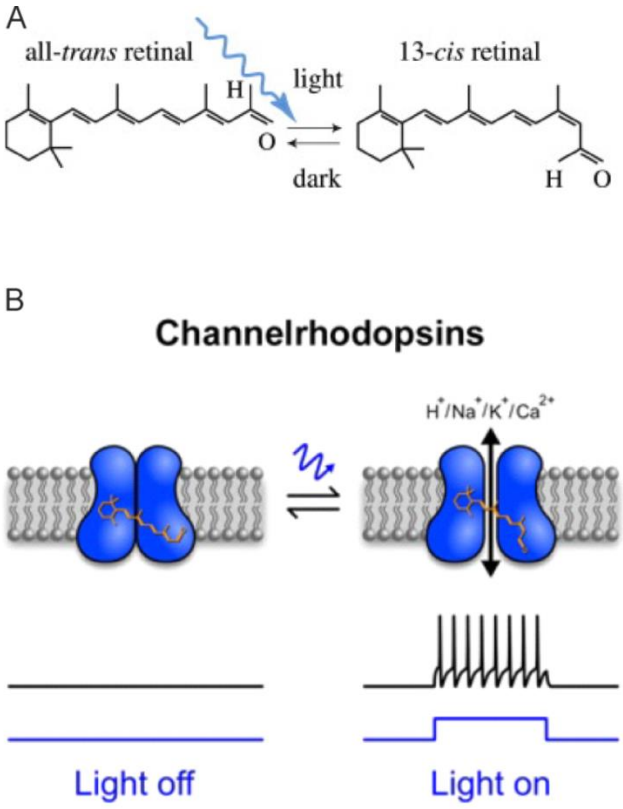

Figure 1.1-4 The mechanism of light-induced neural activity

A) ChR2 is activated through photoisomerization of all-trans retinal to 13-cis retinal when illuminated by 473 nm light. After photoisomerization, the covalently bound retinal spontaneously relaxes to all-trans when swiching off the light, providing closure of the ion channel

and regeneration of the chromophore. This figure is reproduced with permissions from (Abilez et al., 2011). B) ChR2 can be used to control neuronal activity with millisecond precision. When stimulating ChR2 by blue light, action potentials could be fired. Membranes are represented with the extracellular side toward the top. This figure is adapted with permissions from (Dugué et al., 2012).

Mutations of the ChR2 DNA that alter certain amino acids could effectively improve properties such as the absorption, conductance or kinetics of the channel, producing novel optogenetic tools (Hegemann and Moglich, 2011). Recently, based on the natural ChR2, numerous novel tools have been engineered to improve properties, such as expression level, closing dynamics (Dawydow et al., 2014) (Gunaydin et al., 2010), and stable photo-switching (Berndt et al., 2009). In addition to triggering action potentials, ChR2 can be employed to silence neuronal activity by changing its ion selectivity to anions (Wietek et al., 2014) (Berndt et al., 2014) (Wietek et al., 2015).

Optogenetic tools will facilitate understanding of neural activity using light illumination. In my thesis, ChR2opt whose codon was optimized on the ChR2 (H134R) for expression in mammalian cells, and ChR2-XXL (D156C) were employed to control neural activity in primary rat cortical neurons (see: **3.1** and **3.2**, **3.3**). The H134R mutation in ChR2 causes larger stationary photocurrents in comparison to wild-type ChR2 when heterologously expressing in oocytes and HEK293T cells (Nagel et al., 2005b). In addition, D156C mutation in ChR2, named ChR2-XXL, is a very powerful tool for controlling neural activity. It displays increased expression, improved subcellular localization, elevated retinal affinity and an extended open-state lifetime, and gives rise to the largest photocurrents of all ChRs published so far. Moreover, it was demonstrated to increase light sensitivity more than 10,000-fold over wild-type ChR2 in *Drosophila* larvae (Dawydow et al., 2014).

1.1.3 *Guillardia theta* ACR 1

Channelrhodopsin-2 variants have been generated as a very important series of tools for activating or inhibiting neural activity in response to light and are widely applied to study neural circuits for understanding brain functions. In contrast, inhibitory tools are much less efficient at inactivating neurons. In 2015, Spudich's group published naturally occurring anion channelrhodopsins (ACRs) in the alga *Guillardia theta* that are light-gated anion channels (Govorunova et al., 2015). In this paper, two ACRs, named GtACR1 and

GtACR2, encode channels that produced large currents in response to light. Most important, they were demonstrated to be exclusively anion conducting, making Spudich's group the first to describe naturally occurring light-gated chloride channels as illustrated in **Figure 1.1-5B**. This discovery of light-gated inhibitory anion channels opens new opportunities in the field of neuroscience.

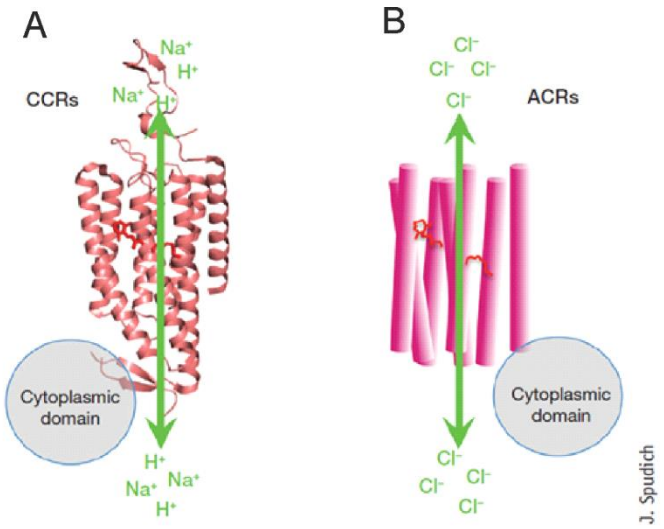

Figure 1.1-5 Ion permeability of cation channelrhodopsins (CCRs) and anion channelrhodopsins (ACRs)

A) After opening by light, cation channelrhodopsins (CCRs) are permeable for cation such as sodium. B) Naturally occurring anion channelrhodopsins (ACRs) in the alga *Guillardia theta* are permeable for the chloride ion. Figure is reproduced with permissions from (Vogt, 2015).

Also, the gating mechanisms of a natural anion channelrhodopsin has been clearly deciphered (Sineshchekov et al., 2015;Sineshchekov et al., 2016) (Yi et al., 2016). Through analyzing the photocurrents of *Guillardia theta* ACR 1 (GtACR1) and its mutants in response to light, they proposed that two different amino acid residues are involved in two separate gating mechanisms. Glu-68 regulates the first mechanism, which is characterized by slow opening and fast closing of the channel. Cys-102 controlls the second mechanism, which is characterized by fast opening and slow closing of the channel. They have demonstrated that the structural basis for anion conductance in ACRs is fundamentally different from that of Cl^--conducting CCR mutants (Wietek et al., 2014)

(Berndt et al., 2014) (Wietek et al., 2015). In 2016, they have characterized the GtACR1 photocycle (Sineshchekov et al., 2016), which contributes to understanding of the coupling between photochemistry of the chromophore and the conformation changes of GtACR1 resulting in the appearance of ion conductance.

Through light-gated chloride conduction, ACRs are able to silence neuronal activity with highly sensitive and efficient (Govorunova et al., 2015). They strictly conduct anions such as Cl^- , completely excluding protons and larger cations, and effectively hyperpolarize the membrane of cultured neurons when chloride ions flow into these neurons through ACRs. In my thesis, GtACR1 was applied to silence neuronal activity in primary cortical neurons, including spontaneously activity (see: **3.4**). ACRs could be used as strongly potent optogenetic tools to inhibit neural activity (**Figure 1.1-6B**). ACRs together with CCRs will provide a complete toolbox for optical control to help decode neural circuits and understand brain function (**Figure 1.1-6**).

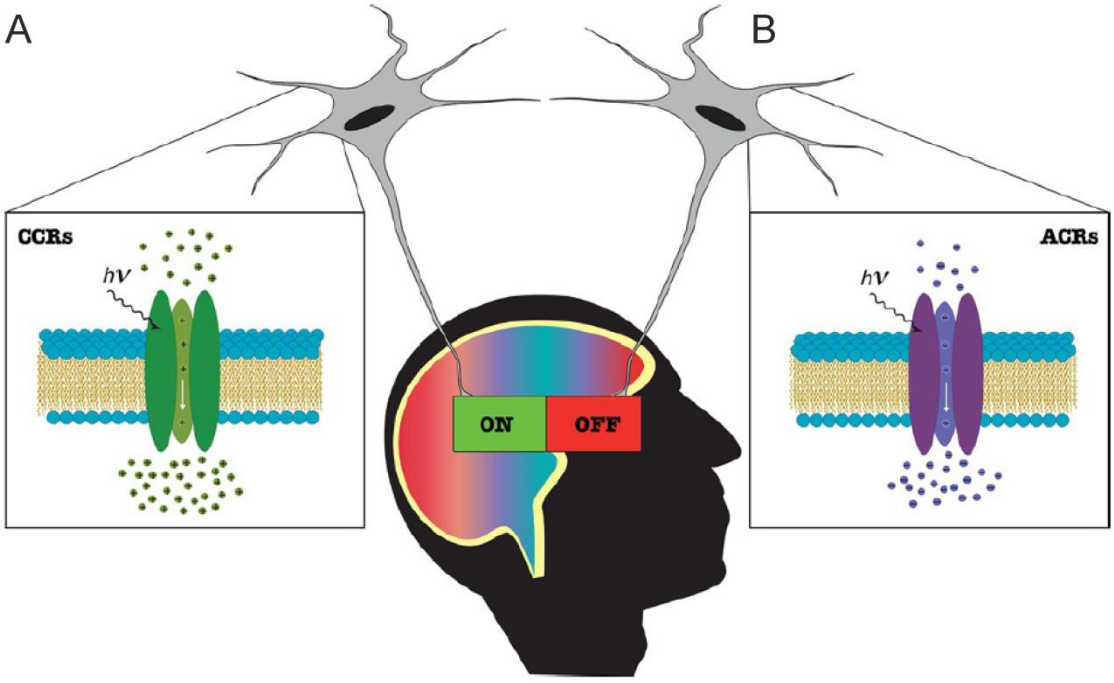

Figure 1.1-6 The new type of light-gated inhibitory anion channels for monitoring and controlling neuronal function

A) Activation of neuronal activity by cation channelrhodopsins (CCRs) that can be opened for cation influx by stimulating light. B) New inhibitory tools for silencing neuronal function by channelrhodopsins (ACRs). Figures are reproduced with permissions from (Peralvárez-Marín and Garriga, 2016).

1.2 Adeno-associated virus (AAV)

Powerful gene delivery approaches are needed for effective optical control of neuronal activity. Recombinant adeno-associated viruses (rAAVs) are used as a potential tool for gene transfer in the optogentics field (Yizhar et al., 2011a). With rAAVs to deliver optogenetic tools into neurons, neuroscientists can manipulate the activity of targeted neurons using light. The steps of the application of virus are not complicated. As depicted in **Figure 1.2-1**, before injecting virus into animal brain for controlling neuronal activity using light, they just need to create a genetic construct including light-gated ion channel and insert this construct into virus. Moreover, AAVs are non-pathogenic, have a low immunogenicity, and are known to transduce dividing and non-dividing cells (Blacklow et al., 1968)(During, 1997)(Hernandez et al., 1999). Therefore, rAAVs are widely applied in optogenetics. The following subsections present the principle and restrictions of rAAVs.

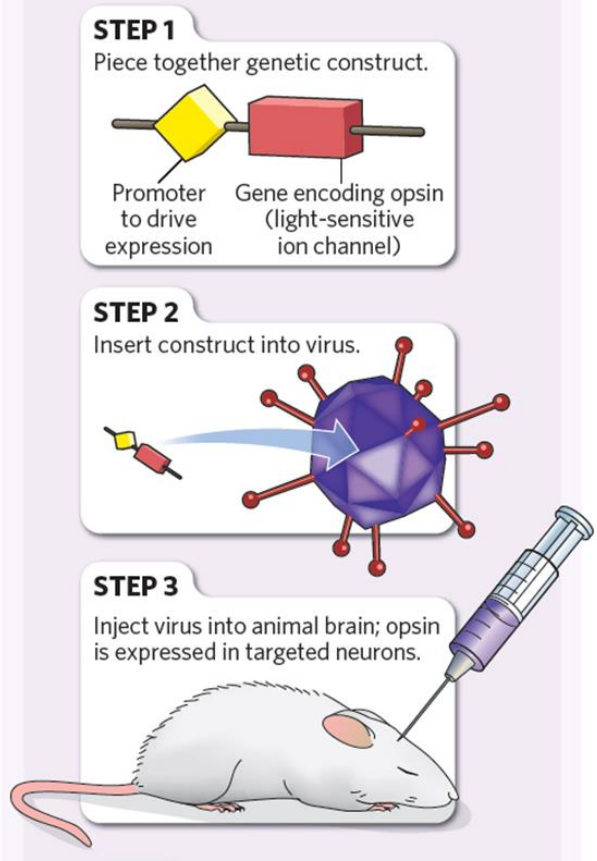

Figure 1.2-1 Virus Injection into animal brain for controlling neuronal activity using light

Figure is adapted with permissions from (Buchen, 2010).

1.2.1 Genome structure of AAV

AAV is a small, nonenveloped virus including a single-stranded linear DNA that is approximately 5 kb long (Srivastava et al., 1983). In terms of the co-infection of an unrelated helper virus, AAV belongs to the Parvoviridae family. It was discovered in 1965 as a contaminant of adenovirus (Ad) isolates (Atchison et al., 1965). As depicted in **Figure 1.2-2**, the AAV genome consists of three open reading frames (ORFs) for coding functional proteins including rep (red color in **Figure 1.2-2B**) for un-structural proteins and cap (yellow color in **Figure 1.2-2B**) for structural capsid proteins. The rep ORF codes for four Rep proteins (Rep78, Rep68, Rep52, and Rep40) that are promoted by the p5 and p19 promoters; the cap ORF codes for three capsid proteins VP1, VP2 and VP3 controlled by the p40 promoter. The two minor capsid proteins, VP2 and VP3, contain the same amino acid sequence that is shown in VP1 but consists of additional N-terminal sequences. Differences among the capsid protein sequence of the various AAV serotypes account for interacting with different cell surface receptors for infection. In addition, the VP2/VP3 mRNA codes for an assembly-activating protein (AAP) (green color in **Figure 1.2-2B**) starting from a weak CTG codon (asterisk) but in a different reading frame (Sonntag et al., 2010). Two 145-base T-shaped AAV inverted terminal repeats (ITRs) (blue color in **Figure 1.2-2B**) are present, which serve as origin of replication and play an important role in viral genome integration into the host.

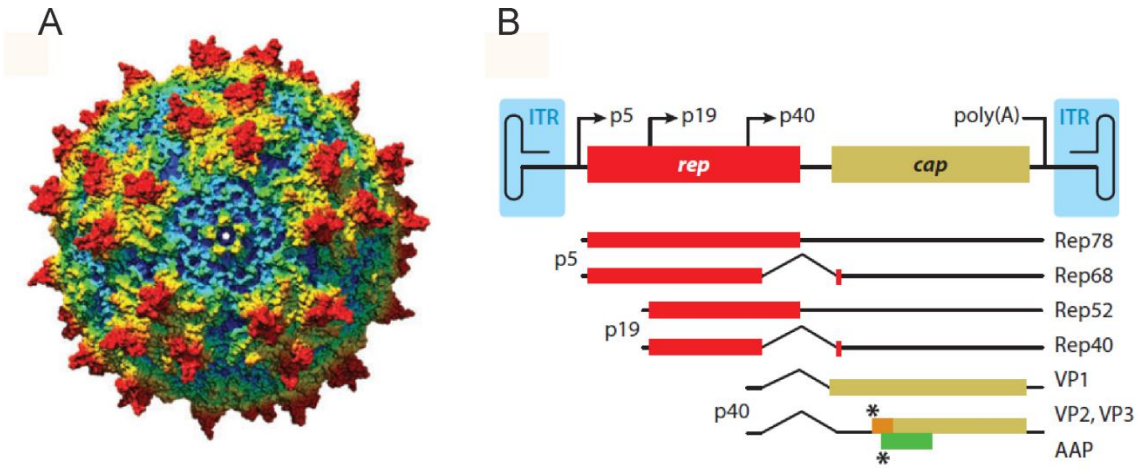

Figure 1.2-2 The AAV capsid surface and its genetic map

A) The AAV capsid surface is shown. Surface amino acids are colored in terms of their relative distance from the center of the capsid, in the following order: blue < cyan < green < yellow < red. B) AAV genetic map. The ~5-kb AAV genome contains three open reading frames (ORFs) for coding functional proteins. Two 145-base T-

shaped AAV inverted terminal repeats (ITRs) (blue color) are shown. Figures are reproduced from (Samulski and Muzyczka, 2014).

1.2.2 Restrictions

AAVs are non-pathogenic which makes them attractive for gene therapy (Samulski and Muzyczka, 2014). However, one potential source of toxicity when using AAVs has emerged; that of insertional mutagenesis and tumor induction. The McCarty group (Rosas et al., 2012) studied tumor formation by self-complementary AAV (scAAV) vectors in a mouse liver model prone to hepatocyte tumor formation. Using either rAAV-GFP or a null vector including only the enhancer or promoter to inject in mouse liver increased the frequency of tumor formation. It implies insertional mutagenesis may happen in liver due to the scAAV itself. Another restriction is the packaging capacity of AAV vectors. While single-stranded AAV (ssAAV) vectors carry ~4.4 kb of unique transgene sequence, scAAV can only deliver 2.2 kb. With a more substantial penalty in efficiency if this is exceeded since the scAAV genome is double-stranded DNA (McCarty, 2008). Therefore, AAVs are not suitable for large genes, many of which are of great interest to scientists.

1.3 Patterned neuronal networks *in vitro*

The patterned neuronal network with controlled geometry is of particular interest in the field of bioelectronics (Sprössler et al., 2001)(Mourzina et al., 2006a)(Mourzina et al., 2006b)(Marconi et al., 2012)(Li et al., 2014). In order to achieve cell patterning, microcontact printing (µCP) technology is widely employed, which was originally developed for producing alkanethiol patterns on the surface of gold (Kumar et al., 1994). This technology provides a simple and efficient way to obtain a neuronal network with well-defined geometry. The procedure consists of two main steps (**Figure 1.3-1**): incubating an elastomeric stamp with the molecular 'ink' solution, and then transferring the molecules to the substrate by printing. Numerous biomolecules can be used to print onto a variety of substrates such as a mixture of poly-lysine and extracellular matrix proteins (ECM)-gel (Vogt et al., 2003). Dissociated neuronal cultures patterned with µCP have generated much information regarding connectivity in neuronal networks (Vogt et al., 2005a) (Albers et al., 2015) and short-term plasticity (Vogt et al., 2005b).

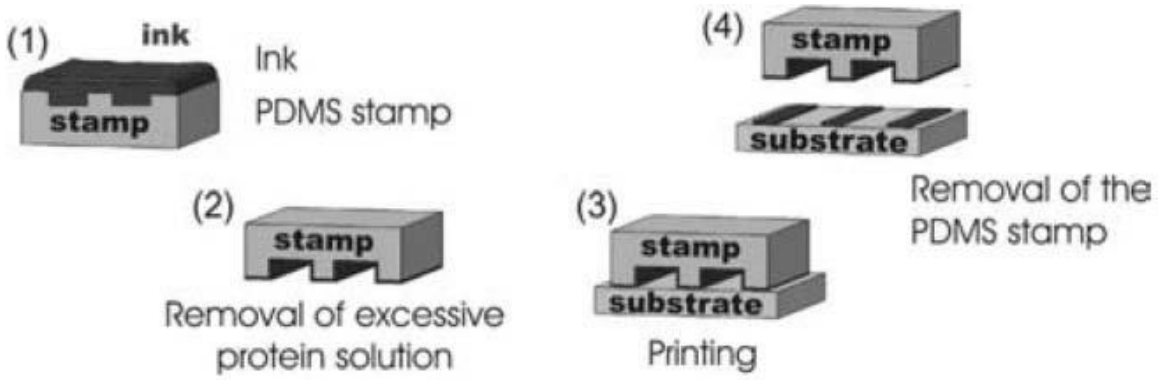

Figure 1.3-1 Schematic of the micro-contact printing method

(1)The PDMS stamp is wet with the inking solution (GBSS with PLL-FITC and Laminin) and (2) dried in a stream of nitrogen, leaving a thin layer of material on the stamp surface. (3) The stamp is pressed to the coverslips by hand, leaving the PLL-FITC and Laminin only on the regions defined by the designed structures of the stamp. (4) The stamp is removed from the substrate. Figure is adapted with permissions from (Offenhäusser et al., 2007).

1.4 The Aim of this work

Recently, optogenetics has been widely applied to decode neural circuits underpinning behavior as well as inducing neural activity to be recorded with bioelectronic devices. However, powerful gene delivery approaches are required for effective optical control of neuronal activity. Standard transfection strategies can be problematic due to low cell viability and low specificity, especially for primary post-mitotic neurons (Watanabe et al., 1999); (Martinez and Hollenbeck, 2003); (Hamm et al., 2002); (Zeitelhofer et al., 2009); (Karra and Dahm, 2010). AAVs are non-pathogenic, have a low immunogenicity, and are known to transduce dividing and non-dividing cells (Blacklow et al., 1968); (During, 1997); (Hernandez et al., 1999). There are numerous serotypes with different tissue tropisms, permitting specific transduction of a wide range of cell types (Howard et al., 2008); reviewed in (Asokan et al., 2012). Therefore, we assessed recombinant adeno-associated viruses (rAAVs) as a potential tool for gene transfer in the section **3.1**. Consequently, we have successfully achieved high-efficiency transduction of primary neurons by recombinant adeno-associated virus to specifically express ChR2opt for optogenetic manipulation.

In addition, patterned neuronal networks with well-defined topology may be a promising way to investigate the microcircuits on the single-cell level. The understanding of how neurons in microcircuits interact is one of the most fundamental questions in

neuroscience today. The brain consists of various microcircuits with specific functions (Cutsuridis et al., 2009). Comparison of the functional strengths of multiple sources of input to individual neurons is necessary for understanding their underlying circuit mechanisms (Hooks et al., 2015). However, it is still challenging to excite a neuron with specific input in brain regions where different neural networks are spatially intermingled. Fine-scale manipulation and measurement of neural activity is required. ChR2 (Nagel et al., 2003a) (Boyden et al., 2005) could elicit action potentials with blue light. ChR2 provides a high speed and powerful method for mapping neuronal circuits (Petreanu et al., 2007)(Augustine et al., 2013)(Wang et al., 2007)(Asrican et al., 2013)(Mancuso et al., 2011). Thus, using optogenetic method together with neuron patterning, mapping of cortical microcircuits with high spatial to understand neural network signaling is of considerable interest. In my work, the section **3.2** aims to achieve mapping of cortical microcircuits combing these promising technologies - optogenetic and neuron patterning. Based on the results of the section **3.1**, we have successfully controlled the activity of patterned neurons transduced with rAAVs.

Moreover, two new optogenetic tools, ChR2-XXL (see: **3.3**) and GtACR1 (see: **3.4**), were introduced into primary rat cortical neurons for activating or inactivating their activity, respectively. ChR2-XXL is a very powerful optogenetic tool (Dawydow et al., 2014), which can give rise to the largest photocurrents of all ChRs published so far and increases light sensitivity more than 10,000-fold over wild-type ChR2 in *Drosophila* larvae. Also, it has a long open-state lifetime. As a result, it can be opened using diffuse, ambient light to allow the ion influx into neurons and activate them. However, ChR2-XXL has not been applied to mammalian neurons yet. In the section **3.3**, depolarization block and neurotransmission in primary cortical neurons have been manipulated using ChR2-XXL.

In addition, channelrhodopsin-2 variants have been generated a very important role for activating neural activity in response to light and widely applied to study neural circuits for understanding brain functions. In contrast, inhibitory tools are much less efficient at inactivating neurons. Natural anion channel rhodopsins (ACRs) provide optogenetic inhibition tools through light-gated chloride conduction with unprecedented light sensitivity and temporal precision (Govorunova et al., 2015). *Guillardia theta* anion channel rhodopsins 1 (GtACR1) is a natural light-gated anion channels. Therefore, in the subsection **3.4**, I have validated the function of GtACR1 in primary cortical neurons and successfully achieved photoinhibition of spiking induced by pulsed current and spontaneous activity using blue light.

2 Materials and methods

2.1 Subcloning

2.1.1 psc-CMV-ChR2opt and psc-hSyn-ChR2opt

The rAAV vector pscAGFPFG2 was kindly provided by Hildegard Büning (CMMC, Cologne, Germany). The pAAV-hSyn-RFP construct was obtained from Addgene (Addgene plasmid #22907). ChR2opt was synthesized by GeneArt and is available from Addgene (plasmid #67958). The rAAV vectors psc-CMV-ChR2opt and psc-hSyn-ChR2opt were generated using restriction digest-based strategies. For the generation of the psc-CMV-ChR2opt vector, the ChR2opt-encoding fragment was inserted into the pscAGFPFG2 vector after excision of GFP. Based on this plasmid, the psc-hSyn-ChR2opt vector was generated by exchanging the CMV promoter for the hSyn promoter fragment.

2.1.2 psc-hSyn-ChR2-XXL

The original plasmid named pGEM ChR2-XXL-YFP was kindly provided by Dr. Shiqiang Gao and Prof. Dr. Georg Nagel (Universität Würzburg, Germany) for cooperation. ChR2-XXL-YFP fragment was amplified through Polymerase Chain Reaction with Phusion High-Fidelity DNA Polymerase (2 U/µL, # F-530S, Thermo Scientific, Germany). Primer pair for its amplification was listed below (**Table 2.1-1**). For ChR2-XXL subcloning, the psc-hSyn-ChR2-XXL was generated using restriction digest-based strategies, with the backbone produced from psc-hSyn-ChR2opt (Ref. **2.1.1**) using double-digest with *Hind* III and *Bam* HI.

Name	Sequence	Remark
XXL-Forward	5'- CCC **AAGCTT** **GCC ACC** *ATG GAT TAT GGA GGC GCC CTG AGT*	5' Enzyme site: ***Hind* III** Kozark sequence(**GCCACC**)
XXL-Reverse	5'- CG **GGATCC** *T TAC TTG CCG GCG GCC GCT TTA CTT GT*	3' Enzyme site: ***Bam* HI**

Table 2.1-1 Primer pair for amplification of ChR2-YFP

5' Enzyme site is marked in red color, 3' Enzyme site is marked in blue color. Kozark sequence (Kozak, 1991) improving efficient initiation of translation is marked in black color with bold font.

2.2 Maxi preparation of Plasmids

Pick a single colony from a freshly streaked selective plate and inoculate a starter culture of 5 ml LB medium containing the antibiotic Ampicillin (50 µg/mL). Incubate for approx. 8 h at 37°C with vigorous shaking (approx. 225 rpm). Dilute the starter culture 1/1000 to 1/2000 with selective LB medium. For low-copy plasmids (psc-hSyn-ChR2opt, psc-hSyn-ChR2-XXL belong to low-copy plasmids), inoculate 500 ml medium with 250–500 µl of starter culture. Grow at 37°C for 12–16 h with vigorous shaking (approx. 225 rpm). To purify plasmids with high concentration for AAV production or electroporation, EndoFree Plasmid Maxi Kit (#12362 Qiagen, Germany) was used. Following the protocol the kit provided. In the last step, dissolve the DNA in 200 µL of TE buffer. To determine the yield, DNA concentration was determined by both the microvolume UV-Vis spectrophotometer (NanoDrop 1000, Thermo Fisher Scientific, MA, USA) at 260 nm and quantitative analysis on an agarose gel through electrophoresis.

2.3 AAV production

This part was carried out by Baumann's group(Institute of Complex Systems ICS-4, Forschungszentrum Jülich, Germany).

Recombinant adeno associated viral (rAAV) vectors were generated by transient transfection of HEK293 cells (obtained from ATCC). HEK293 cells were cultivated in DH10 medium (DMEM + Glutamax (Invitrogen), 10% (v/v) FBS (Gibco), 1% (v/v) antibiotics/antimycotics (Invitrogen)) at 37°C, 5% CO_2, and 95% relative humidity. Briefly, 24 h prior to transfection 10^7 cells were seeded on Ø 14.5 cm dishes (10 dishes/rAAV construct). Cells were triple-transfected with the vector plasmid providing the transgenic viral genome, as well as the helper plasmids pRC (Girod et al., 1999) and pXX6-80 (Xiao et al., 1998), using the calcium phosphate method modified from (Chen and Okayama, 1987). Plasmid DNA was diluted in $CaCl_2$ (250 mM) and HEPES-buffered saline (50 mM HEPES, 280 mM NaCl, 1.5 mM Na_2HPO_4, pH 7.12), incubated for 3 min at RT, and added to HEK293 cells. After 24 h incubation at 37°C, 5% CO_2, and 95% relative humidity, the medium was exchanged for DH10 with reduced FBS (DMEM + Glutamax, 2% (v/v) FBS, 1% (v/v) antibiotics/antimycotics). Cells were harvested in PBS-M/K (in mM: NaCl 130, KCl 2.5, $MgCl_2$ 1, Na_2HPO_4 70, NaH_2PO_4 30, pH 7.4) after 24 h and collected by centrifugation.

Cells were lyzed in lysis buffer (in mM: NaCl 150, Tris/HCl 50, pH 8.5) by four freeze/thaw-cycles in liquid nitrogen and at 37°C. Nucleic acids were digested with benzonase (50 U/ml; Merck) for 30 min at 37°C. After removal of cell debris by

centrifugation rAAV particles were enriched by density gradient centrifugation. The rAAV suspension was sub-layered with iodixanol (Sigma-Aldrich, Taufkirchen, Germany) solutions (15%, 25%, 40%, and 60% iodixanol) and centrifuged (264,000 g, 4°C, 2 h). The 40% iodixanol phase containing the virus particles was collected and viral titers were determined by quantitative PCR. Briefly, viral genomes were isolated using the DNeasy Blood & Tissue Kit (Qiagen, Hilden, Germany) and genomic titers were determined. Primer pairs framing defined DNA segments of promoter or transgene sequences were used: for the CMV promoter (CGCTATTACCATGGTGATGCG, CCTCCCACCGTACACGCC), for the hSyn promoter (CCTGCGTATGAGTGCAAGTG, GGTGCTGAAGCTGGCAGTG), and for the eGFP-encoding sequence (GACGTAAACGGCCACAAGTTC, GAAGTCGTGCTGCTTCATGTG).

2.4 Primary Rat Cortical Neurons

Primary cortical cultures were prepared as described previously (Brewer et al., 1993). Briefly, cortices from embryonic day 18 (E18) Wistar rat brains were dissected and mechanically dissociated by trituration with a fire-polished, silanized pasteur pipette in 1 ml Hank's balanced salt solution without calcium or magnesium (HBSS-) (0.035% sodium bicarbonate, 1mM pyruvate, 10 mM HEPES, 20 mM glucose, pH 7.4). The cell suspension was diluted 1:2 in HBSS+ (with calcium and magnesium) and non-dispersed tissue was allowed to settle for 3 min. The supernatant was centrifuged for 2 min at 200 g. The pellet was resuspended in 1 ml Neurobasal medium (Gibco, Paisley, UK) with 1% B-27 (Gibco, Grand Island, NY, USA) and 0.5 mM L-glutamine (Gibco, Paisley, UK) and 50 µg/ml gentamicin (Sigma, Steinheim, Germany) (NB) per hemisphere. The cells were counted in a Neubauer counting chamber and plated in a concentration of 50,000 cells per well (24-well-plate) on poly-D-lysine (PDL, 10 µg/ml) coated 12 mm coverslips. Cells were kept at 37°C, 5% CO_2 and 100% humidity in 500 µl NB. After 4 hours, the medium was exchanged for 500 µl NB per well. Every third day, half of the medium was exchanged or, for rAAV transduced cultures, 100 µl NB medium was added.

This work except for GtACR1 experiments was carried out with the approval of the Landesumweltamt für Natur, Umwelt und Verbraucherschutz Nordrhein-Westfalen, Recklinghausen, Germany, in accordance with §6 TierschG., §4 TSchG i.V. and §2 TierSchVerV. GtACR1 experiments (see: **3.4**) were carried out with the approval of the Landesumweltamt für Natur, Umwelt und Verbraucherschutz Nordrhein-Westfalen, Recklinghausen, Germany, number 84-02.04.2015.A173.

2.5 Patterned neural network with Micro-contact printing

The grid pattern was designed in order to guide neurons to grow into a network as illustrated in **Figure 3.2-4**. 12 µm-diameter nodes were for the adhesion of neuronal somas, which were interconnected with eight neighbors via 4 µm-wide lines. The distance was 200 µm between vertically or horizontally connected nodes or 283 µm between two neighboring nodes along a diagonal. The production of microstamps was similar to that described previously (Fricke et al., 2011). Briefly, the pattern (**Figure 3.2-4**) was transposed into a chrome mask through an electron beam writer. A silicon wafer was spin coated by a layer of photoresist. The structure was transferred from the chrome mask to the resist in a mask aligner by applying UV-photolithography. After deep reactive ion etching, a 4 µm-deep structure was produced on the silicon wafer. Then the silicon mold was passivated by linking Tridecafluoro-1,1,2,2-tetrahydrooctyl (FOTCS) to the surface by a vapor deposition process in order to support the easy release of the plastomer. Poly(dimethylsiloxane) (PDMS) microstamps were produced by pouring Sylgard 184 (Dow Corning, Midland, USA) onto the silicon mold and curing at 60 °C for 6 h. After one separation release from the master, PDMS microstamps were cured for 1 h at 110 °C and ready for the micro-contact printing.

The protein mixture was transferred onto glass coverslips by micro contact printing (µCP, **Figure 1.3-1**). In order to increase the efficiency of protein transfer and the cellular repulsive effects of the unstamped substrate, glass coverslips (Menzel, Germany) were fully cleaned with 2% Helmanex solution for 15 min in an ultrasonic water bath, rinsed with milli-Q water for 5 min, and dried with nitrogen gas. The clean coverslips were activated in an oxygen plasma oven to form a layer of hydroxyl groups (-OH) on the surface. Then salinization was conducted in the glove box with the vapor of 3-glycidoxpropyltrimethoxysilane (GPTES) in order to introduce epoxy groups, which can form a layer of negative charged surface in the cell culture medium. The negative charged surface has a repulsive effect on the cell adhesion. On the other hand, epoxy groups can react with the amino-group of proteins and covalently immobilize the protein onto the substrate. Then the coverslips were rinsed with milli-Q water for three times and dried in the oven. Coverslips were sterilized by UV for 15 min before micro-contact printing. The ink solution was Gey's Balance Salt Solution (GBSS) containing 10 µg/mL PLL-FITC (Sigma P3069) and 20 µg/mL Laminin (Sigma L2020). PDMS stamps were sterilized with 75% ethanol, and dried with nitrogen gas. Then stamps were incubated in the ink solution for 20 min on ice. After incubation and drying with nitrogen gas, PDMS stamps were first

pressed on coverslips with a slight force, and kept in contact for 20 min. After removing the PDMS stamp from the coverslip, the printed coverslips were ready for the cell culture.

2.6 Gene delivery to Rat primary cortical neurons

2.6.1 Transduction with AAV virus

Primary cortical cells, grown on PDL coated coverslips (12 mm), were transduced with rAAVs on DIV1 or DIV8 with different multiplicities of infection (MOI). The medium (500 µl) was completely exchanged with NB containing 10^8, 10^9, 10^{10} or 10^{11} viral genomes to achieve MOIs of $2{\cdot}10^3$, $2{\cdot}10^4$, $2{\cdot}10^5$ and $2{\cdot}10^6$ viral particles per cell (vp/cell), respectively. As a control, the same volume of 40% Iodixanol was added to individual wells. Three days post transduction (DPT), 100µl NB medium was added. The cells were electrophysiologically measured after DIV14 or fixed for immunofluorescence DPT7-9.

2.6.2 Electrofection

The preparation of primary cortical neurons remains as described in **2.4**. Amaxa Rat Neuron Nucleofector® Kit (Cat.No. VPG-1003) from Lonza Cologne GmbH (Germany) was used to transfer circular, double stranded, plasmid DNA directly into cells. Each electrofection experiment used two fresh cortices. After centrifugation for 2 min at 200 g, the cell pellet was carefully resuspended in 200 µl room temperature Nucleofector® Solution from the Kit (163.6 µl of Rat Neuron Nucleofector® Solution mixed with 36.4 µl of Supplement), to which was added 6 µg of psc-hSyn-ChR2-XXL plasmid or 8.5 µg pBK-CMV-GtACR1-TYE plasmid. Avoid leaving the cells in Rat Neuron Nucleofector® Solution for extended periods of time (longer than 15 minutes), as this may reduce cell viability. Transfer cell/DNA suspension into certified cuvette (sample must cover the bottom of the cuvette without air bubbles). Using Nucleofector® Device (AAD-1001S, Lonza, Germany), select the Nucleofector® Program G-013 (Chicken DRG). Insert the cuvette with cell/DNA suspension into the Nucleofector® Cuvette Holder and apply the selected program. Take the cuvette out of the holder once the program is finished. Add 800 µl of the pre-equilibrated RPMI medium (Gibco, Grand Island, NY, USA) with 1% FBS (Gibco, Grand Island, NY, USA) and 0.5 mM L-glutamine (Gibco, Paisley, UK) to the cuvette and gently transfer the sample immediately into the prepared 24 wells culture dish with the coated coverslip and added 500 µl RPMI medium per well. Use the supplied pipettes and avoid repeated aspiration of the sample. After 4 hours carefully replace medium with 500 µl fresh Neurobasal medium (Ref. **2.4**) per well to remove cellular debris. Every third day, half of the medium was exchanged.

2.7 Immunofluorescence staining

For the immunostaining, cells were fixed with 4% (w/v) paraformaldehyde in PBS (PFA) at RT for 20 min, washed with 1x PBS (pH 7.4) and blocked overnight in blocking solution (1% (w/v) BSA, 2% (v/v) goat serum in PBS). Cells were permeabilized with 0.1% (w/v) TritonX-100 in blocking buffer for 15 min. The following primary antibodies were used: rabbit anti-MAP2 (dilution 1:500, Chemicon/Millipore) and mouse anti-GFAP (dilution 1:100, Chemicon/Millipore). Bound primary antibodies were visualized using Alexa-488, Alexa-568, Alexa-546 or Alexa-633-conjugated secondary antibodies (Life technologies, Eugene, Oregon, USA; dilution 1:500 in blocking solution). Nuclei were stained with TOPRO (Life technologies, Eugene, Oregon, USA; dilution 1:500 in blocking solution). Samples were mounted in Dako Fluorescence Mounting Medium (Agilent Technologies, Waldbronn , Germany) and analyzed by using a Zeiss Apotome microscope (Carl Zeiss Microscopy GmbH, Göttingen, Germany) or Confocal laser scanning microscope (Leica TCS SP5, Leica Microsystems, Heidelberg, Germany).

2.8 Electrophysiology

Whole cell patch clamp experiments were performed using an EPC9 amplifier (HEKA Elektronik, Lambrecht/Pfalz, Germany) controlled by the TIDA 5.240 software (HEKA Elektronik). The recordings were performed in extracellular patch clamp buffer solution (mM: NaCl 120, KCl 3, $MgCl_2$ 1, HEPES 10, $CaCl_2$ 2; pH 7.3, 248 mosm/kg). For synaptic input blocking measurement, the following (all from Tocris Bioscience, Bristol, UK) were added to the extracellular solution above: D-AP5 (25 µM), NBQX (10 µM), SR 95531 hydrobromide (alternative name: Gabazine, 20 µM). Patch pipettes were pulled from borosilicate glass capillaries (Sutter Instrument Co., Novato, CA, USA) using a micropipette puller (P-2000, Sutter) to achieve a pipette resistance of 6-9 MOhm. The pipettes were filled with the standard intracellular patch solution (mM: NaCl 2, KCl 120, $MgCl_2$ 4, HEPES 5, EGTA 0.2, Mg-ATP 0.20, pH 7.3, 255 mosm/kg). Special for GtACR1 measurements, an intracellular solution with low chloride concentration (mM: K_2SO_4 67.5, $MgCl_2$ 2, adjusted to 248 mosm/kg with glucose) was prepared to replace the standard solution.

2.9 Laser stimulation

Optogenetic tool-expressing neurons were stimulated with a 473 nm diode laser (Rapp OptoElectronic GmbH, Hamburg, Germany), which was guided through an optical fiber and reflected with a dichroic mirror (UGA-40, Rapp OptoElectronic GmbH) into the light path of a Zeiss Axioscope microscope equipped with an Olympus (x20) objective

(UMPLFLN20xW). For the ChR2opt construct, the laser spot diameter was adjusted to about 24 µm, resulting in a laser intensity of approximately 1.74 W/mm^2. The different delay times (150ms or 200ms or 500ms) and different laser pulse times (ranging from 1 msec to 50 msec) were applied for ChR2opt stimulation targeting somas/axons/dendrites. For the ChR2-XXL and GtACR1 construct, different delay times (500 msec to 60 sec) and different laser pulse times (ranging from 0.25 msec to 100sec) were applied for light stimulation. Light intensity was 1.68 W/mm^2 for ChR2-XXL stimulation (laser spot diameter was about 24 µm); Light intensity was 0.21 W/mm^2 for GtACR1 (laser spot diameter was about 61.2 µm).

2.10 Data analysis

Data were analyzed in TIDA 5.240, Excel, Matlab or Origin 9. All data are given as mean ± standard error of the mean. The following statistical test was used One-way ANOVA. Significance levels are indicated as follows: ** ($P \leqslant 0.01$), ***($P \leqslant 0.001$), n.s. (not significant). Findpeaks script with MATLAB (Ref: **Appendix A1**) was used to analyze action potentials. Stationary photocurrents of GtACR1 were measured for the last 50 ms of the illumination period. Reversal potentials were calculated by linear fit of the two data points between crossing of I=0 pA occurs. In the subsection **3.3.2**, the spikes whose amplitudes were more than 35 mV were selected to determine the oscillation. Each frequency point was the average value of 5 milliseconds window.

3 Results

3.1 psc-CMV-ChR2opt and psc-hSyn-ChR2opt

In this section, the present work aims to provide a useful tool for specifically manipulating neuronal activity with ChR2opt (H134R) using rAAV transduction. The subsections from **3.1.1** to **3.1.3** have been published (Jin et al., 2016), which was titled 'High-efficiency transduction and specific expression of ChR2opt for optogenetic manipulation of primary cortical neurons mediated by recombinant adeno-associated viruses'.

3.1.1 Transduction efficiency of rAAV serotypes in primary cortical cultures

In order to compare the transduction efficiencies of different rAAV serotypes in rat primary cortical cell cultures, rAAV serotypes 1, 2, 4, 5, 6, 8, and 9 mediating expression of eGFP under the control of the constitutively active cytomegalovirus (CMV) promoter (Wilkinson and Akrigg, 1992) were applied. Viral vectors were applied with different multiplicity of infection (MOI) values, i.e. $2•10^3$, $2•10^4$, $2•10^5$ and $2•10^6$ vp/cell, on cortical-glial mixed cultures after 8 days in vitro (DIV8). All of the applied rAAV serotypes mediated expression of eGFP, but transduction efficiencies and eGFP expression levels varied between serotypes (**Table 3.1-1** and **Fig. S 1**). Due to vector design eGFP expression was driven by the constitutive CMV promoter and thus eGFP expression was observed in neuronal as well as glial cells. The ratio of transduced neuronal vs. transduced glial cells was examined using a neuronal marker (microtubule-associated protein 2, MAP2) and an astrocyte marker (glial fibrillary acidic protein, GFAP). Serotype 6 mediated the most efficient transduction in primary cortical cultures (**Table 3.1-1** and **Figure 3.1-1**). However, even though the highest neuron transduction rate was observed for serotype 6, glial cells were also detected (**Figure 3.1-1**). The specificity of serotype-dependent tropisms was not sufficient for cell-type specific transgene expression.

Serotype	Expression level	Transduced neurons (total MAP2 positive)	Transduced glial cells (total GFAP positive)
1	++	++	+++
2	+	+	++
4	+	+	+++
5	+	+	+
6	+++	+++	++
8	+	+	-
9	+	+	+++

Table 3.1-1 Transduction efficiency of different rAAV serotypes in primary cortical cultures

Primary cultures were transduced on DIV8 with rAAV serotypes 1, 2, 4, 5, 6, 8, and 9 expressing eGFP under the control of the CMV promoter (MOI $2•10^4$ vp/cell). Transduction efficiencies were estimated based on eGFP fluorescence (DPT9) and cell types were identified using the neuronal marker MAP2 and the glial marker GFAP. Percentages of transduced neurons and glial cells were estimated based on total MAP2 or GFAP-positive cells, respectively. Mean values (*n*=3) were calculated and are depicted as – (no transduced cells), + (⩽ 30%), ++ (30 – 66%), and +++ (⩾ 66%).

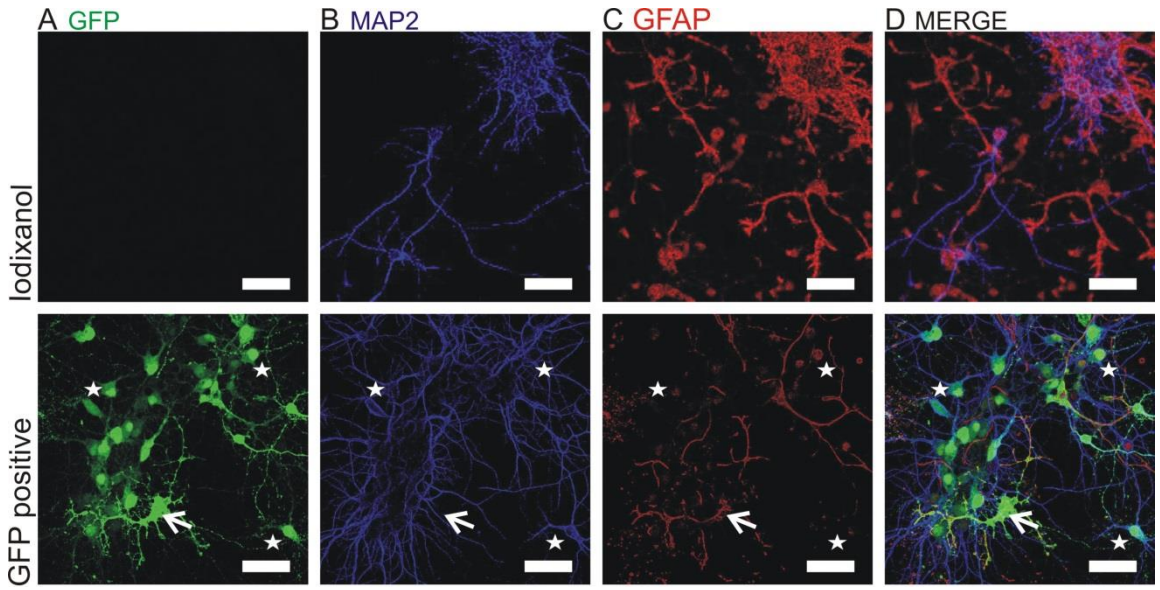

Figure 3.1-1 Expression of eGFP in primary cortical cultures.

Primary cortical cultures were transduced with rAAV6-CMV-eGFP (MOI $2•10^4$ vp/cell) on DIV8 (lower panel) or treated with iodixanol as a control (upper panel). Immunocytochemistry was performed on DIV15 and cultures were stained using specific antibodies for MAP2 (B, blue) and GFAP (C, red). Fluorescence of eGFP is shown in green (A) and the merged images are depicted in (D). Arrows identify eGFP-positive glial cells and stars mark eGFP-expressing neurons. Scale bars indicate 50 µm.

3.1.2 Neuron-specific expression of ChR2opt in primary cortical neurons

Based on the results described above, we selected rAAV6 as the most suited serotype for transgene expression in cortical neurons. For optogenetic approaches, we generated a

rAAV6 vector mediating expression of ChR2opt under the control of the CMV promoter. The rAAV6-CMV-ChR2opt construct mediated expression of the transgene in about 72% of cells. In order to assess transduction of neuronal cells vs. glial cells, immunocytochemistry was performed using MAP2 and GFAP on these cultures (**Figure 3.1-2**). ChR2opt was mainly detected in neuronal cells, but also in a moderate amount of GFAP-positive cells (**Figure 3.1-2**). Fluorescence of the C-terminal mKate tag could be detected on DPT3 and increased until DPT7. These results corroborate the data for CMV promoter-mediated eGFP expression after transduction with different rAAV serotypes (**Figure 3.1-1**).

Accordingly, we substituted the CMV promoter for the neuron-specific human synapsin 1 (hSyn) promoter. Firstly, we assessed the neuron-specificity of the rAAV6-hSyn-RFP vector in primary cortical cultures based on RFP fluorescence. Immunocytochemical staining with MAP2 and GFAP antibodies revealed a very high percentage of RFP-positive neurons, whereas glia cells did not express the fluorescent protein (**Figure 3.1-3A**). The neuron transduction efficiency of 92% ± 5% achieved with rAAV6-hSyn-RFP (MOI $2 \cdot 10^2$ vp/cell) was higher than observed for rAAV6-CMV-eGFP (MOI $2 \cdot 10^4$ vp/cell). Application of rAAV6-hSyn-RFP with an MOI of $2 \cdot 10^4$ vp/cell further increased the neuron transduction efficiency to 96% ± 2% (**Figure 3.1-3B**). In summary, the hSyn promoter not only mediated neuron-specific transgene expression, but furthermore improved the overall observed transduction efficiency.

Next, we probed whether ChR2opt could also be specifically expressed in primary rat cortical neurons with the hSyn promoter via rAAV6-mediated transduction. A transduction efficiency of 70% ± 8% was achieved (**Figure 3.1-3B**). Strong ChR2opt expression could be identified in neurons based on mKate fluorescence, whereas glial cells did not express the transgene (**Figure 3.1-3C**). These results correspond to our observations for the rAAV6-hSyn-RFP construct (**Figure 3.1-3A**).

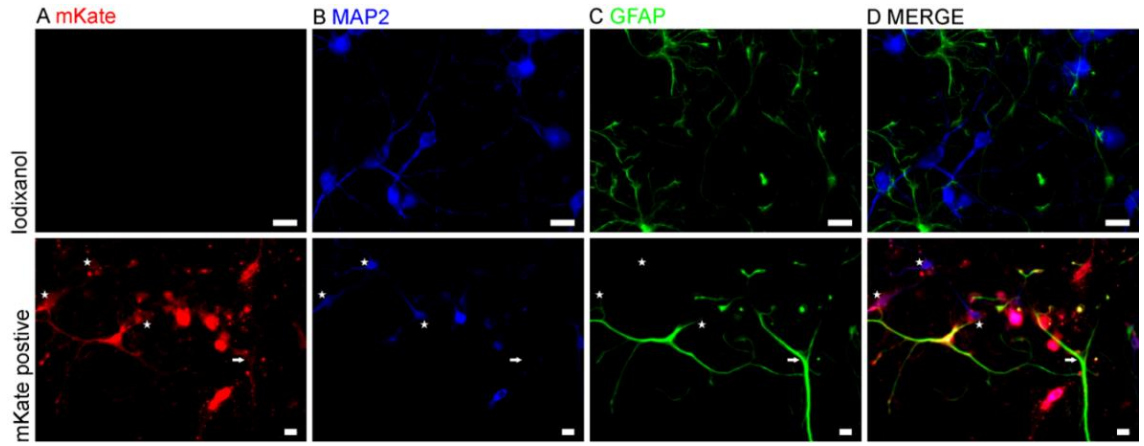

Figure 3.1-2 Expression of ChR2opt in primary cortical cultures.

Primary cortical cultures were transduced with rAAV6-CMV-ChR2opt (MOI $2 \cdot 10^4$ vp/cell) on DIV8 (lower panel) or treated with iodixanol as a control (upper panel). Immunocytochemistry was performed on DIV15 and cultures were stained using specific antibodies for MAP2 (B, blue) and GFAP (C, green). Fluorescence of mKate is shown in red (A) and the merged images are depicted in (D). Arrows identify mKate-positive glial cells and stars mark mKate-expressing neurons. Scale bars indicate 20 µm.

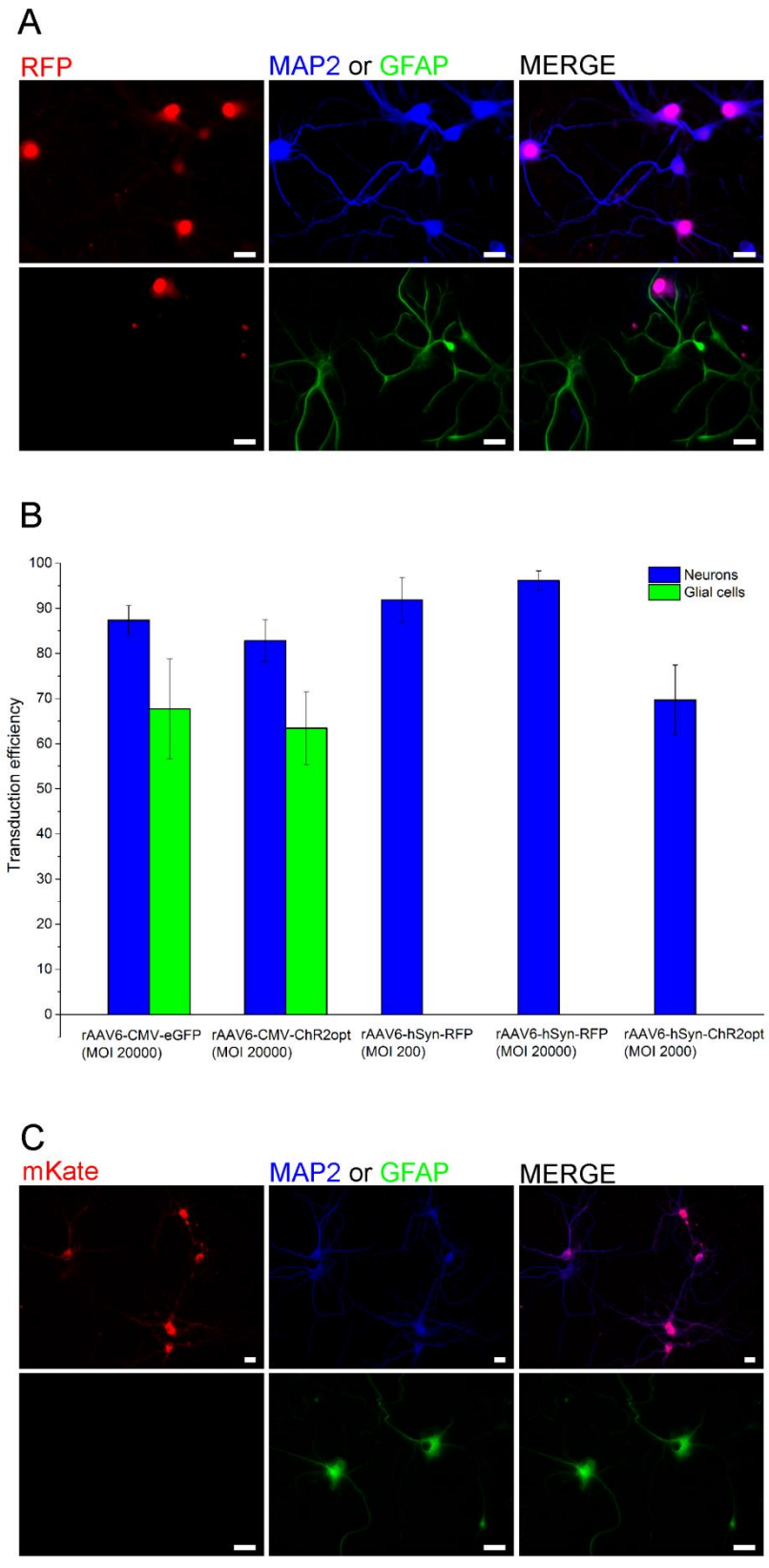

Figure 3.1-3 Neuron-specific expression of ChR2opt in primary cortical cultures.

A) Primary cortical cultures were transduced with rAAV6-hSyn-RFP (MOI $2 \cdot 10^4$ vp/cell) on DIV8 and stained immunocytochemically on DIV14 for MAP2 (blue) and GFAP (green). Fluorescence of RFP is shown in red and the merged images are depicted on the right. Scale bars indicate 20 µm. B) Neuron transduction efficiencies of rAAV6 vectors (DIV14) harboring different promoters. The data are mean values ± SEM (*n*=3 independent experiments. In one experiment, 10 different areas of each coverslip containing neurons were imaged for analysis). C) Primary cortical-glial mixed cultures were transduced with rAAV6-hSyn-ChR2opt (MOI $2 \cdot 10^3$ vp/cell) on DIV8 and stained immunocytochemically on DIV15. Autofluorescence of mKate is depicted in red, MAP2 in blue, and GFAP in green. The merged images are shown on the right. Scale bars indicate 20 µm.

3.1.3 Optical Stimulation of ChR2opt-expressing neurons

In order to test ChR2opt-mediated triggering of action potentials in neurons, we performed optical stimulation experiments. Single ChR2opt-expressing neurons were stimulated using blue laser light (473 nm) with a spot size of approximately 24 µm in diameter (laser intensity of 1.74 W/mm^2). Stimulated cells were analyzed using the whole cell patch clamp technique.

We probed how many action potentials (= spikes) were elicited with different light pulse durations using the same interstimulus delay times for ChR2opt recovery. In **Figure 3.1-4A** experiments are shown where ChR2opt was expressed under the control of the CMV promoter (rAAV6-CMV-ChR2opt). Two different delay times (150 ms or 200 ms) and five different laser pulse times (ranging from 1ms to 30 ms) were applied for ChR2opt stimulation. It was easier to evoke spikes with longer pulse times than with shorter pulse times. Using a 10ms laser pulse, spikes were triggered with a success rate of 83% ± 8%. Successive stimuli were applied with interpulse delay times of 150ms. The stimulation success rate increased to 97% ± 2% if the delay time was extended to 200ms. Accordingly, measurements of cells transfected with hSyn-ChR2opt were performed with stimulation pulses interrupted with delay periods of 200ms. With the hSyn promoter, pulse times of ≥5ms resulted in successful spike generation rates of up to 99%. Furthermore, we addressed eventual triggering of extra spikes. As depicted in **Figure 3.1-4B** pulse times of 50ms evoked an extra spike. Using 30ms pulses, a second depolarization was

measured but it did not reach the threshold level to induce another action potential. The photocurrent of Channelrhodopsin consists of a peak current and a stationary current (Berndt et al., 2011). Our data suggest that during the stationary photocurrent, that can be induced with a longer pulse, some channels remain open. These channels can be used to depolarize the cell over the threshold and to trigger an additional action potential when long light stimuli (50 ms) are applied.

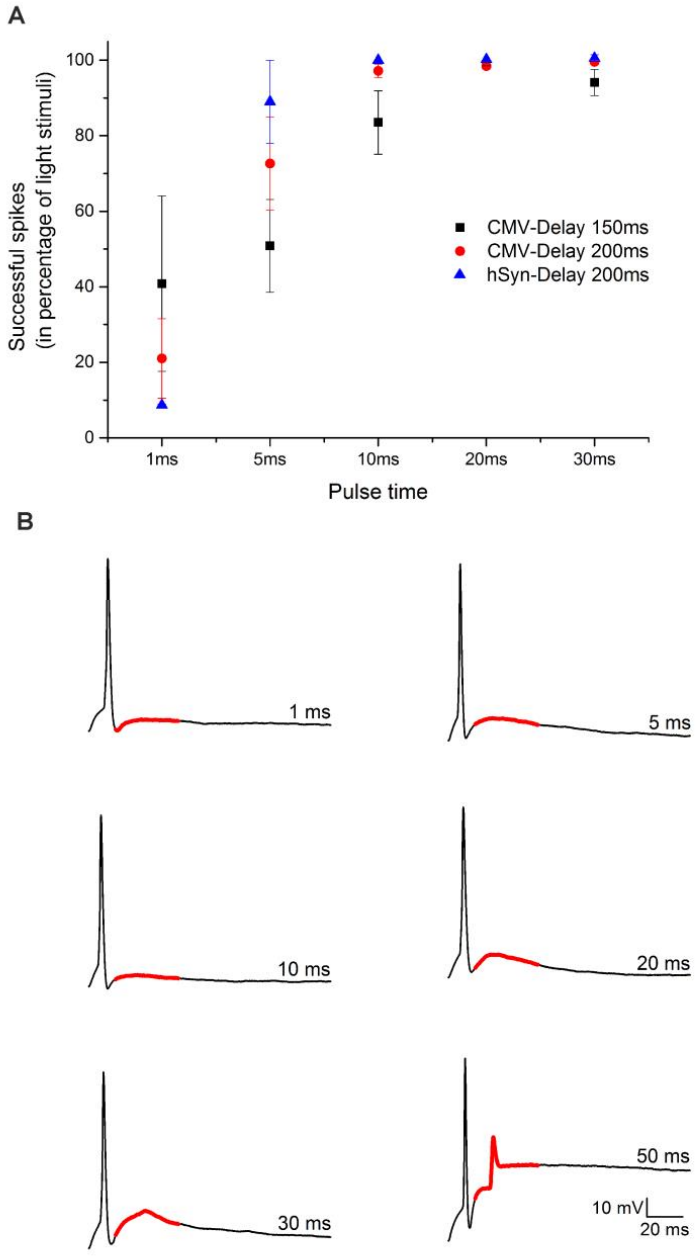

Figure 3.1-4 Stimulation of ChR2opt - expressing neurons.

A) Neurons transduced with a rAAV6 construct harboring either the CMV promoter (black, red) or the hSyn promoter (blue) were examined. Successful generation of action potentials (%) is displayed vs. pulse duration of the light stimulus. Data (n=3-7 for rAAV6-CMV-ChR2opt group; n = 3-4 for rAAV6-hSyn-ChR2opt group) are presented as mean ± SEM. Each stimulation repeated 100 times. B) An extra spike was triggered by longer pulse times in a rAAV6-CMV-ChR2opt transduced neuron.

Having demonstrated the ability of ChR2opt to trigger action potentials at the soma, we next investigated whether illumination of axons or dendrites of a neuron were sufficient to trigger action potentials. Five different sites including the soma of a ChR2opt expressing neuron were selected for stimulation (**Figure 3.1-5A**, asterisks). Action potentials were recorded at the soma with whole cell patch clamping. As shown in **Figure 3.1-5B**, action potentials were observed after blue light illumination at each of these sites. As we had measured before (Lange et al., 2014), action potentials could be precisely and repeatedly triggered at each of 5 different sites with 100 laser pulses of 50ms and a delay time of 500ms (**Figure 3.1-5B**). We also examined the dependence of the response time and spike amplitude to the distance of the stimulation site. The time from the onset of illumination to spike peak measured at the soma was defined as response time. As depicted in **Figure 3.1-5C**, response times decreased with reducing the distance between the stimulation site and the patch pipette. Stimulation at position 5 (see **Figure 3.1-5A**) triggered an action potential after 18.4 ± 0.2ms, whereas stimulation at the soma (position 1) caused an action potential approximately after 12.1 ± 0.2ms. The amplitudes of the action potentials were very similar and were independent of the stimulation site (**Figure 3.1-5D**).

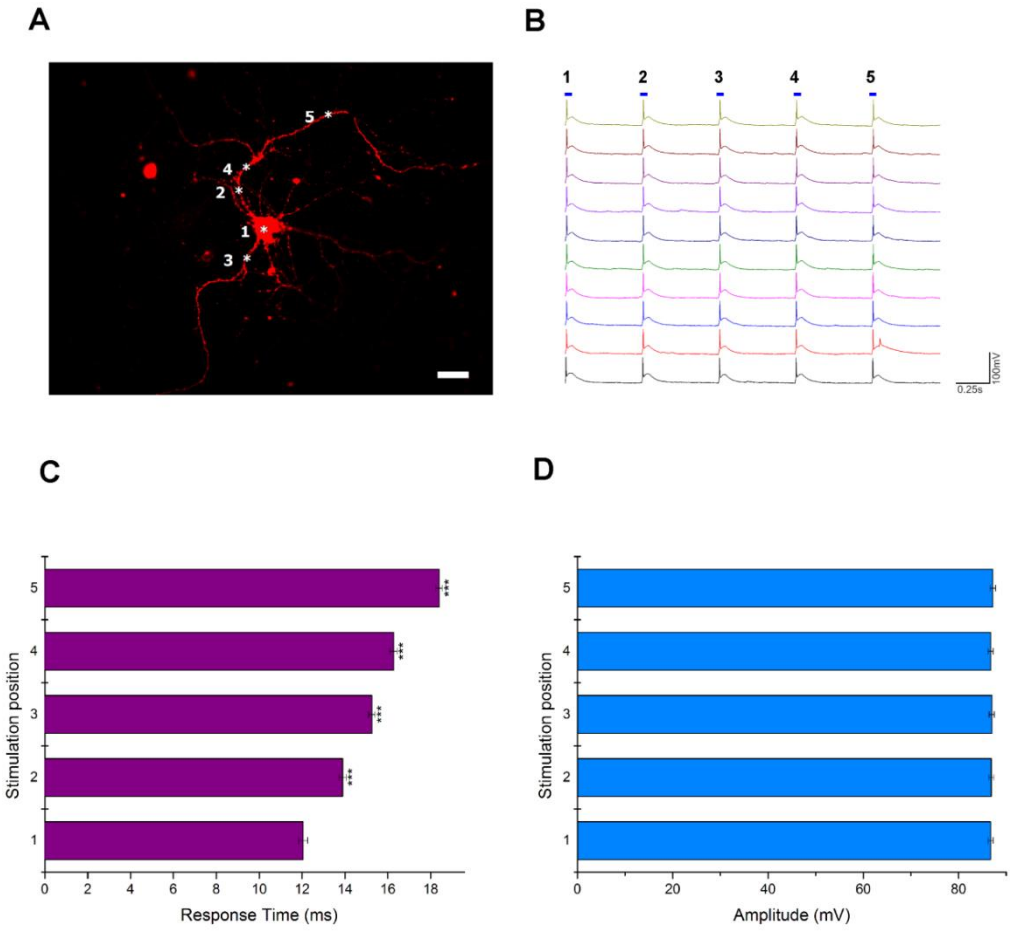

Figure 3.1-5 Stimulation of rAAV6-CMV-ChR2opt-transduced neurons.

A) Fluorescence of mKate tagged to ChR2opt is displayed. The 5 stimulation sites targeted are indicated by asterisks (positions 1 – 5). The scale bar represents 50 µm. B) Voltage traces of 10 successive stimulations (50ms pulses with 500ms interpulse delay times) initiated at the 5 different stimulation sites (see **Figure 3.2-5A**) were recorded from a single cell by whole cell patch clamping. C) Response time to evoke an action potential measured at the soma after laser light stimulation at each of the 5 different stimulation sites (one-way ANOVA, $p < 0.001$) are depicted. D) Action potential amplitudes measured after laser light stimulation at each of the 5 different stimulation sites are shown. Data (*n* =50 trials from one cell) are presented as mean ± SEM.

Similar to CMV-driven expression of ChR2opt, neurons transduced with rAAV6-hSyn-ChR2opt generated action potentials after stimulation with blue laser light (n=15). In **Figure 3.1-6A**, a representative trace is depicted using a laser pulse of 50ms and a delay time of 500ms. When applying 50ms pulses, again, often more than one spike was

evoked. The success rate of triggering the first spike was 100%, whereas the success rate to trigger a second spike was 55% ± 22% (**Figure 3.1-6B**). A comparison of the FWHM (Full-Width Half-Maximum) and the amplitude of both the first and second spike after light stimulation revealed that the FWHM of the first spike was smaller than that of the second one (**Figure 3.1-6C** and **E**), while the amplitude of first spike was larger than that of the second one (**Figure 3.1-6D**).

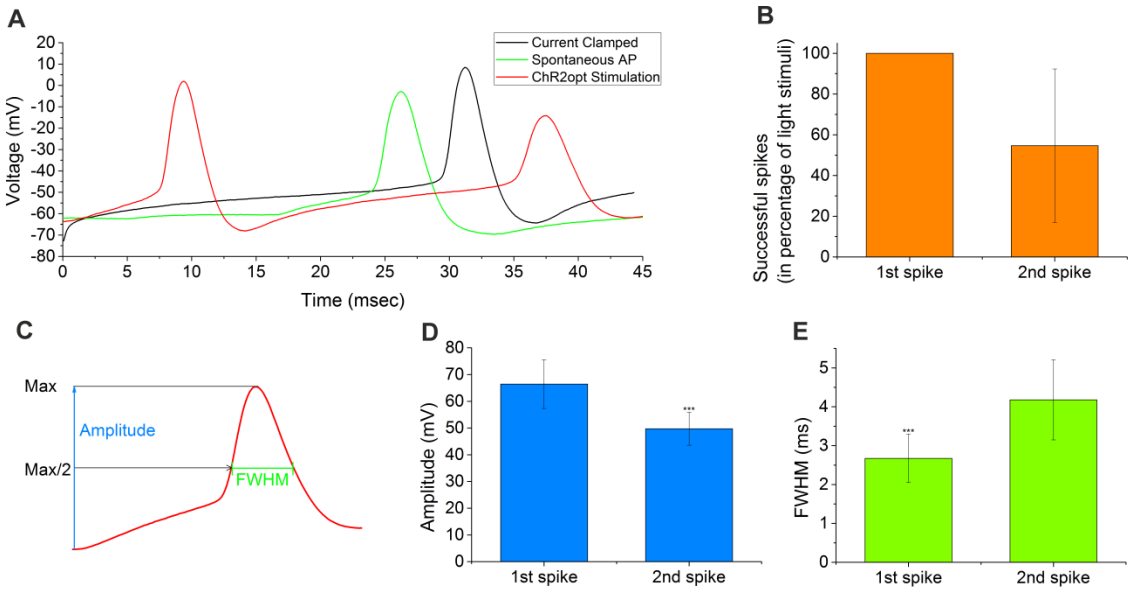

Figure 3.1-6 Triggering of action potentials in rAAV6-hSyn-ChR2opt transduced neurons

A) Comparison of action potentials in a typical rAAV6-hSyn-ChR2opt transduced neuron. A voltage trace (black) driven by 80 pA injection from the patch pipette, a representative voltage trace (red) of APs evoked by laser pulse application for 50 ms separated by a delay time of 500 ms, and a spontaneous action potential (green) are shown. B) Success rate (%) of action potential generation in response to a light stimulus is depicted for the first and second spike. C) The scheme of the amplitude and FWHM (Full-Width at Half-Maximum) in one spike are depicted in blue and green color, respectively. 'Max' indicates the maximum of depolarization from the resting potential. D) Amplitudes of the first and second spikes (one-way ANOVA, $p < 0.001$) were analyzed. E) FWHM of the first and second spikes (one-way ANOVA, $p < 0.001$) is shown. Data (n=300 spikes from one cell for the first spike group; n=164 spikes from the same cell for the second spike group) are presented as mean ± SD.

3.2 Optical control of neuronal network *in vitro* with ChR2opt

Microcircuit is a specific pattern of connectivity between neurons within a region. I want to explore if ChR2opt can be employed to study the microcircuit of neuronal network in a small region. In addition, controlling neural activity on single-cell level is very promising in neuroscience field. I want to explore the possibility whether neural activity can be controlled with optical method on single-cell level including just stimulating the axon or dendrite of a neuron. Here two kinds of patterning structures (X-shape and branch patterns) were used to investigate these goals described above. The subsection **3.2.1** focuses on optogenetic mapping of cortical microcircuits of the random network with ChR2opt. Then, the subsection **3.2.1** shows the results on mapping microcircuits of X-shape patterned neural network by ChR2opt; the subsection **3.2.3** aims to optical control of neural activity on single-cell level through the branch pattern.

3.2.1 Optogenetic mapping of cortical microcircuits in the random network

In this subsection, we aim to map microcircuit of cortical neural network with ChR2opt and investigate synaptic behaviors of a pair of pre-postsynaptic neurons using two kinds of stimulation protocols. The first protocol is to apply for repetitive laser stimulations on only one region (the soma or axon of the recorded neuron, or the presynaptic neuron) to measure the response of the recorded neuron in a small neural network. The second one is to apply for sequential and repetitive photostimulations in a small neural network including two or three pairs of the pre-postsynaptic neurons. The general positions setting for laser illumination is followed: 1) position 1 (cell-1, also postsynaptic neuron) is always used as a recorded neuron to measure the response to laser stimulation with patch clamp. 2) other positions are the axon of the cell-1 or the soma of the presynaptic neuron. The laser spot diameter was adjusted to about 24 μm, resulting in a laser intensity of approximately 1.74 W/mm^2. Using these protocols, we have measured 6 small neural networks and here we present the results with two typical individual networks to demonstrate: 1) ChR2opt allows optogenetic control of neuronal network signaling; 2) it allows mapping of cortical microcircuits *in vitro*; 3) ChR2opt can be applied to analysis synaptic behaviors in the neural network.

To scrutinize whether ChR2opt allows optogenetic control of neuronal network signaling, we established 4 small laser spots of light illumination in a ChR2opt-tranduced neuronal network (**Figure 3.2-1a**) and selected the soma of a neuron as the recording site, indicated in the figure by number 1. As data **Figure 3.2-1c** shows, blue light stimulation of ChR2opt at the soma or axon of the recorded neuron successfully elicited its action

potentials (see **Figure 3.2-1c** stimulation 1 or 3). In addition, stimulated action potentials of other cells could propagate to the recorded neuron that was away from the stimulated cells (see **Figure 3.2-1c** stimulation 2 and 4). The laser spots, 24 µm in diameter, are smaller than the distances between the distant neurons stimulated and the recorded neuron, which strongly enables the laser light not stimulate other unexpected regions. This demonstrated ChR2opt enables optical control the neuronal network signaling. Next, we mapped the spatial distribution of synaptic circuits connecting neurons (**Figure 3.2-1b**). By comparing the response time and amplitude of the stimulated action potentials that were recorded by whole cell patch clamp, we found that the response time from the distant stimulation site 4 that was dramatically longer (39.88 ± 0.96 msecs, see **Figure 3.2-1d**); the amplitudes of the action potentials were different among these four stimulation sites. In general, the voltage traces of a postsynaptic neuron involve in its postsynaptic currents that are induced by neurotransmitters from the presynaptic neurons; the higher intensity current could elicit faster action potential. Therefore, based on the basic knowledge above, these data show the synaptic inputs from different neurons in one network elicit different responses in the postsynaptic neuron due to the induction of different postsynaptic currents. In summary, optogenetic control of neural network signaling with ChR2opt can be applied to map microcircuits of cortical neural networks and analysis synaptic inputs connecting neurons.

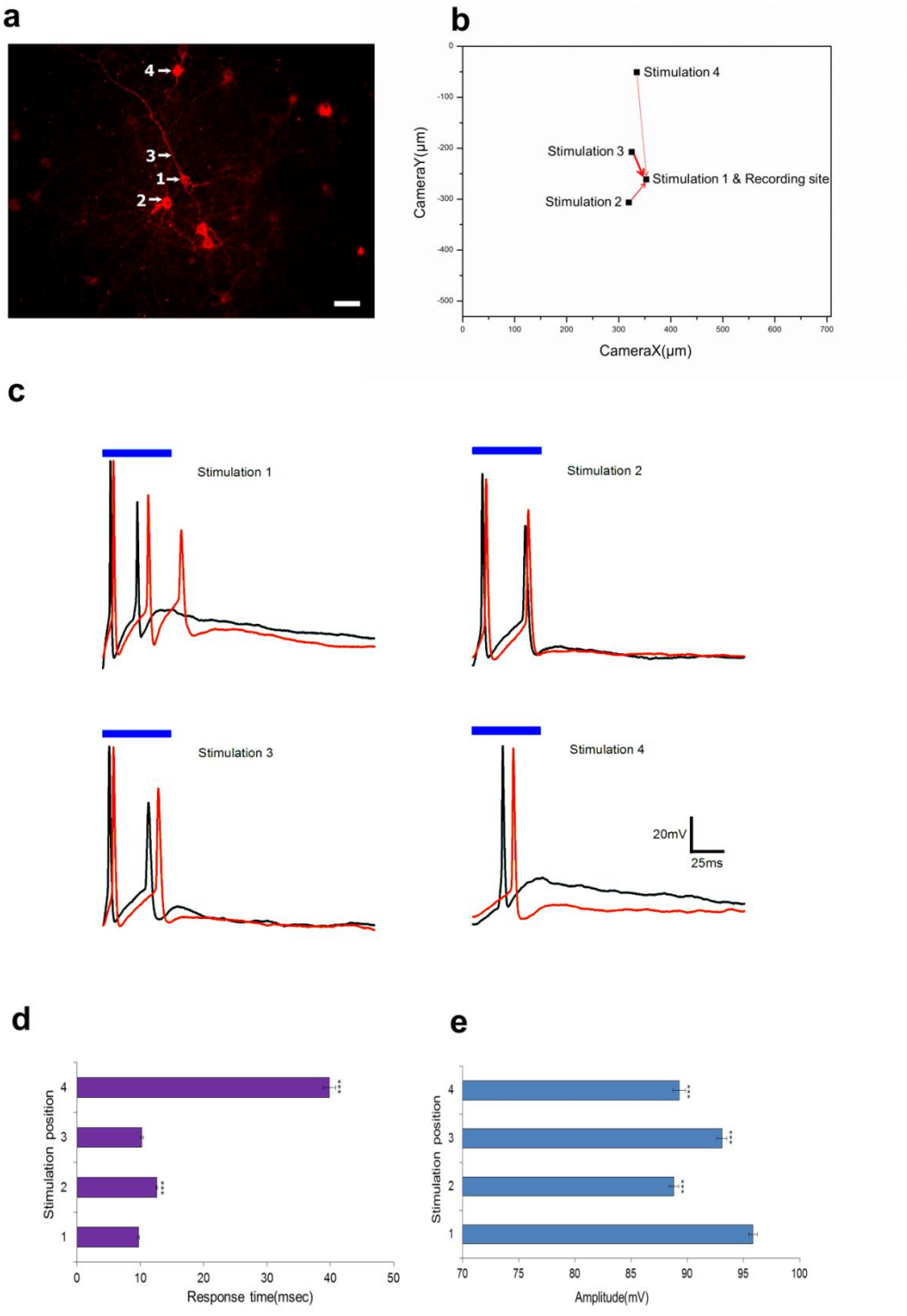

Figure 3.2-1 Mapping of cortical microcircuit with ChR2opt

a) Image of CMV-ChR2opt-mKate fluorescence in primary cortical neurons (scale bar 50 µm). 50k cortical neurons on one PDL coated coverslip were transduced with 10µl rAAV6-CMV-ChR2opt ($4.97*10^7$ viral particles per µl) on DIV7, which achieved a MOI of $9.94*10^3$ viral

genomes per cell. These cells were measured on DIV17. Numbered sites (white digits) indicate locations where four small laser spots were positioned when the responses indicated in c) were driven. b) Map of the cortical microcircuit in neuron network a). Red arrow indicates the connection direction between presynaptic and postsynaptic neurons. c) Light-evoked voltage traces of the postsynaptic neuron from four different small laser spots. The repetitive laser stimulations were applied for only one position to measure the response of the recorded neuron in this small neural network. Each recoding repeated 100 times, each figure shows the results from the first 2 laser stimulations (Black: the first stimulation; Red: the second stimulation). d) The response time of stimulated action potentials in four different stimulation positions (one-way ANOVA, $p < 0.001$, against the position 1). e) The amplitude of the stimulated action potentials in four different stimulation positions (one-way ANOVA, $p < 0.001$, against the position 1). Data is presented as mean ± SEM.

We probed the characteristics of ChR2opt during sequential and repetitive photostimulations in optogenetic mapping of cortical microcircuit experiments. As depicted in **Figure 3.2-2a**, we recorded the soma of cell-1 with whole cell patch clamp under current clamp mode, while laser light illuminated cell-1 to cell-3, sequentially. This sequence was repeated 34 times in one independent measurement. We defined the response time as the time from light onset to depolarization peak. **Figure 3.2-2c** shows three voltage traces, which had different response times, measured from cell-1 under laser stimulation at three different sites. Analysis showed the 1st stimulus on cell-1 to have a response time of 5.28 msec, which is shorter than other response time under subsequent stimuli on cell-1 (**Figure 3.2-2d**). This means the photocurrent from the 1st stimulus is larger than other ones. We concluded from this data during continuous illumination on cell-1, desensitization of ChR2opt was found in this system. The response time from the stimulated cell-2 to the recorded cell-1 is 40.67 ± 1.98 msec, which is longer than the cell-3 to cell-1 or for direct stimulation on cell-1 (**Figure 3.2-2b**). The response time from the stimulated presynaptic neuron to the postsynaptic neuron means how long the action potentials of the stimulated neuron propagating to its postsynaptic neuron need. These data indicate the action potential of the stimulated cell-2 spent longer time to send to the cell-1 compared with other pairs of the pre-postsynaptic neurons in this case. Optogenetic control of neural network signaling with ChR2opt provides a possible way to investigate the propagation of action potentials in neural networks.

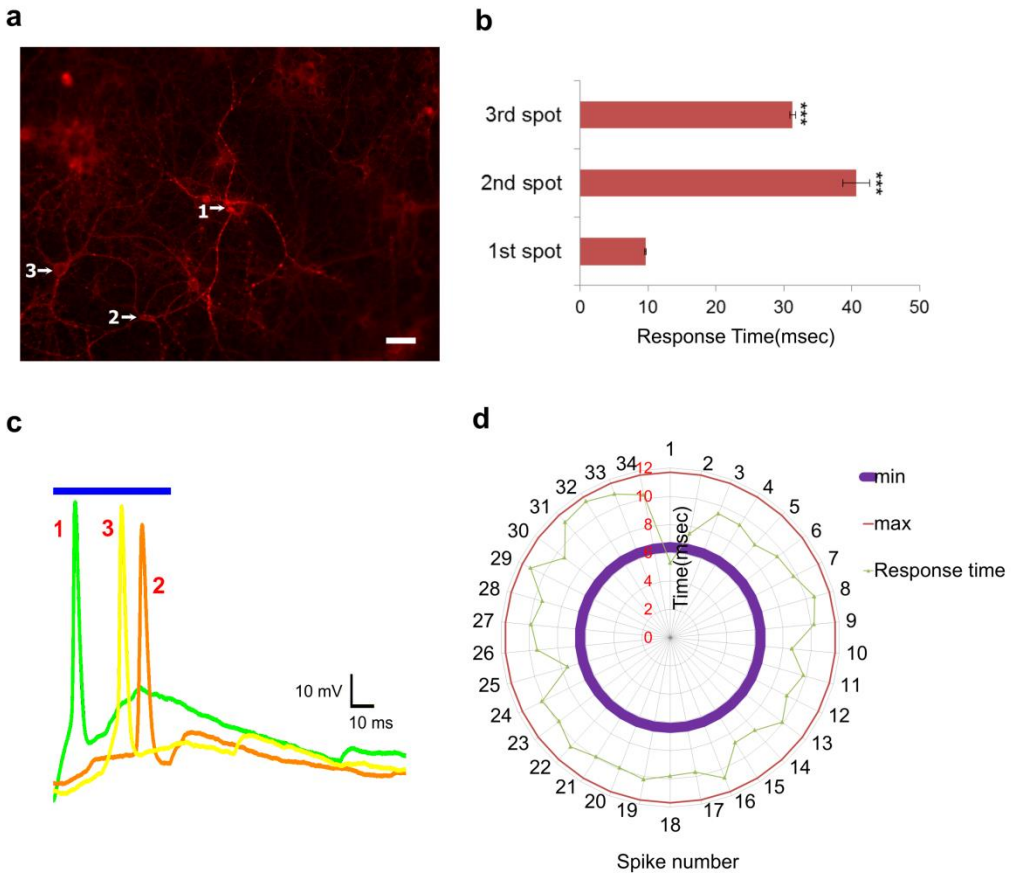

Figure 3.2-2 Desensitisation of ChR2opt by repetitive photostimulation.

The stimulus order is spot 1 (cell-1), spot2 (cell-2), then spot3 (cell-3), pulse 50ms and delay 500ms were applied for each photostimulation. Only cell-1 was recorded with whole cell patch clamp. 50k cortical neurons in one PDL coated coverslip were transduced with 15µl rAAV6-hSyn-ChR2opt ($4.43*10^6$ viral particles per µl) on DIV7, which achieved MOI of $1.329*10^3$ viral genomes per cell. The cells were measured on DIV14. a) Image of hSyn-ChR2opt-mKate fluorescence in primary cortical neurons (scale bar 50 µm). Numbered sites (red arrows) indicate locations where three small laser spots (about 24 µm) were positioned when the responses indicated in c) were elicited. The first spot is located directly on the the patched neuron and spots two and three are located on two different presynaptic neurons' somas. b) The response time of stimulated action potentials in three different stimualtion positions. d) The response time during repetitive photostimulation of cell-1, which was measured by patch clamp. Spike numbers from 1 to 34, mean repetitive photostimulation on cell-1 from 1st to

34^{th} (The interval time between two simulations on cell-1 is 1.65 sec). Data are presented as mean ± SEM.

From this concept that cortical microcircuits can be mapped by optogenetics, we could also study synapse plasticity induced by low-frequency repetitive photostimulation. Only the postsynaptic neuron was measured by whole cell patch clamp, while laser light illuminated the postsynaptic neuron to the presynaptic neuron, sequentially. A laser pulse of 50 msec and a delay time of 1050 msec was applied for the postsynaptic neuron; a laser pulse of 50 msec and a delay time of 500 msec was applied for the presynaptic neuron. Therefore, the interval time between two simulations on the presynaptic neuron or the postsynapstic neuron is 1.65 sec (0.60 Hz). The response time of the first stimulation on the presynaptic neuron is shorter than the response time from other subsequent stimuli on the presynaptic neuron due to subsequent desensitization of ChR2opt that persists for the duration of the experiment (**Figure 3.2-2d** and **Figure 3.2-3**). Also, the response time of the postsynaptic neuron shows subsequent desensitization of ChR2opt (Blue curve in **Figure 3.2-3**). Moreover, as depicted in **Figure 3.2-3a**, the response time under stimulation of the presynaptic neuron increases dramatically following repeated illumination, but the response time directly stimulating the neuron is stable. **Figure 3.2-3** also shows the response time of directly stimulating the postsynaptic neuron is about 10.45 msec, but for stimulation on the presynaptic neuron, response times increase from 27.58 msec to 37.38 msec following repeated illumination. Because the action potential of the directly stimulated neuron is not associated with synaptic transmission, its response time is stable. However, when stimulating the presynaptic neuron, the involvement of the synapse causes the response time dramatically increasing via the mechanism of synapse depressing. These data demonstrate the repeated illuminations on the presynaptic neuron successfully induced synapse depressing. In summary, synapse depressing phenomenon can be induced through the low-frequency repetitive photostimulation by ChR2opt.

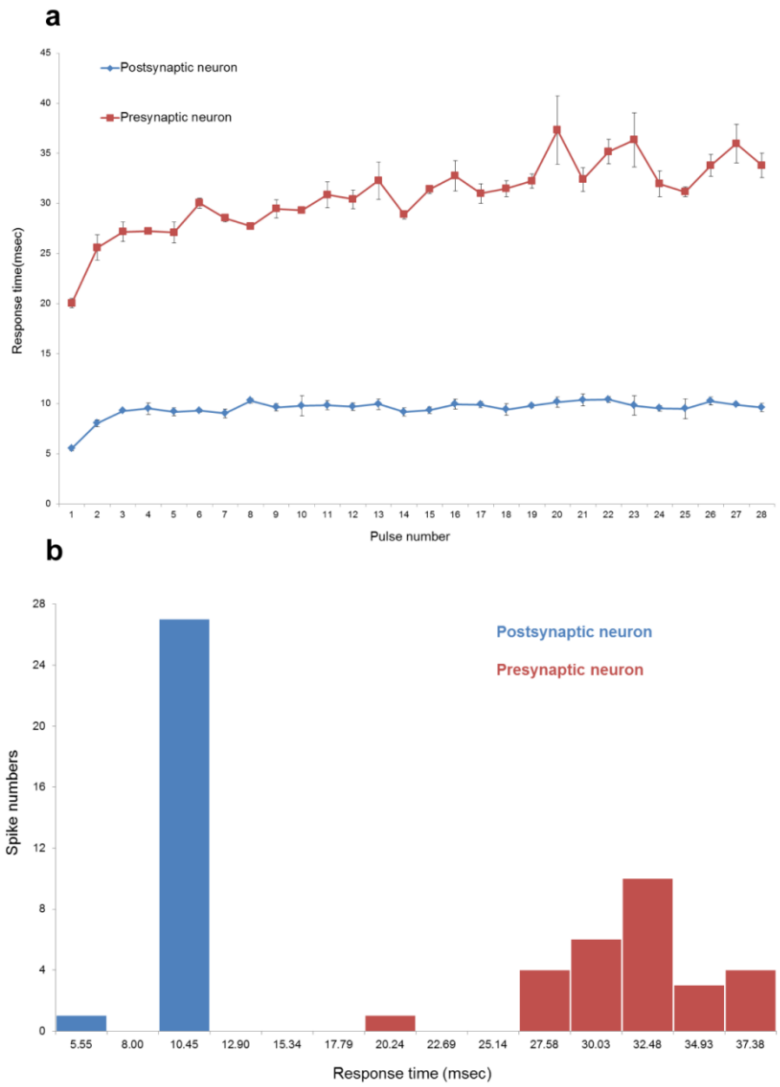

Figure 3.2-3 Delayed synaptic response induced by low-frequency repetitive photostimulation

a) Response time of ChR2opt-expressing neuron under the low-frequency repetitive photostimulation. Only the postsynaptic neuron was measured by whole cell patch clamp, while laser light illuminated the postsynaptic neuron to the presynaptic neuron, sequentially. This sequence was repeated 28 times in one independent measurement, which was repeated three times. A laser pulse of 50 msec and a delay time of 1050 msec was applied for the postsynaptic neuron; a laser pulse of 50 msec and a delay time of 500 msec was applied for the presynaptic neuron. Therefore, the interval time between two simulations on the presynaptic neuron or the postsynapstic neuron is 1.65 sec (0.60 Hz). b) Histogram of spike number vs response time.

Blue color bars represent direct stimulation of the neuron, red color bars for the response time when the presynaptic neuron is stimulated. Data are presented as mean ± SEM.

3.2.2 Mapping microcircuits of X-shape patterned neural network

Microcircuits play a very important role in the communication between brain cells (neurons). However, lot of connections in the native neural network result in the difficulty on decoding these neural circuits. Patterning neural network *in vitro* can be designed a simple one with less connections between neurons, which can dramatically reduce this dilemma. Therefore, I want to validate whether ChR2opt can be employed to study the microcircuit of patterned neurons in a small region.

An X-shape micropattern was used for studying neuronal microcircuits (**Figure 3.2-4A**) since it is a design with multiple connections, but those connections are well defined. In this pattern, 12 µm-diameter nodes were printed for the adhesion of neuronal somas, and were interconnected with eight nodes via 4 µm-wide lines. The distance was 200 µm between vertically or horizontally connected nodes or 283 µm between two neighboring nodes along a diagonal. After micro-contacting printing with PLL-FITC on coverslips (Ref. **2.5)**, clear green fluorescence of FITC can be detected and formed X-shape as we designed (**Figure 3.2-4B**). PLL supports neurons to adhere on the surface of coverslips.These data enables that the adhesion of neurons would form the X-shape. Then, rat primary cortical neurons were seeded into these coverslips. At DIV3, rAAV6 harboring a construct with the hSyn promoter to promote expression of ChR2opt was transduced into these patterned neurons. After 7 days, patterned neurons showed very strong mKate fluorescence (**Figure 3.2-5A**, **Figure 3.2-6A** and **Fig. S 2A**) by a fluorescence microscopy. mKate was tagged the C-terminal of ChR2opt. These images of mKate fluorescence indicate ChR2opt expressed very well in patterned neural network at DIV10, which enables that controlling their activity and mapping microcircuits with optical is possible.

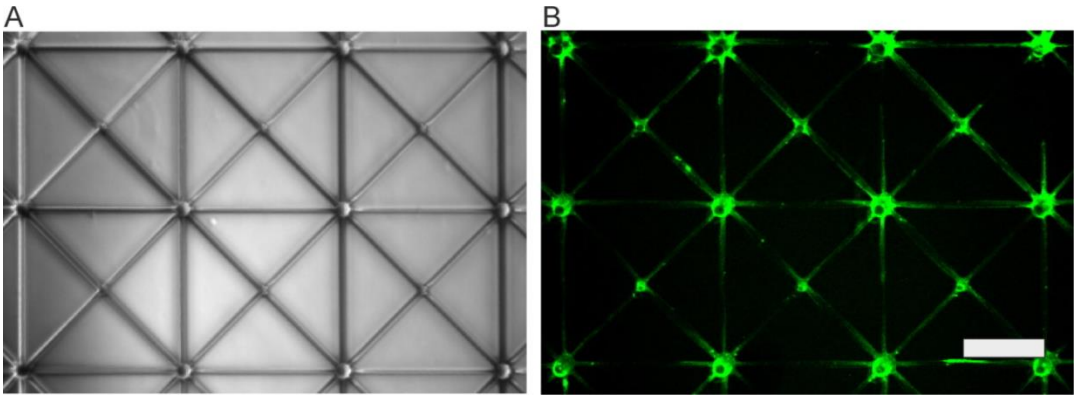

Figure 3.2-4 The design of X-shape pattern

A) DIC micrograph of a stamp shows the shape of the pattern that will guide the neurons. The grid pattern was designed in order to guide neurons to grow into a network with defined connections. 12 µm-diameter nodes were printed for the adhesion of neuronal somas, and were interconnected with eight nodes via 4 µm-wide lines. The distance was 200 µm between vertically or horizontally connected nodes or 283 µm between two neighboring nodes along a diagonal. B) PLL-FITC fluorescence graph shows that PLL was transferred to glass coverslips with the fine structures of the stamp. The black spots in the nodes indicate the FITC fluorescence is weaker than the edge of nodes. The scale bar represents 100 µm.

Subsequently, in order to confirm the function of ChR2opt in patterned neurons, patch clamp was employed to measure single neuron activity of patterned neurons during optical stimulation of the network. In **Figure 3.2-5A**, **Figure 3.2-6A** and **Fig. S 2A**, the schematic pipette indicates the point where patch clamp was used to measure neural activity. Using 473 nm laser light, this single neuron was stimulated at the soma position where it was patched. The laser spot diameter was adjusted to about 24 µm, resulting in a laser intensity of approximately 1.74 W/mm^2. The membrane potential of the recorded neuron was measured in current clamp mode with current injection of -59 pA. Action potentials (**Figure 3.2-5B**) and current (**Figure 3.2-5C**) were successfully elicited by 473 nm laser illumination. Some smaller depolarizations or the second action potentials were detected in this neuron (**Figure 3.2-5B**), which indicate action potential evoked by light may propagate through the patterned network back to the patched neuron. However, the amplitude of action potentials in response to repeated pulses of 50 milliseconds light stimulation at 1.8 Hz gradually decreased (**Figure 3.2-5D**) and the membrane potential depolarized by about 21 mV after these stimulations, which demonstrated maybe this patterned neuron at DIV10 was easy to arrive at depolarization block state (Ref. **4.1.1**). I had measured 10 patterned neurons growing on the X-shape pattern and found this

phenomenon was common among these patterned neurons. I also analyzed the current during repeated light stimulation and found the current from the first pulse was higher than currents from subsequent pulses. These data demonstrated that the desensitization of ChR2opt existed in these patterned neurons, which was consistent with what **Figure 3.2-2d** described in the subsection 3.2.1. In summary, using optogenetic methods to map microcircuits of patterned neurons is possible but suited for a few pulses. Analyzing the first pulse would be the best way to achieve this goal.

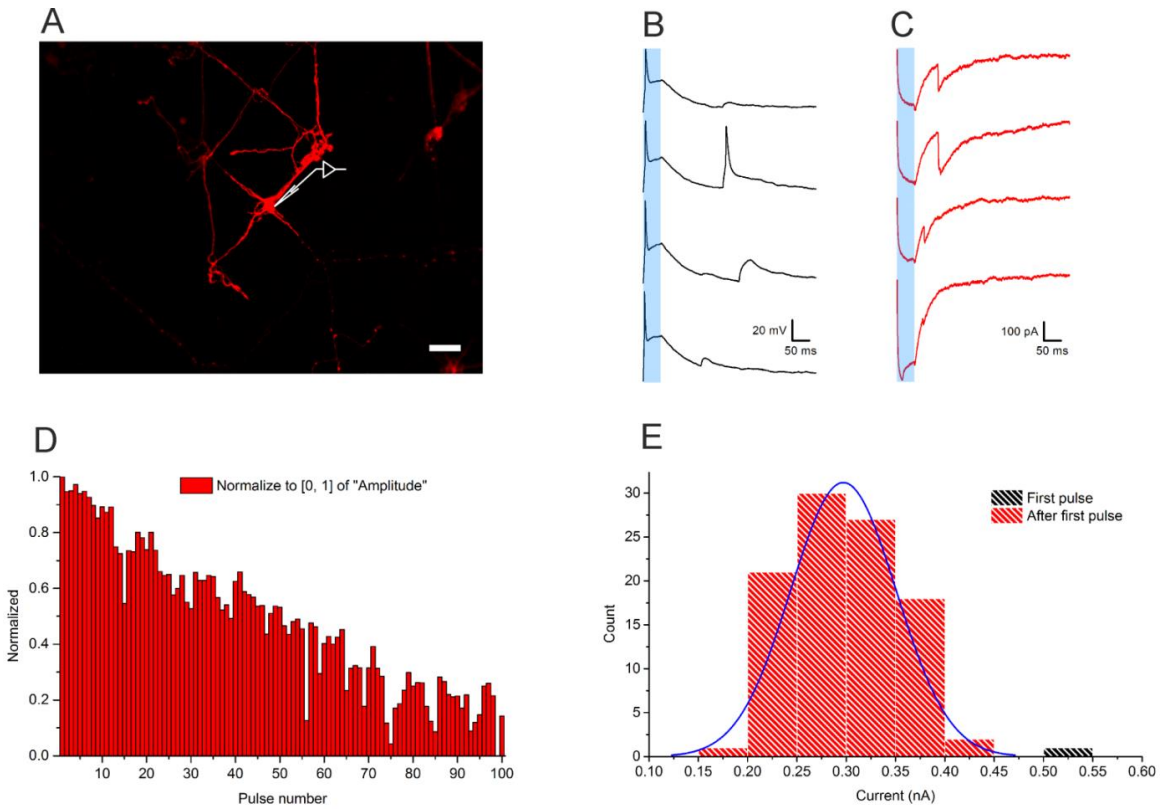

Figure 3.2-5 Optogenetic manipulation in a single patterned neuron

A) mKate fluorescence of a typical patterned neuron (DIV10, DPT7) was very strong on the X-shaped grid pattern. The patterned neurons were transduced with AAV6-hSyn-ChRopt-mKate at DIV3. White pipette indicates the patch clamp to measure neural activity. Scale bar represents 50 µm. B) Voltage traces of the 1st, 2nd, 13th and 28th laser pulses (from bottom to top) show evoked action potentials by a 50 milliseconds pulse (blue bar) of blue laser. Moreover, the smaller depolarization could be seen after the first action potential. The laser spot diameter was adjusted to about 24 µm, resulting in a laser intensity of approximately 1.74 W/mm^2. The membrane potential of the recorded neuron was measured in current clamp mode with current injection of -59 pA. C) Current traces of the 1st, 17th, 27th and 42nd laser pulses (from bottom to top) show photo-activated currents in patterned neuron by

blue light illumination. Holding potential is – 70 mV. D) Normalized amplitude of action potentials evoked by 100 sequential light stimulations. A 50 msec light pulse with followed by a delay time of 500 msec was applied to evoke action potentials. The amplitude of the first spike was set as the standard for normalization. E) The distribution of current evoked by light is normally distributed (Blue curve), except for one of the first stimulation. The current at first stimulation was 0.53 nA.

Having validated the function of ChR2opt in X-shape patterned neurons, I studied whether mapping microcircuits of the small pattered neural network is feasible by optogenetics. Both **Figure 3.2-6A** and **Fig. S 2** show two small pattered neural networks that were selected to map their microcircuits. Strong mKate fluorescence can be detected in these network (**Figure 3.2-6A** and **B**), indicating ChR2opt expressed very well in these patterned networks. It enables the role of ChR2opt on evoking action potentials. **Figure 3.2-6A** shows that five positions were selected to stimulate using laser light. Each marked number indicates the soma of a different stimulated neuron - only the soma of neuron 1 was measured with patch clamp, but it has connections with the other neurons. If the patched neuron can receive electrical signals from other distant stimulated neurons, the response can be measured on the patched neuron numbered 1 (see: **Figure 3.2-6A**). As depicted in **Figure 3.2-6C**, current traces show the signals of the patched neuron in response to laser stimuli at five different positions. Stimulation at the different positions delivers different amounts of charge transfer into the patched neuron (**Figure 3.2-6D**). Action potentials of the patched neuron can be elicited when 473 nm laser light stimulated the neuron 1, other distant neuron 2 and 3 (**Figure 3.2-6E**). When light stimulated position 4 and 5, charge transferred into the recorded neuron was not enough to fire one action potential (**Figure 3.2-6D** and **Figure 3.2-6E**). In general, when blue laser directly stimulates the soma of neuron, how much charge transferred into itself is associated with the amounts of ChR2opt; when light illuminates the soma of other distant neurons that connect the recorded neuron, charge transferred into the recorded neuron involves in neurotransmitters release via synapses, which induced by light-activated action potentials of the stimulated neurons. These data indicate between the patched neuron 1 and other distant neuron 2 or 3 have enough connections.

Moreover, the mKate fluorescence image and its statistic at positions (**Figure 3.2-6A** and **B**) show the amount of ChR2opt at neuron 4 was higher than neuron 3. Also, the neuron 5 at the inside of laser spot has higher fluorescence than the position 1 in **Fig. S 2** that can evoke action potential to send to the patched neuron. The mKate levels should positively correlate with the ability to depolarize a neuron above its threshold. These two neurons are expected to be able to activate the patched neuron since they show brighter

fluorescence than other positions that could trigger electrical activity. However, the patched neuron 1 did not generate the action potentials when laser stimulated at neuron 4 or neuron 5. Their currents recorded by patch clamp maybe come from a little bit of the excited ChR2opt expressing at the end of neurites of the patched neuron 1 that located at the inside of the laser spot 4 or 5. Therefore, these data suggests that neurons 4 and 5 could not send enough electrical signals to the patched neuron for activating its activity.

Subsequently, mapping microcircuit of this patterned network was done in **Figure 3.2-6G**, where indicates whether the studied neurons communicate with the neuron 1 using two colors. Combining with mKate fluorescence (**Figure 3.2-6F**), the map with full information was drawn in **Figure 3.2-6H**. These data shows the neuron 2 and 3 could communicate with the patched neuron but the neuron 4 and 5 not. In summary, mapping microcircuits of a small pattered neural network is feasible by stimulating ChR2opt that expressed very well in the patterned network.

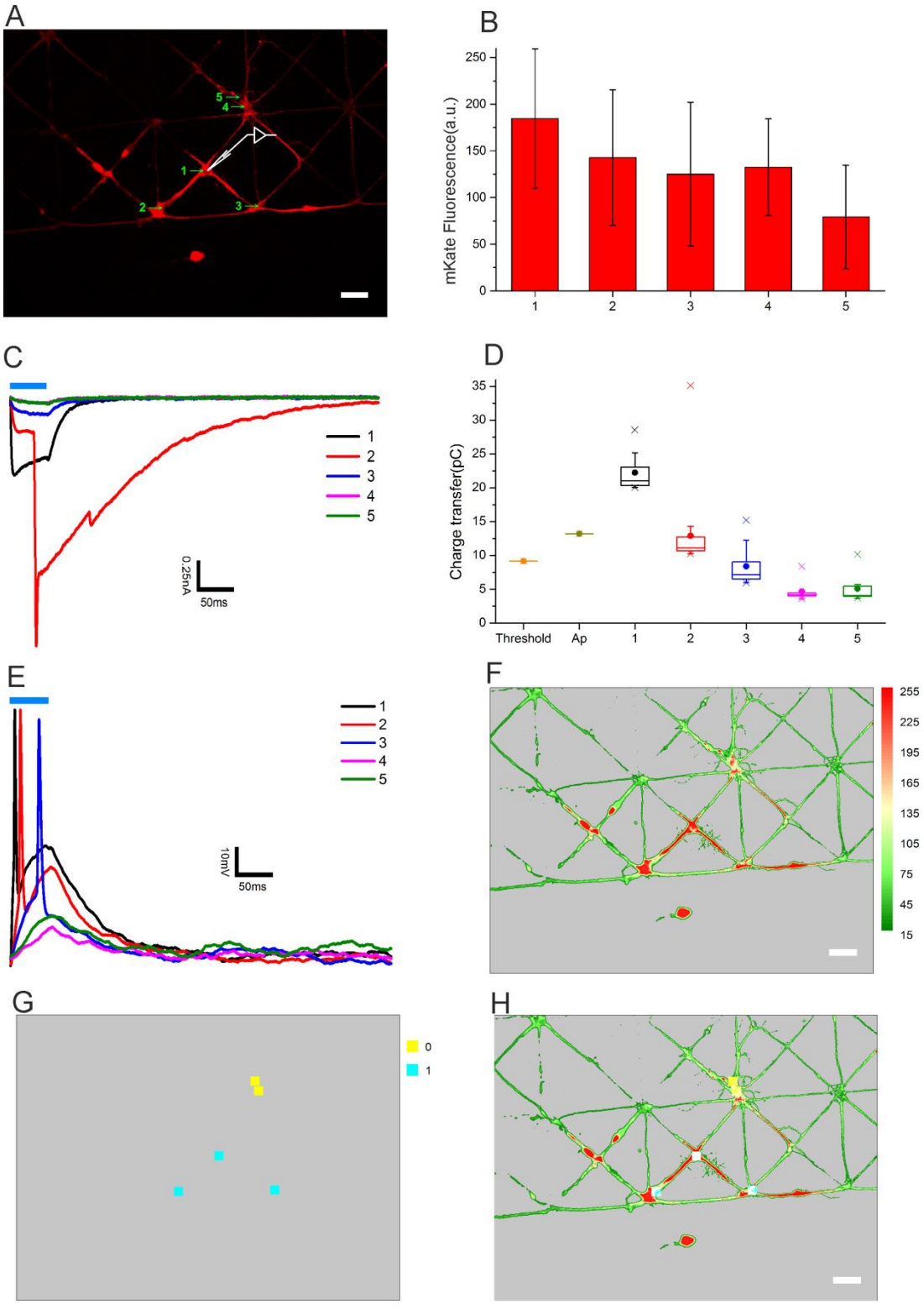

Figure 3.2-6 Mapping microcircuit of a small patterned neural network

A) A typical patterned neural network with X-shape shows strong mKate fluorescence. The numbered sites were sites stimulated with blue laser. The laser spot was about 24 µm diameter, resulting in a laser intensity of approximately 1.74

W/mm^2. Patch clamp was employed to measure neural activity at the neuron 1, where is marked white pipette. Scale bar represents 50 µm. B) The average intensity of mKate fluorescence located at the inside of these numbered laser spots is shown. Data (n= 2200 pixels) are presented as mean (per pixel) ± SEM (blue dash). C) Current traces show photo-activated currents in the patterned neural network. Holding potential is - 70 mV. D) Comparison of charge transferred to the neuron 1 when stimulating at different positions. Data were calculated by integration. When blue stimulate the soma of patched neuron the photocurrent of ChR2pt is too large to fire sodium current at holding potential at – 70 mV. E) Voltage traces show evoked action potentials by a 50 milliseconds pulse (blue bar) of blue laser at 5 sites. F) The map of mKate fluorescence in the studied neural network was drawn. The right side of this figure is the scale of fluorescent intensity in a.u.. White bar at the right bottom represents 50 µm. G) The evoked action potentials of the patched neuron were applied to map microcircuits. Yellow indicates no evoked action potential; cyan indicates the elicited action potential by light. H) The microcircuit of one patterned neural network was mapped combing figure F and G. The neuron 1 is assumed as a postsynaptic neuron. This microcircuit focuses on the connectivity of the neuron 1 with other distant neurons.

3.2.3 Single-cell optogenetic control of neuronal activity

Using the X-shape pattern, it is difficult to control neural activity on single-cell level since one node of X-shape pattern has 8 connections with other nodes (see: **Figure 3.2-4**). I explored the possibility of whether a branch pattern (pattern courtesy of Dr. Liping Du) can be used to characterize the optical method on a single-cell level. The branch patterns are designed to guide neuronal growth as shown in **Figure 3.2-7**. These two kinds of branch patterns consist of one 20 µm-diameter node in the middle for for the adhesion of neuronal somas, one 160 µm-long straight line, and two other symmetrical trajectories. All lines are 2 µm-wide. In these patterns, trajectories in the each direction consist of seven 30 µm minor branches. The angles between each two subtree are 120° (**Figure 3.2-7A**) and 60° (**Figure 3.2-7B**).

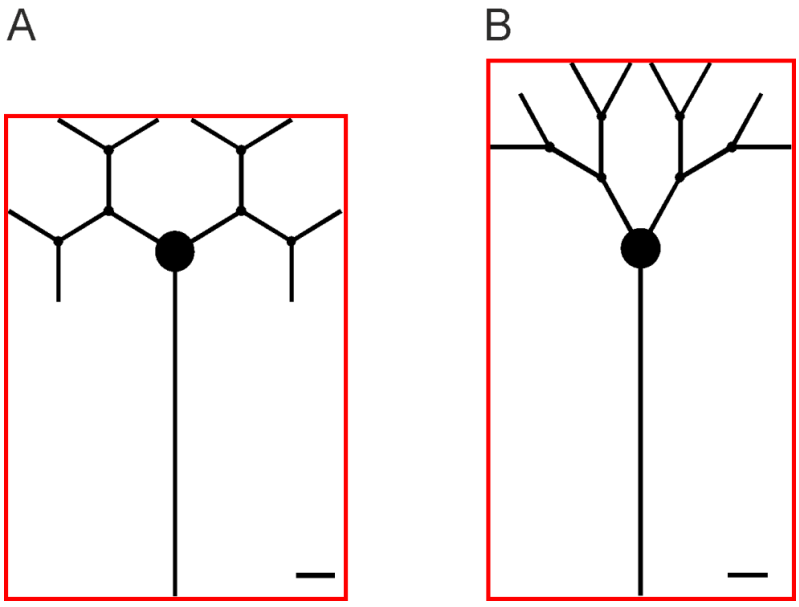

Figure 3.2-7 The schematic of two branch patterns

These two branch patterns consist of one 20 µm-diameter node in the middle for for the adhesion of neuronal somas, one 160 µm-long straight line, and two other symmetrical trajectories. All lines are 2 µm-wide. In these patterns, trajectories in the each direction consist of seven 30 µm minor branches. The angles between each two subtree are 120° (A) and 60° (B). The scale bar represents 20 µm.

First, before printing on the coverslips, the stamps were incubated by 10 µg/mL PLL-FITC and 20 µg/mL Laminin. Then, primary rat cortical neurons were seeded on these coverslips with well-defined structure of the branch pattern. At DIV3, a rAAV6 construct harboring the hSyn promoter was transduced into these neurons. After six days (DIV9) to allow ChR2opt to express enough for optogenetic experiments, very clear mKate fluorescence can be measured with fluorescence microscopy (**Figure 3.2-8B**). This enables ChR2opt under laser stimulation wound allow more ions to depolarize the membrane potential. Next, blue laser and patch clamp were used to stimulate and measure, respectively, single neural activity. As depicted in **Figure 3.2-8A**, the marked numbers indicate the sequence and position of laser pulses to activate ChR2opt and the pipette was injected into the soma at the position marked number 7 to measure the cell's response to laser. Other laser sites from 1 to 6 were put into the crosses of two branches on opposite sides of the cell. The laser spot diameter was adjusted to about 24 µm, resulting in a laser intensity of approximately 1.74 W/mm^2. At all stimulation sites by light illumination, action potentials can be measured at the soma with whole cell patch clamp

(**Figure 3.2-9**). Moreover, these action potentials can be repeated once to elicit (see: **Figure 3.2-9A**). These data demonstrate it is successful that optogenetic method can control neural activity at single-cell level with branch patterns.

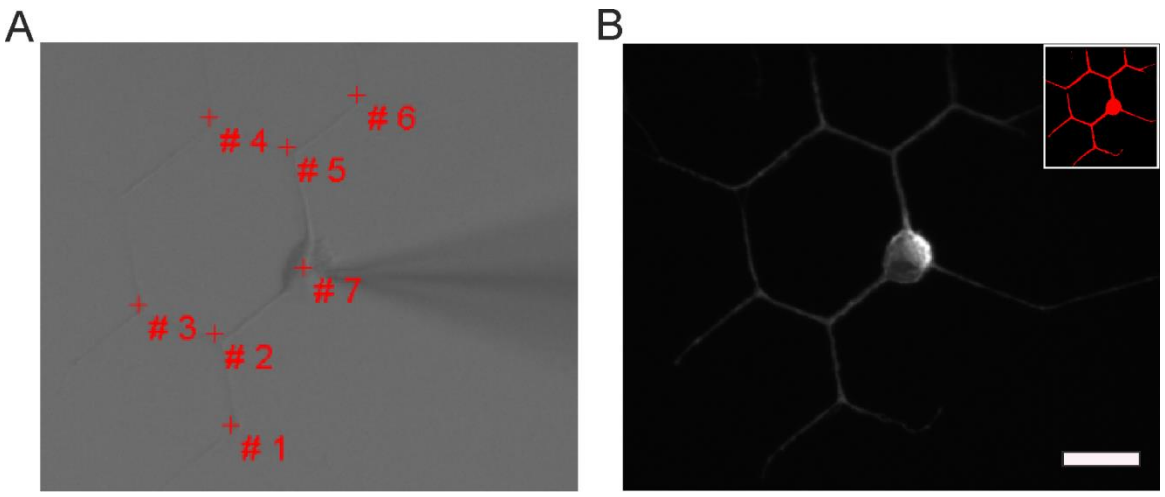

Figure 3.2-8 Images of a single patterned neuron

A) Bright field image of one typical patterned neuron with numbers that indicate the positions of laser stimulation. This neuron was guided with the branch pattern as shown in **Figure 3.2-7A**. The laser spot diameter was adjusted to about 24 µm, resulting in a laser intensity of approximately 1.74 W/mm^2. B) mKate fluorescence image as the patterned neuron in **Figure 3.2-8A**. To present the clearer structure of this patterned neuron, a small image with brighter mKate fluorescence (red) is inserted into the top right. At DIV3, the patterned neurons were transduced with the rAAV6 construct harboring the hSyn promoter to promote expression of ChR2opt. Both images were taken from this neuron at DIV9. Scale bar represents 30 µm.

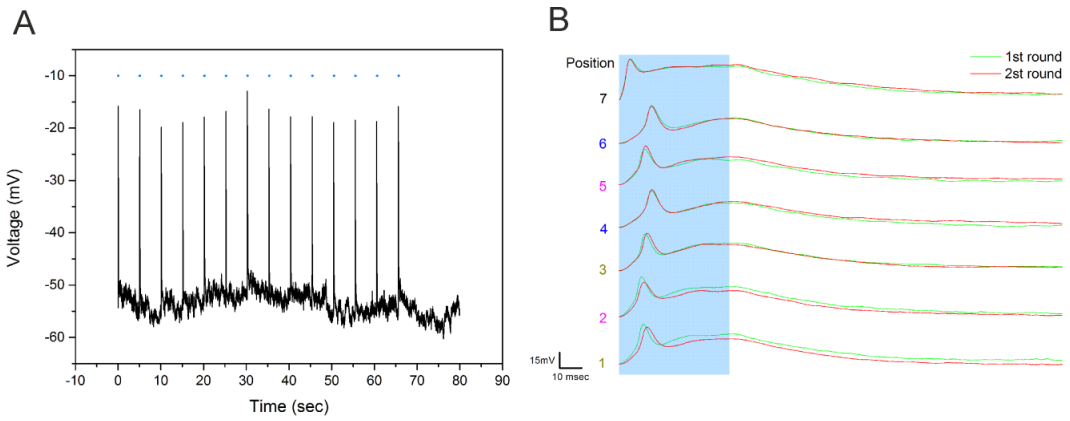

Figure 3.2-9 Action potentials of the single patterned neuron evoked by light

A) The patterned neuron in **Figure 3.2-8** was measured with whole cell patch clamp under laser stimulation. The illuminating sequence of one round is from site 1 to 7, running two rounds without a pause. An action potential was evoked at each stimulus. Blue dot indicates one pulse of 50 milliseconds separated by 5 seconds. B) The magnification of action potentials as shown in **Figure 3.2-9A**. Blue bar indicates blue laser pulse. The shapes of action potentials were grouped what is marked with different colors in position numbers (dark yellow, magenta, blue, black; on the left of this figure).

Having successfully evoked action potentials in the single neuron, I wanted to compare the shape of depolarization by light at different sites that have different distances to the recording site at the soma. The slope indicates how fast the neural membrane potential changed during laser illumination. First, three groups were defined by the distance to the soma from these stimulated sites. Site 1 and 3, Site 4 and 6 were selected as one group, since they have about 60 µm from the soma and include a branching point. In addition, site 2 and 5 were picked up as another group since they have about 30 µm from the soma and do not involve a branch. The typical action potentials of these three groups were depicted in **Figure 3.2-9B** and **Figure 3.2-10A**. The first 4.5 milliseconds of voltage traces were extracted to analyzed the shape of depolarization by 473 nm light (**Figure 3.2-10B**). Most interesting, the slope of depolarization by light is different for these groups (**Figure 3.2-10C**). Compared with the slope of the soma stimulation (site 7), all other three slopes have significant differences (one-way ANOVA, $p < 0.001$). These differences are associated with the amounts of ChR2opt. These data demonstrate this neuron has different amounts of ChR2opt at the inside of these stimulating sites.

In addition, the rise times of these groups (**Figure 3.2-10D**) are different, which demonstrate an action potential propagating from the stimulated site to the recorded soma needs a few milliseconds. In summary, these data indicate the response to laser light at the single-cell level shows different behavior on the shape of depolarization.

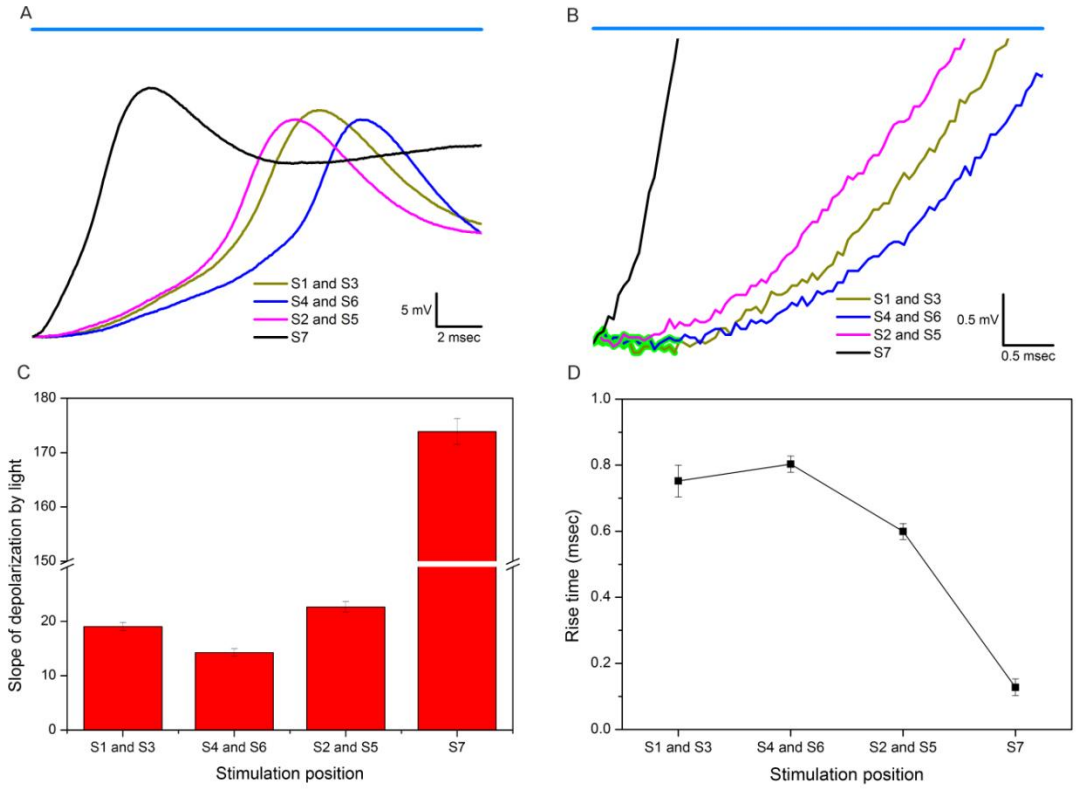

Figure 3.2-10 Comparison of depolarization by light at different sites

A) The typical shape of evoked action potentials in these three groups, plus direct somal stimulation as depicted in **Figure 3.2-9B**. B) The shape of depolarization by light is zoomed in from **Figure 3.2-10A**. Blue bar of both A) and B) indicate blue laser pulse. The traces with green highlighting indicate the stationary state before depolarization by light. C) The slope of depolarization (mV/msec) by light is compared between the three groups and the soma site (S7). D) The rise time of different stimulation sites. The rise time and slope were determined by linear fitting the normalized original trace of depolarization as **Figure 3.2-10B** shows - the total length of time is 4.5 milliseconds from light on. Data (n=4) are presented as mean ± SEM.

Controlling neural network with light is of great interest in neuroscience field. Next, small networks of paired neurons growing on the branched pattern were selected to study neural activity under optogenetic stimulation. In order to measure the responses of the neural network depicted in **Figure 3.2-11A** to light, the soma of neuron where was marked # 11 was selected as the recorded position. 473 nm laser pulses were applied at the marked numbers from #1 to #11, orderly. As depicted in **Figure 3.2-11A** and **Fig. S 3**, strong mKate fluorescence was detected at DIV10 (DPT7) that indicates ChR2opt expressed very well in these neurons, which is the first condition to optically control them.

The membrane potential of the recorded neuron was depolarized at all 11 stimulation sites (**Figure 3.2-11B** and **Figure 3.2-12A**). Also, action potentials and currents generating action potentials could be measured in the small network (**Fig. S 4**).

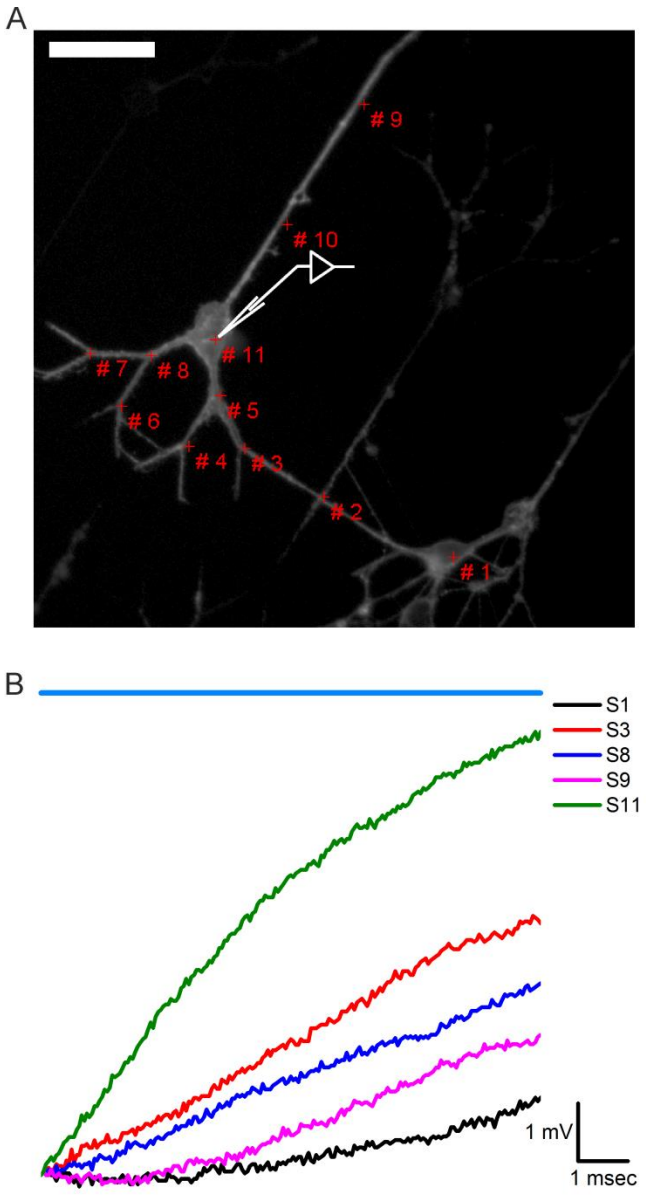

Figure 3.2-11 Optical control a small patterned neural network

A) mKate fluorescence image of a typical branch patterned neural network on DIV10, which was transduced on DIV3 with the rAAV6 construct harboring the hSyn promoter to promote expression of ChR2opt. The marked numbers indicate laser stimulation sites (laser spot is about 24 µm in diameter). The illuminating order of one round is from site #

1 to # 11, running four rounds. The soma of neuron marked # 11 was measured with patch clamp (white pipette). Scale bar represents 51 μm. B) The representative traces of depolarization by laser light (blue bar). The black one indicates the presynaptic neuron marked # 1 that connected with the patched neuron (see: **Figure 3.2-11A**). All measurements were done at holding potentials about -30 mV that indicated this neuron had already entered into the depolarization block state.

Subsequently, the slopes of depolarization by light in the patterned neural network were calculated by linear fitting of the normalized original traces for the first 10 milliseconds. As depicted in **Figure 3.2-12A**, the slopes of light induced depolarization show different patterns. The detailed patterns are below: 1) For the presynaptic neuron at # 1 (synapse group in **Figure 3.2-12A**), its slope is lower than all other regions by light, which indicates the depolarization by directly stimulating at all areas of the recorded neuron itself is faster than depolarization by synaptic transmission from the neighboring neuron. Maybe neurotransmitter release through synapse contributed to this phenomenon. 2) For stimulating neurites of the recorded neuron, their slopes of depolarization by light are at same level except for right branches (site # 3, # 4 and # 5). Most interesting, these slopes of stimulating the right branches are larger than other's slopes. Maybe the reason is that this neurites connect the presynaptic neuron at site # 1, which resulted in the membrane of this branches grew bigger than the left branches(**Figure 3.2-11A**) so that more ChR2opt could be activated. 3) For directly stimulating the soma of the recorded neuron, its slope is the largest since there has lots of ChR2opt that can be activated with laser. The slope indicates how fast the membrane potential of the recorded neuron depolarized by light. The different slopes implied there have different amounts of ChR2opt proteins that can elicit action potential by light.

In addition, as depicted in **Figure 3.2-12B**, the propagating time of the action potential and the average speed were analyzed. The time from light on to the time point that started depolarizing by light is defined as the propagating time. In this case, the propagation time from the presynaptic neuron to the recorded neuron needed about 2 milliseconds (S1 in **Figure 3.2-12B**). For other sites, the times are shorter than 2 milliseconds since these sites are close to the recorded neuron. Moreover, the propagating speed of action potentials is in the range from 65 μm to 205 μm per millisecond. These data demonstrated optical control of the patterned network can be applied to decode the details of how fast the presynaptic neuron communicate

postsynaptic neuron. In short, optical control of neural activity of the patterned network can be successfully achieved with ChR2opt, which would facilitate bioelectronics field.

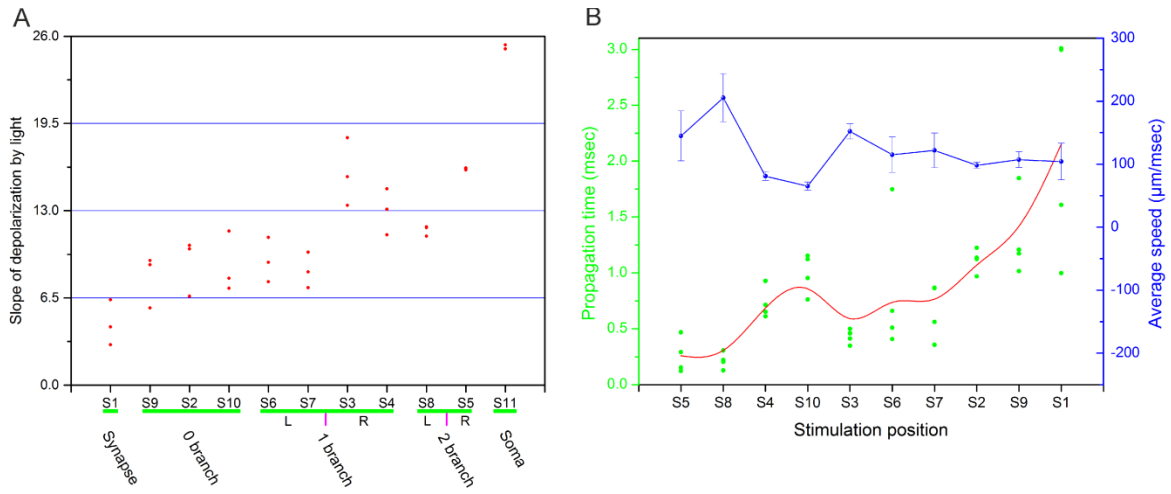

Figure 3.2-12 Comparison of depolarization by light in a small network

A) Comparison of the slope of depolarization (mV/msec) by light at different sites (marked in **Figure 3.2-11A**). Green bar indicates different groups (synapse, 0-2 branch, soma). L and R indicate the left branch and right branch of the recorded neuron depicted in **Figure 3.2-11A**. Blue line indicate four ranges of the slope of depolarization by light. B) Comparison of the propagation time (green dots) and the average speed (blue curve) of evoked action potentials at different stimulation positions. X axis was made in terms of the distance between the stimulated site and the recorded site (S5: nearest; S1: farthest). Red curve indicates the trend of the propagation time. The slopes and propagation times were determined by linear fitting the normalized original traces of depolarization as shown in **Figure 3.2-11B**. Data (n=4 repeated stimuluses) are presented as mean ± SEM.

3.3 Channelrhodopsin-XXL (D156C)

ChR2-XXL (D156C) (Dawydow et al., 2014) can give rise to the largest photocurrents of all ChRs published so far and increases light sensitivity more than 10,000-fold over wild-type ChR2 in *Drosophila* larvae. As a result, it can be opened using diffuse, ambient light to allow the ion influx into neurons and activate them. In this section, the functions of ChR2-XXL in rat primary cortical neuron are presented. The subsection **3.3.1** aims for depolarization block induced ChR2-XXL; the subsection **3.3.2** aims for neurotransmission promoted by ChR2-XXL.

3.3.1 Depolarization block induced by ChR2-XXL (D156C)

To functionally validate the powerful optogenetic tool named Channelrhodopsin-XXL (Dawydow et al., 2014) in primary rat cortical neurons, the DNA of ChR2-XXL (provided by Dr. Shiqiang Gao who is working in Prof. Dr. Georg Nagel's group) was sub-cloned to form psc-hSyn-ChR2-XXL plasmid using restriction digest-based strategies (Ref. **2.1.2**). After psc-hSyn-ChR2-XXL plasmids were delivered into neurons by electrofection (Ref. **2.6.2**), very clear YFP fluorescence (yellow color) was detected on DIV13 (**Figure 3.3-1**) that indicates ChR2-XXL expressed very well in primary rat cortical neurons.

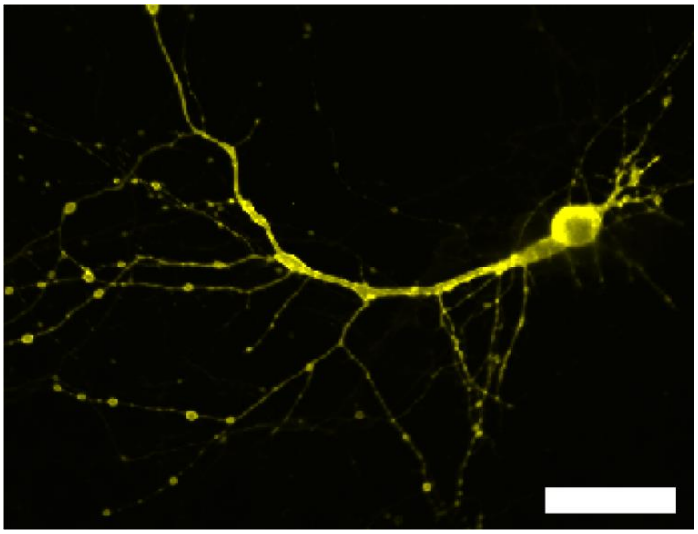

Figure 3.3-1 Expression of ChR2-XXL in primary rat cortical neuron

In this figure, very strong YFP fluorescence (yellow color) was shown in the ChR2-XXL (+) neuron on DIV13. YFP was tagged onto the C-terminal of ChR2-XXL, which was delivered by electroporation before neuron seeding. Scale bar represents 50 µm.

Because ChR2-XXL could generate the largest photocurrents of all ChRs published so far and showed light sensitivity more than 10,000-fold over wild-type ChR2 in *Drosophila* larvae (Dawydow et al., 2014), I had the idea that ChR2-XXL may induce the neuron to go into a depolarization block state under exposure to white light for a few minutes. In order to achieve depolarization block, all neurons were illuminated 10 minutes with white light before any measurement. Then, patch clamp was applied to measure the response after exposure to white light. What's very interesting is that ChR2-XXL positive neurons needed more injected current than control neurons for holding membrane potential at -70 mV

regardless of DIV (**Figure 3.3-2A**).The reason for this should be a change in the resting potential of these ChR2-XXL positive neurons caused by white light. Next, we measured the resting potential using patch clamp without any current injection. Obviously, the resting potential of most of ChR2-XXL positive neurons (red filled circles) was higher than control cells (black filled circles) across different culture days (DIV7 to DIV14) (**Figure 3.3-2B**). From my measurements in primary rat cortical neurons , a depolarization to about -50 mV produces an action potential (see: **Figure 3.3-3B**). Most of ChR2-XXL positive neurons surpassed this threshold. Depolarization block drives the membrane potential over threshold and holds it there. These data indicated depolarization block happened in ChR2-XXL positive neurons.

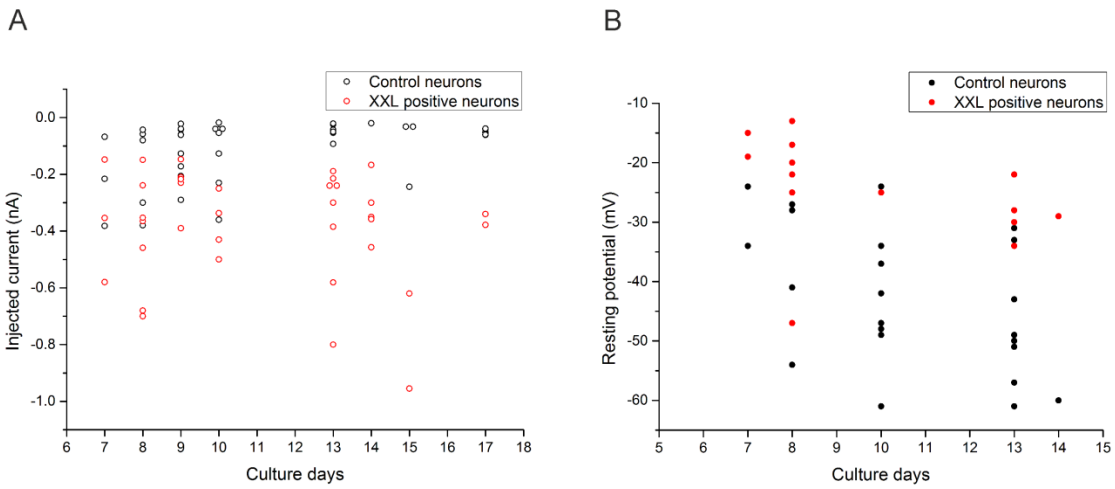

Figure 3.3-2 Current injection needed and resting potential

After 10 minutes exposure to white light, A) ChR2-XXL positive neurons (red unfilled circles) needed more injected currents than control neurons (ChR2-XXL negative neurons, black unfilled circles) to hold the membrane potential at -70 mV on DIV7 to DIV17. B) The resting potential of ChR2-XXL positive neurons (red filled circles) was higher than control cells (ChR2-XXL negative neurons, black filled circles) on DIV7 to DIV14. The resting potentials were measured without any current injection. In A and B, each circle is the average value over 1 second for one neuron.

Depolarization block forces the neuron into a refractory state that cannot conduct action potentials due to the inability of the voltage-gated sodium channels to open in that zone (Sassen and Zimmermann, 1973). Because of this, we designed an approach with voltage clamp to measure how sodium current was changed and confirm whether it could be recovered in ChR2-XXL positive neurons after neurons were blocked. In the approach (**Figure 3.3-3A**), voltage was stepped from -70 mV to -20 mV, and each step increased

by 10 mV and was held for 20 msec. Then a hyperpolarization pulse was applied and the steps repeated. Hyperpolarization was used at different voltages and durations to recover voltage-gated sodium channels (Bendahhou, 2012). **Figure 3.3-3B** shows no inward current was detected both before and after hyperpolarization at -130 mV for 5 secs in a ChR2-XXL positive neuron, whereas the amplitude of voltage-gated inward current is slightly increased after hyperpolarization in a control neuron. These data indicate hyperpolarization can un-block a control neuron, but those particular conditions were not enough for un-blocking the ChR2-XXL expressing neuron. Next, I wanted to change the protocol to make it work in the ChR2-XXL positive neurons with lower potential for hyperpolarization. Finally, at -170 mV or -210 mV for 2 secs, the recovery of current was seen, whereas it still did not appear at -150mV for 2 secs (**Figure 3.3-3C**). Moreover, compared with the hyperpolarization at -170 mV for 2 secs, voltage-gated current is slightly increased after hyperpolarization at -210 mV (**Figure 3.3-3C** blue and red traces), but it is still lower than the voltage-gated current in the control neurons (black trace in **Figure 3.3-3B**). These data indicate depolarization block could be successfully induced using ChR2-XXL and it could be recovered by hyperpolarization to -170 mV or -210 mV for 2 secs.

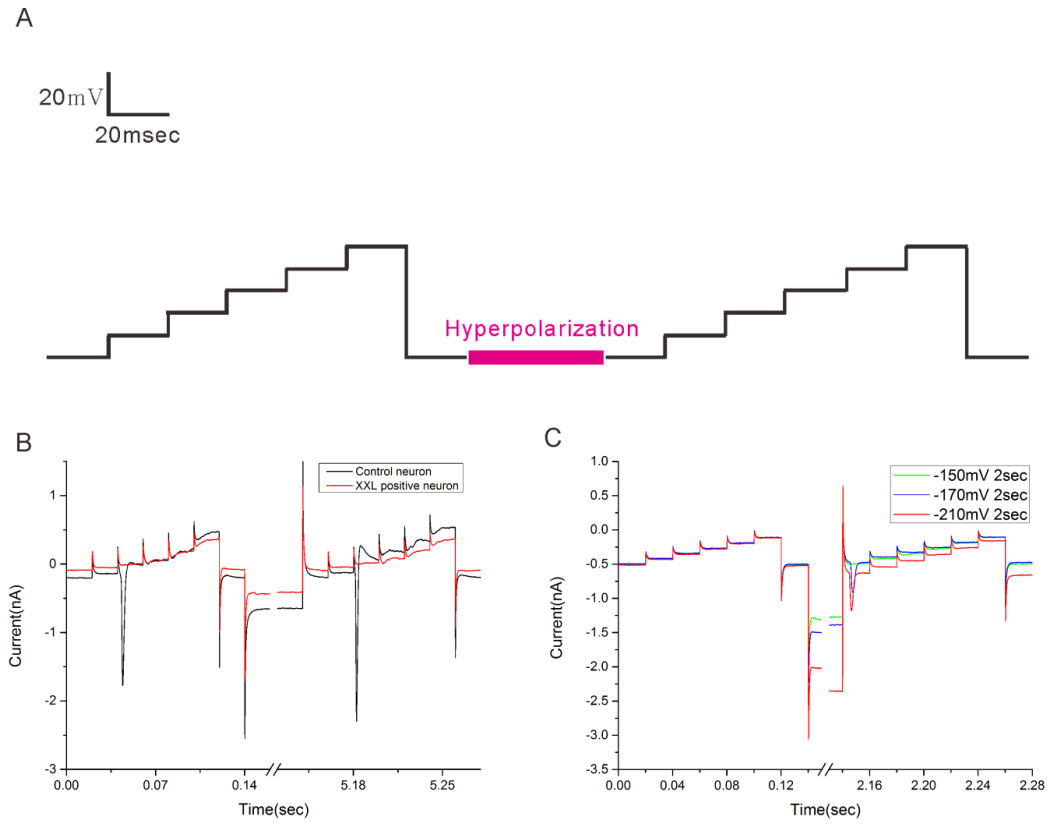

Figure 3.3-3 Recovery from depolarization block through hyperpolarization

A) Schematic of hyperpolarization protocol to recover from depolarization block is depicted. Voltage steps before and after hyperpolarization were applied, where voltage was stepped from -70 mV to -20 mV (each step increases by 10 mV and is held for 20 msec). Hyperpolarization with different voltage and duration was used to recover voltage-gated sodium channels. B) Recovery of ChR2-XXL positive neurons was not achieved by hyperpolarization to -130 mV for 5 secs. A typical current trace of ChR2-XXL positive neurons is shown in red, while one of control neuron (ChR2-XXL negative neuron) is shown in black. C) Recovery of ChR2-XXL positive neurons was successfully achieved by hyperpolarization at two different conditions (Blue color: -170 mV for 2 secs; Red color: -210 mV for 2 secs). Hyperpolarization with -150 mV for 2 secs (green color) still didn't recover voltage-gated sodium channels. Three traces are from the same neuron but different one as depicted in **Figure 3.3-3B**.

Subsequently, I have tested whether the membrane potential could be depolarized in ChR2-XXL positive neurons by laser stimulation after depolarization block. Together with laser stimulus, patch clamp was employed to characterize ChR2-XXL in primary rat cortical neurons (**Figure 3.3-4**). ChR2-XXL-expressing neurons at three different culture days were measured under laser illumination. All representative voltage traces in **Figure 3.3-5** indicate two kinds of patterns. The first pattern shows a declining membrane potential prior to laser stimulation due to exposure to white light when setting up the experiment, which demonstrates ChR2-XXL channels in neurons had opened but gradually closed. This is consistent with ChR2-XXL's long open state and high light sensitivity (Dawydow et al., 2014). The second pattern is that depolarization took place but without action potential after laser light stimulating ChR2-XXL-expressing neurons, which indicates voltage-gated channels still inactivated in neurons. Moreover, compared **Figure 3.3-5B** (1 second laser stimulation) with **Figure 3.3-5C (**30 seconds stimulation), longer laser stimulation does not help the activation of action potentials. These data demonstrated ChR2-XXL can be used to induce stable state of depolarization block.

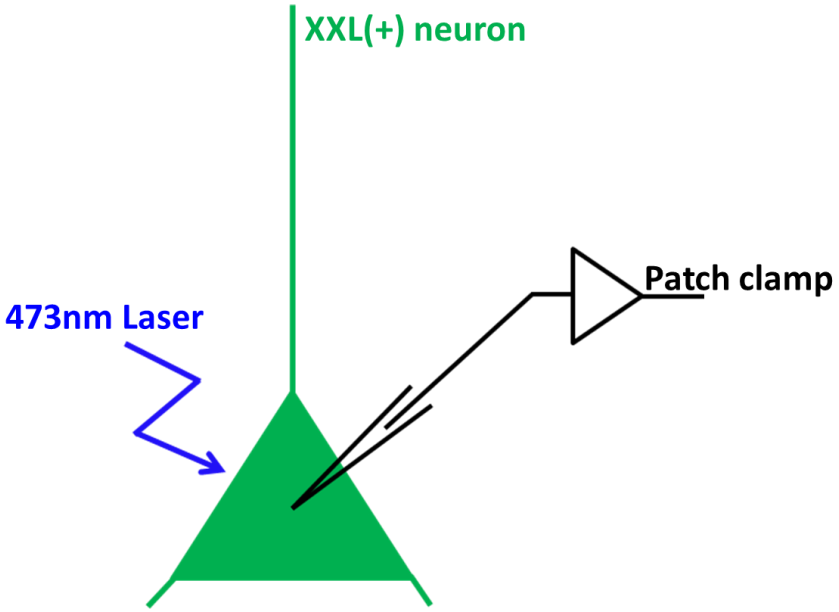

Figure 3.3-4 Schematic of measurement of ChR2-XXL (+) neuron in response to light

Measurement of ChR2-XXL's function in a primary rat cortical neuron was executed by patch clamp and 473nm blue laser stimulation. All neurons were illuminated 10 minutes with while light before any measurement.

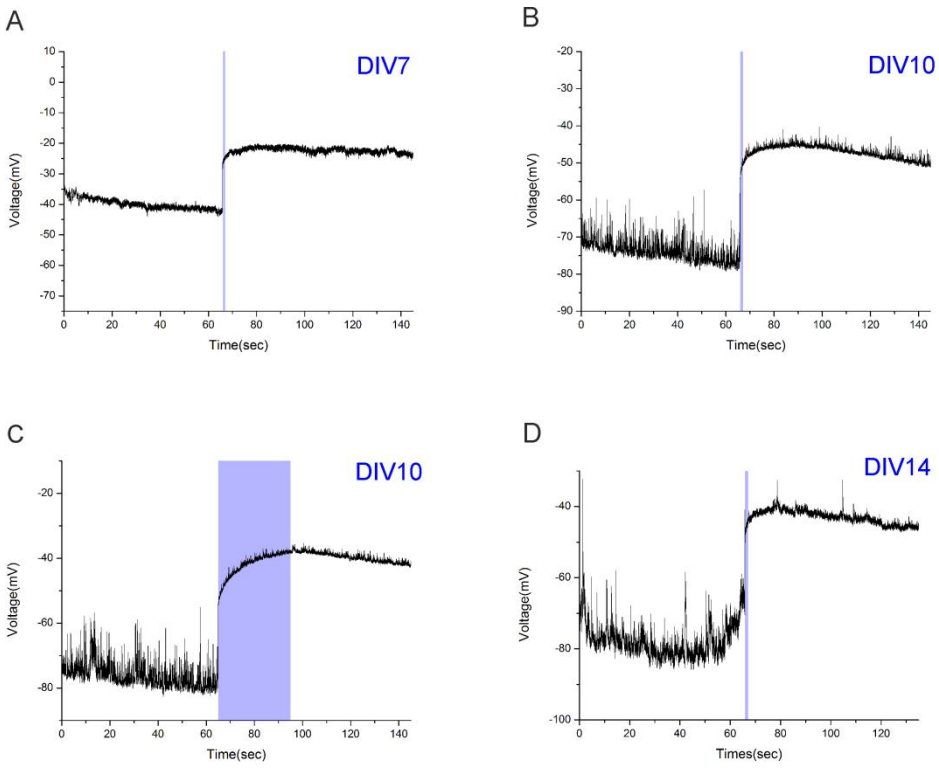

Figure 3.3-5 Representative voltage traces of the ChR2-XXL expressing neurons

After 10 minutes exposure to white light, membrane potentials were measured with current clamp at DIV7 (A, laser stimulation 1 sec, injected current: -16 pA), DIV10 (B: laser stimulation 1 sec, injected current: -190 pA; C: laser stimulation 30 secs, injected current: -170 pA), DIV14 (D: laser stimulation 1 sec, injected current: -173 pA). All neurons in **Figure 3.3-5** can't been induced the action potential in response to laser light.

3.3.2 Neurotransmission induced with ChR2-XXL (D156C)

Having induced depolarization block with ChR2-XXL, I wanted to investigate whether ChR2-XXL can facilitate neurotransmission using blue light illumination. The protocol of this experiment is indicated in **Figure 3.3-6**. A ChR2-XXL-expressing neuron (putative presynaptic neuron) was illuminated with the 473nm laser, while a ChR2-XXL negative neuron (putative postsynaptic neuron) was measured with patch clamp. YFP fluorescence was used as the standard to determinate ChR2-XXL expressing neurons since YFP was tagged to the C-terminal of ChR2-XXL. In this protocol, neurons with YFP fluorescences were selected as the putative presynaptic neurons. In contrast, the ones without fluorescence were identified as the putative postsynaptic neurons. In order to laser illumination with high-fidelity, the distance between the putative presynaptic and postsynaptic neurons is longer than 200 µm but located in the same frame with 20x objective. 473 nm laser light was applied for stimulation with different durations from 1 second to 100 seconds. Each measurement lasted 2 minutes, and the patched-neurons were from different culture days, including DIV8 to DIV17. All measurements were done in dark environment in order to avoid the activation of ChR2-XXL by stray light. The principle of neurotransmission is that neurotransmitter release from the ChR2-XXL positive presynaptic neuron under the stimulus of blue light could elicit excitatory postsynaptic current (EPSC) in the postsynaptic neuron, which can make the postsynaptic neuron surpass its threshold to fire action potentials.

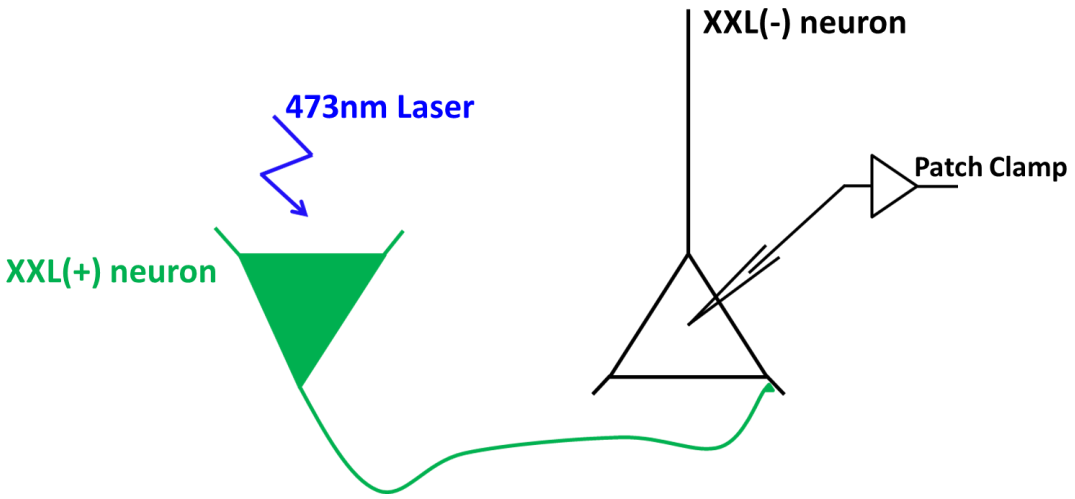

Figure 3.3-6 Schematic of measurement of neurotransmission with patch clamp

Patch clamp was employed to measure the response of the ChR2-XXL negative postsynaptic neuron when the 473nm laser illuminated the presynaptic neuron that expressed ChR2-XXL. ChR2-XXL positive neurons were identified by their yellow fluorescence before selecting neuron pairs.

In the beginning, based on the protocol I designed, neurons without YFP fluorescence were measured by current clamp (**Figure 3.3-7A**) and voltage clamp (**Figure 3.3-7B**) from DIV8 while a laser pulse of 10 seconds was applied to the ChR2-XXL positive neuron. From these data, action potentials and inward currents were successfully evoked on the putative postsynaptic neurons from DIV8 when illuminating the putative postsynaptic neurons (ChR2-XXL positive). Moreover, very interesting is that more action potentials were seen at the postsynaptic neurons from DIV15 (**Figure 3.3-7C**). Spontaneous activity was detected from neurons of DIV15 (**Figure 3.3-7C** and **D**) at before laser stimulation. In one word, older neurons are more excitable than young neurons.

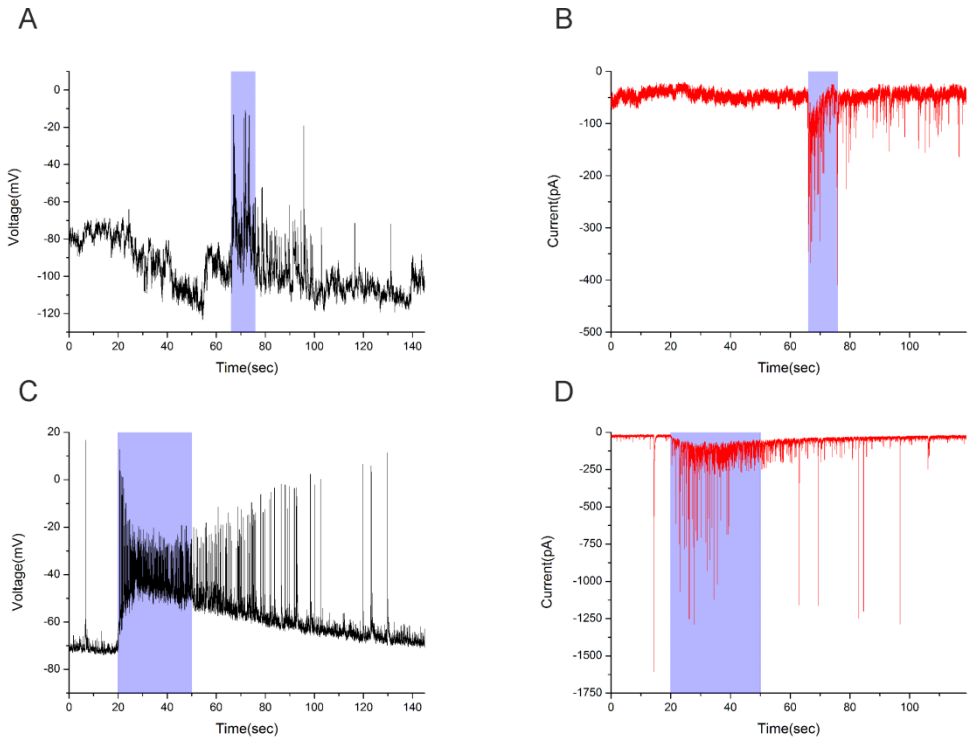

Figure 3.3-7 Representative voltage and current traces at two different culture days

A) Voltage trace shows action potentials of a ChR2-XXL negative neuron (the putative postsynaptic neuron) during laser stimulation at a ChR2-XXL positive neuron (the putative presynaptic neuron) for 10 seconds (Holding current -57.9 pA, for a Vm of -70mV at the start of the experiment.). B) Current trace shows peak currents of a ChR2-XXL negative neuron during laser stimulation at a ChR2-XXL positive neuron for 10 seconds (Holding potential: -70 mV). C) Voltage trace shows burst spiking of ChR2-XXL negative neuron during laser stimulation at ChR2-XXL positive neuron for 30 seconds (Holding current -19 pA, for a Vm of -70mV at the start of the experiment.). D) Current trace shows peak currents during laser stimulation at the presynaptic neuron for 30 seconds (Holding potential: -70 mV). A) and B) are from the same recorded neuron on DIV8; C) and D) are from the same recorded neuron on DIV15. Blue bands indicate the period of laser stimulation.

Next, we wanted to know how the frequency of action potentials in the putative postsynaptic neuron changes while the laser stimulates a ChR2-XXL-expressing presynaptic neuron. The durations of laser light were set 1 second, 10 seconds, 30 seconds, and 60 seconds. In order to hold neurons at about -70 mV before laser

illumination, the amount of current was injected into neurons. Voltage traces from the same neuron are shown in **Figure 3.3-8**. Obviously, action potentials have similar cell behaviors under these conditions. Subsequently, we analyzed the frequency of action potentials elicited by the presynaptic neuron (see: **2.10**). The frequency of action potential shows oscillation behavior (**Figure 3.3-9**). Moreover, the frequency declined after laser stimulation. In summary, the frequency of action potentials of the putative postsynaptic neuron shows oscillation phenomenon while stimulating putative presynaptic neuron by blue laser.

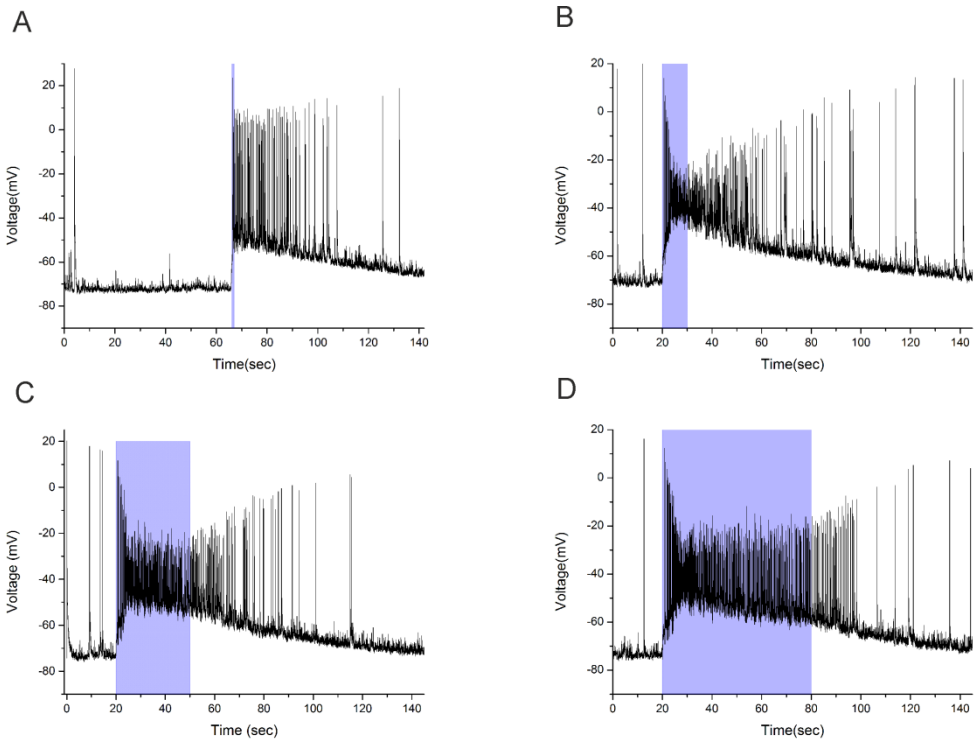

Figure 3.3-8 Spiking associated with neurotransmission from the presynaptic neuron under different durations laser illumination

A) Spontaneous activity of a postsynaptic neuron (DIV15) was measured for 65 seconds before laser illumination of 1 second. Burst spiking was elicited through blue laser stimulation of the presynaptic neuron (Injected current: -27 pA). B) Spontaneous activity of the postsynaptic neuron was measured for 20 seconds. Spiking was achieved through blue laser stimulation on the presynaptic neuron for 10 secs (Injected current: -19 pA). C) Representative voltage trace was shown when stimulating the presynaptic neuron for 30 seconds (Injected current: -19 pA). D) Representative voltage trace as shown when stimulating the presynaptic neuron for 60 seconds (Injected current: -19 pA). These data shows longer

laser stimulation can promote more neurotransmitter release. All traces were measured from the same neuron.

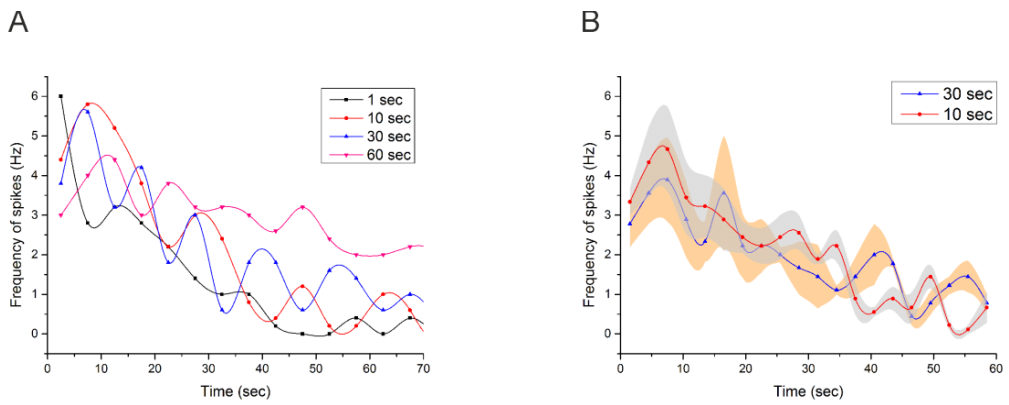

Figure 3.3-9 Frequency oscillation and decreasing in the putative postsynaptic neurons

A) The frequency of action potential of a putative postsynaptic neuron shows oscillation phenomenon but decline, while laser light stimulated a putative presynaptic neuron. The different color curves indicate different durations of laser stimulation. These measurements were from the same cell. B) Three pairs of the putative pre-postsynaptic neurons were measured with the same protocol as A) under laser stimulation of 30 seconds and 10 seconds (Shaded gray indicate s.e.m of red curve, shaded orange indicate s.e.m of blue curve.)

3.4 Photoinhibition of neural activity with *Guillardia theta* ACR 1 (GtACR1)

Natural anion channel rhodopsins (ACRs) provide optogenetic inhibition tools through light-gated chloride conduction with unprecedented light sensitivity and temporal precision (Govorunova et al., 2015). *Guillardia theta* anion channel rhodopsins 1 (GtACR1) is a natural light-gated anion channel. In this section, GtACR1 was employed to inhibit cortical neural activity under blue laser stimulation. In the subsection **3.4.1** and **3.4.2**, the hyperpolarization of cortical neurons could be achieved by GtACR1 and light-gated chloride conduction of GtACR1 was well verified in primary cortical neurons; the subsection **3.4.3** aims for photosuppression of neuronal action potentials including spontaneous activity; the last subsection **3.4.4** focuses on the effects of GtACR1 in primary rat cortical neurons.

3.4.1 Hyperpolarization by GtACR1

To silence neural activity with an optical method, light-gated proton pumps or chloride channels could be used. Here, I employed a very novel light-gated chloride channel to achieve this goal. First, GtACR1 DNA was transfected into primary rat cortical neurons by electrofection (Ref. **2.6.2**) before seeding cells on PDL-coated coverslips. At DIV7, yellow fluorescence was detected in the neurons transfected with GtACR1 (**Figure 3.4-1A**). However, fluorescence was intermittent along the neural membrane including the membrane of axons or dendrites, which was consistent with old neural cells expressing GtACR1 (at DIV16, see: **Figure 3.4-1B**). These data indicate GtACR1 maybe express on the membrane of neurons that provide a very important condition to allow ions influx under laser stimulation.

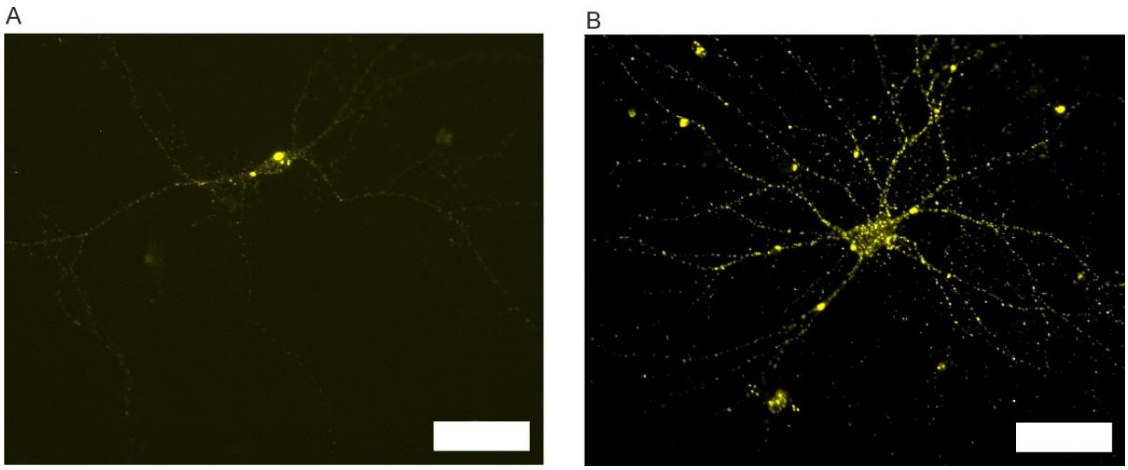

Figure 3.4-1 Expression of GtACR1 in primary rat cortical neurons

A) At DIV7, yellow fluorescence is shown in a typical rat cortical neuron transfected with GtACR1 whose C-terminal was tagged with yellow fluorescence protein (YFP) to detect expression of GtACR1. Scale bar: 50 µm. B) At DIV16, yellow fluorescence is shown in a typical rat cortical neuron transfected with GtACR1. Scale bar: 50 µm.

GtACR1 is a natural light-gated anion channels (Govorunova et al., 2015) (Sineshchekov et al., 2015) (Sineshchekov et al., 2016). Next, the function of GtACR1 was investigated by electrophysiology and light stimulation. The cytoplasmic chloride concentration in most types of cells, including neurons, is low (Bregestovski et al., 2009). Because of this, I have prepared an intracellular solution with low chloride concentration (4 mM) to replace the standard solution (see: **2.8**). Under such conditions, the membrane of cortical neurons was hyperpolarized by blue laser (473 nm) stimulation for 0.25 milliseconds (**Figure 3.4-2A**). The time constants of rise and decay of hyperpolarization were determined by

single exponential fits of the original recorded traces, hyperpolarization was induced by GtACR1 with the mean rise time of 1.23 ± 0.14 milliseconds and the mean decay time of 126.03 ± 19.43 milliseconds (**Figure 3.4-2B**). The rise time is very fast, which is advantageous for silencing the neural activity. The long decay time means the hyperpolarization would be extended more than 100 milliseconds after light is switched off.

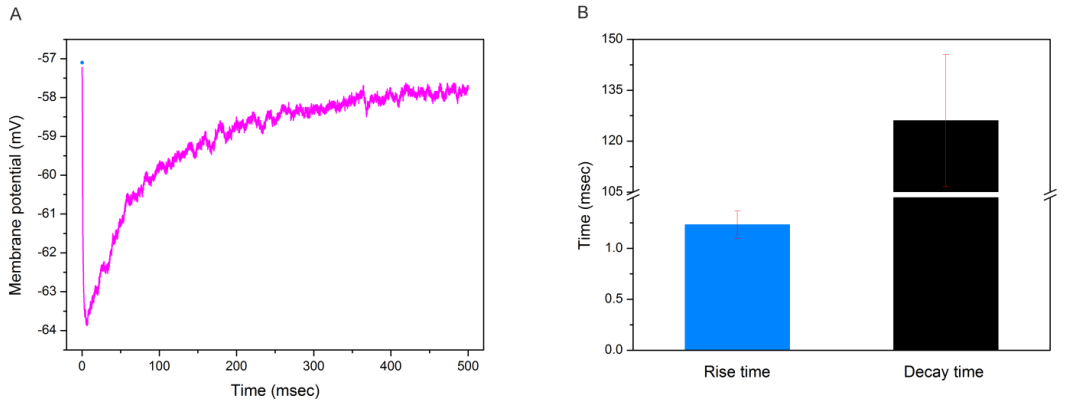

Figure 3.4-2 Hyperpolarization induced by GtACR1

A) Using blue laser stimulation for 0.25 milliseconds (blue dot), hyperpolarization was induced in GtACR1-expressing neurons. No current was injected into neurons when it was measured with whole cell patch clamp. B) Hyperpolarization was induced by GtACR1 with the mean rise time of 1.23 ± 0.14 milliseconds and the mean decay time of 126.03 ± 19.43 milliseconds (n = 5. Error bar: s.e.m.). Blue column indicates the mean rise time of GtACR1, black one indicates its mean decay time. The rise and decay times were determined by single exponential fits of the original recorded traces.

Next, whether GtACR1 can be desensitized following channel opening by blue light was investigated. For this experiments 30 blue light pulses were applied, which each lasted 0.25 milliseconds followed by 4 seconds of light off. A representative outward current trace was depicted in **Figure 3.4-3A**. Moreover, the amplitude of photocurrent evoked by laser pulse is decreasing (**Figure 3.4-3**). At the last pulse, it was declined by around 25%. These data indicate the gating mechanism of GtACR1 involves in a long recovery process.

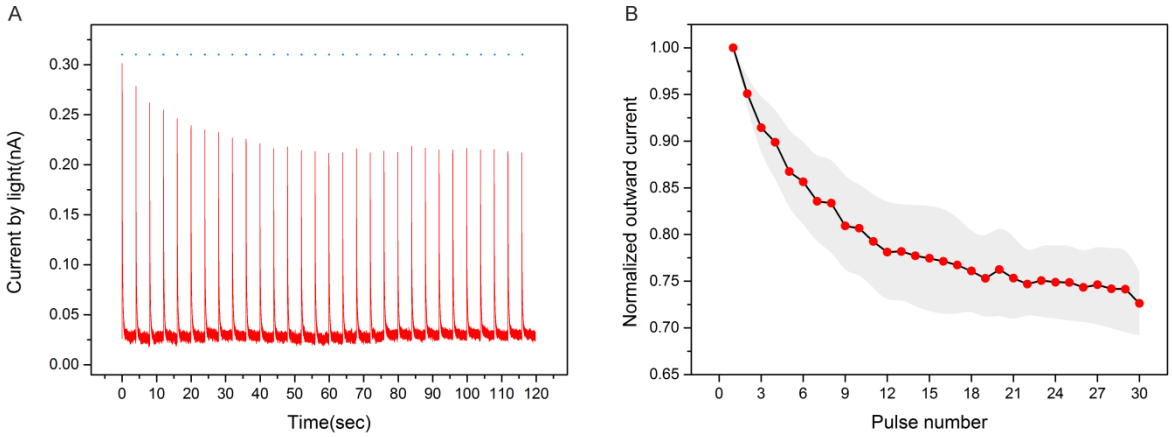

Figure 3.4-3 The desensitization of GtACR1 in neurons

A) A representative outward current trace induced by 30 blue light pulses, which each lasted 0.25 milliseconds followed by 4 seconds of light off. B) Normalized outward current by 30 laser applications. The data are mean values ± SEM (n = 3 cells), gray area indicates SEM. The membrane potential was held at -50 mV while the current were measured under low Cl^- concentration in the pipette and D-AP5 (25 µM), NBQX (10 µM), SR 95531 hydrobromide (20 µM) in the bath. In all light pulses, blue laser intensity was 0.21 W/mm^2.

3.4.2 Light-gated chloride conduction by GtACR1 in cortical neurons

Having determined the time constants of GtACR1, I wanted to depict the current-voltage relationships (IE curves) of GtACR1 in primary rat cortical neurons. Under different holding potentials from - 90 mV to 10 mV, current traces were recorded and representative responses are shown in response to a light pulse of 0.5 seconds in the left of **Figure 3.4-4A**. When switching off the laser, the current decreased a lot under the same holding potentials (right, **Figure 3.4-4A**). The photocurrent of GtACR1 was calculated by subtraction, which the current values of last 50 milliseconds under dark was subtracted from the current values of last 50 milliseconds with light. Moreover, voltage-gated peak current was eliminated by laser illumination (see: **Figure 3.4-4B**). At early stages of neuron growth (DIV6 and DIV8), the IE relationship shows a linear relationship (**Figure 3.4-4C**). However, at the later mature state of neurons (DIV14, DIV17 and DIV20) it doesn't match with linear shape; When voltage is up to -30 mV, the curves of IE relationship show the decline behavior (**Figure 3.4-4C** and **D**). Then, I have investigated whether the synaptic inputs at the mature state result in this decline. D-AP5 (25 µM), NBQX (10 µM) and SR 95531 hydrobromide (20 µM) were applied in the bath solution when the measurements were performed. As depicted in **Fig. S 5**, the later mature state of neurons (DIV14, DIV16 and DIV20) still show the similar behavior as **Figure 3.4-4D**

without blocking neurotransmission. Therefore, the decline behavior is not associated with synaptic inputs in the neuronal network.

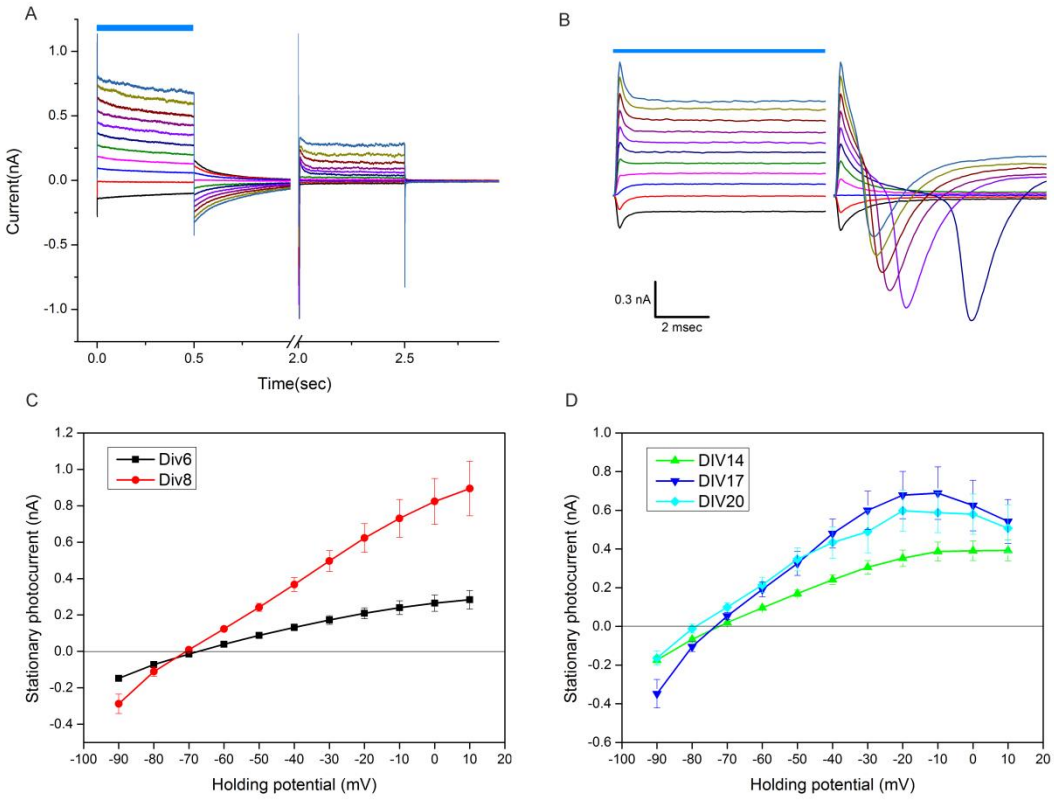

Figure 3.4-4 Light-gated chloride conduction and IE relationship for GtACR1 in primary rat cortical neurons

A) In GtACR1-expressing neurons, representative current traces were shown in response to voltage steps with a light pulse of 0.5 seconds (left, blue bar indicates light pulse) and without light pulse (right). Light intensity was 0.21 W/mm^2. This measurement was done by voltage clamp with voltage steps from – 90 mV to 10 mV; each step increases 10 mV. B) Magnification of current traces from the first 8 milliseconds with and without laser pulse showing voltage-gated current was eliminated by laser illumination. C) IE relationship for GtACR1 in primary rat cortical neurons of both DIV6 and DIV8. D) IE relationship for GtACR1 in primary rat cortical neurons of DIV14, DIV17 and DIV20. The data (mean values ± SEM; n= 3 to 5 neurons) were corrected by subtraction, with current values of the last 50 milliseconds without light was subtracted from current values of last 50 milliseconds with light.

Next, in order to find out the real reason for the decline described above, I wanted to analyze the detailed currents of GtACR1-expressing neurons with light and dark. **Figure 3.4-5B** depicts when the holding potential was up to -30 mV, neurons of DIV17 or 20 showed larger current than other younger neurons. Moreover, these current don't match with linear shape, whereas the ones under light fit well with the linear shape, which contribute to the decline behavior as **Figure 3.4-4D** shows.

In general, the photocurrent value is associated with the amounts of ion channels expressing in neurons. Most interesting, the currents under light (**Figure 3.4-5A**) indicate that neurons at DIV8 show the limitation currents as DIV17 or DIV20. These data imply GtACR1 expression achieved the highest level at DIV8 (I have checked the fluorescence, data not shown), which provide the strongly evidences to determine when is best to transduce with AAV viruses for GtACR1 expression in neurons in future. All data above (**Figure 3.4-4** and **Figure 3.4-5**) demonstrate GtACR1 can produce effective outward currents to inhibit voltage-gated sodium current by 473 nm laser illumination. It would be a powerful optogenetic tool for inhibiting neural activity.

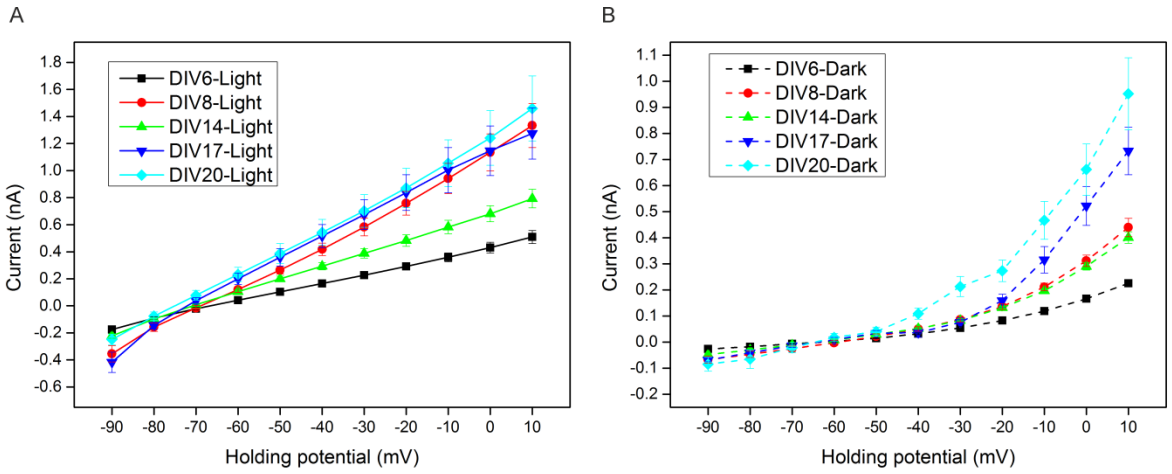

Figure 3.4-5 The current of GtACR1-expressing neurons under light and dark

A) The current of GtACR1-expressing neurons by voltage clamp under blue light. B) The current of GtACR1-expressing neurons by voltage clamp without light. All current were measured at different holding potential from -90 mV to 10 mV. The data indicate mean values of the last 50 milliseconds ± SEM (n= 3 to 5 neurons).

Furthermore, the reversal potential for GtACR1 during neural development (from DIV6 to DIV20) shows two kinds of trends (**Figure 3.4-6**). On the one hand, for younger neurons from DIV6 to DIV8, the reversal potential declined from -66.4 mV ± 3.4 mV to -72.2 mV ± 2.1 mV. Also, up to DIV20, the reversal potential declined to -78.4 mV ± 1.6 mV again. On

the other hand, from DIV8 to DIV17, it was stale around -72 mV. These data imply the chloride concentration in neurons was changing during neural development. Maybe the chloride ion is an important factor to regulate neural development.

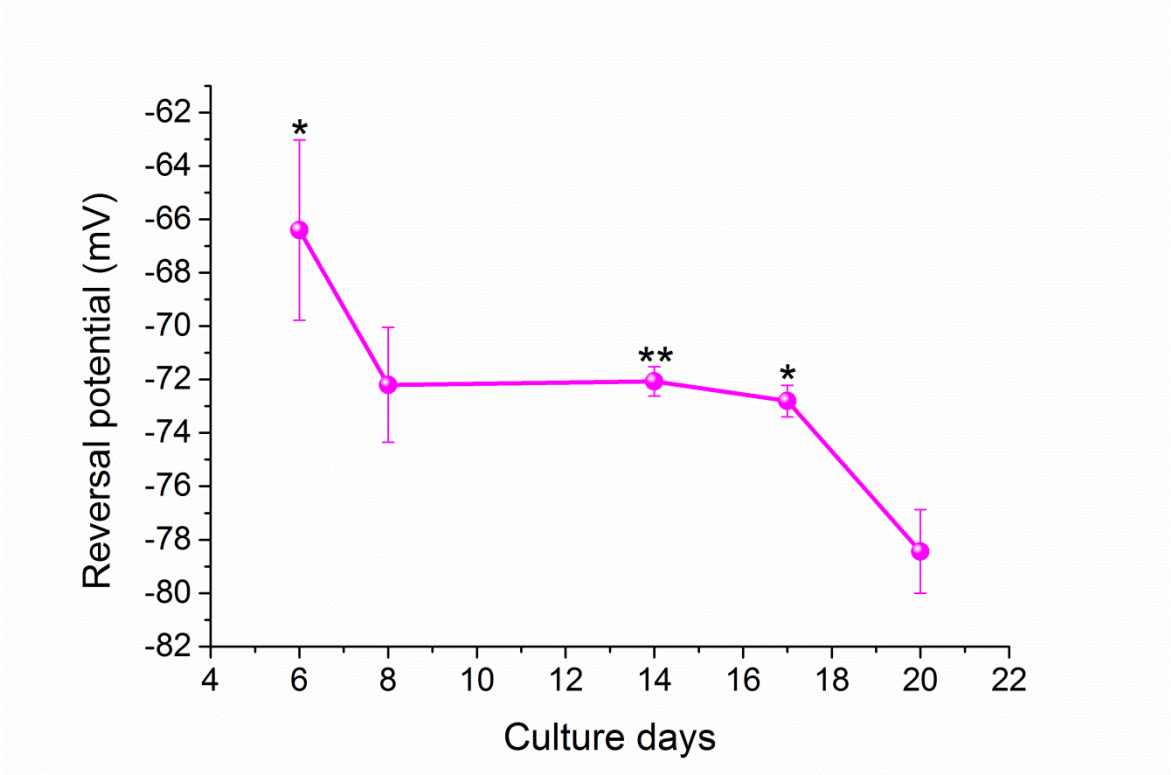

Figure 3.4-6 Reversal potential for GtACR1 during neural development

The reversal potential was defined the point where the stationary photocurrent amplitude was 0 pA. At different culture days, the reversal potentials of GtACR1 (Mean values ± SEM; *n* =3 to 5 cells) were determined by linear fits of the IE relationship curves (**Figure 3.4-4C** and **D**). For younger neurons from DIV6 to DIV8, the reversal potential declined from -66.4 mV ± 3.4 mV to -72.2 mV ± 2.1 mV. However, it was stable from DIV8 to DIV17. From DIV17 up to DIV20, the reversal potential declined again to -78.4 mV ± 1.6 mV. Data were analyzed by one-way ANOVA (* $p < 0.05$ vs. DIV20 group, ** $p < 0.01$ vs. DIV20 group).

3.4.3 Photoinhibition of spiking by GtACR1

Having successfully validated the light-gated chloride conductivity of GtACR1 in primary rat cortical neurons, I wanted to investigate how GtACR1 makes the membrane potential of neurons change. First, I wanted to test photoinhibition of spiking induced by pulsed

current. To induce spiking, the 20 Hz current pulses of 10 milliseconds (300 pA) were applied for primary rat cortical neuron expressing GtACR1 that was measured with whole cell patch clamp. For a typical GtACR1-expressing neuron on DIV8, compared with the voltage trace without light (green trace, see: **Figure 3.4-7A**), under blue light illumination the spiking was successfully inhibited. Also, the same results were recorded at DIV14 (**Figure 3.4-7B**). Because the chloride concentration in neurons was different during neural development (**Figure 3.4-6**), I wanted to verify whether GtACR1 could inhibit neural activity at different culture days. Next, I have tested 4-7 neurons at different culture days (from DIV6 to DIV20). What a very surprising result it is, all spikings induced by pulsed currrent were successfully inhibited by blue light. These data indicate GtACR1 is a powerful tool to inhibit neural activity induced by pulsed current.

Subsequently, I wanted to inhibit spontaneous activity by blue light pulses. Neurons expressing GtACR1 at DIV 20 were picked up to measure with whole cell patch clamp and during light illumination. In response to the blue light, spontaneous activity of all neurons measured (n=10 neurons expressing GtACR1 from DIV20) was successfully inhibited (**Figure 3.4-7C** and **Fig. S 7**). Furthermore, spontaneous activity can be repeatly suppressed as depicted in **Figure 3.4-7D**. These data demonstrate GtACR1 could effectively inhibit spontaneous neural activity by blue light illumination.

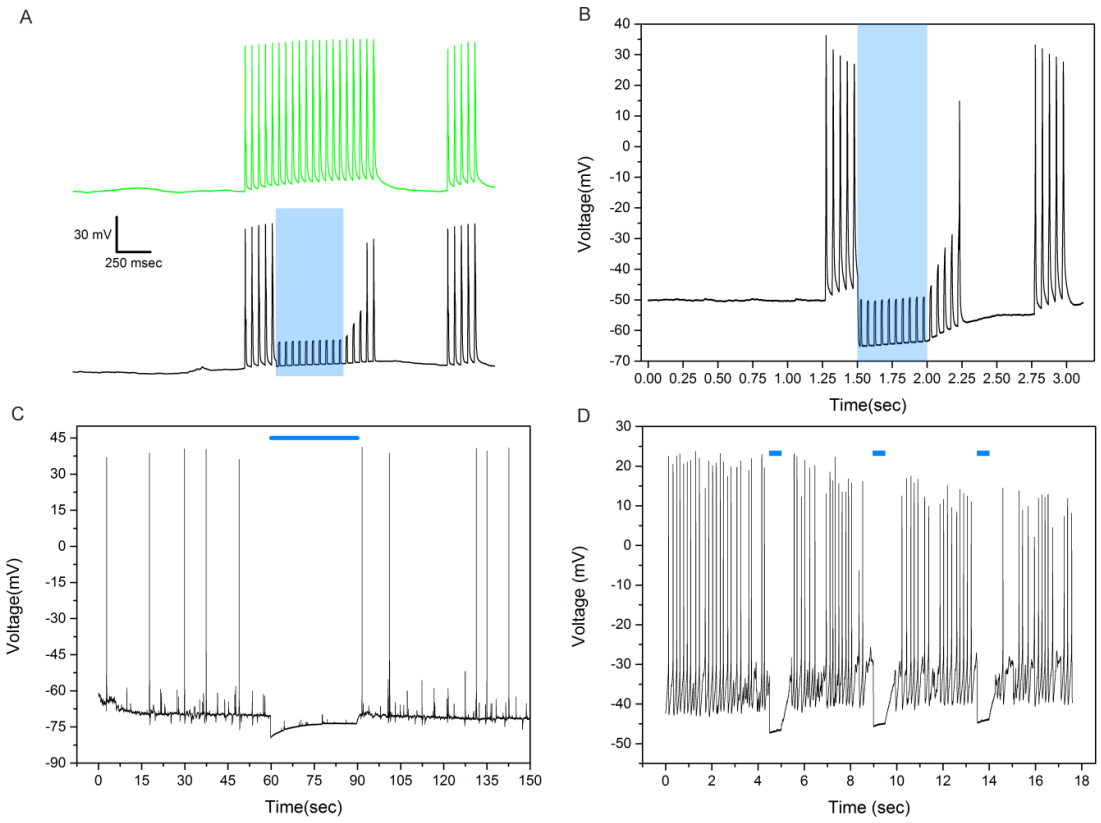

Figure 3.4-7 Photoinhibition of neural activity at different culture days

A) At a typical GtACR1-expressing neuron of DIV8, photoinhibition of spiking induced by pulsed current (300 pA for 10 milliseconds in one pulse, 20 Hz). Green trace indicates the meausurement without light (top), black trace (bottom) indicates the meausurement with light of 500 msec. B) At a typical GtACR1-expressing neuron of DIV14, photoinhibition of spiking induced by pulsed current (300 pA for 10 milliseconds in one pulse, 20 Hz). C) and D) Photoinhibition of spontaneous activity at two different GtACR1-expressing neurons of DIV20 without any current injection. The pulse of blue laser lasts 30 seconds in C) or 500 msec in B) and D). In all measurements, blue laser intensity was 0.21 W/mm^2. Blue area indicates laser on.

3.4.4 The effects of GtACR1 in primary rat cortical neurons

It is very powerful that GtACR1 can effectively inhibit neural activity including spontaneous activity. However, whether hyperpolarization induced by GtACR1 affects the spiking after light illumination is still unknown. In order to investigate this issue, during the measurement of GtACR1-expressing neurons 100 pA was applied to generate continuous action potential activity. At the same time, laser pulses were employed to induce hyperpolarization. In the **Figure 3.4-8**, the amplitude of action potentials after light illumination was slightly increased. It demonstrates that the hyperpolarization by GtACR1 can recover the voltage-gated channels in neurons, which make them fire higher action potentials.

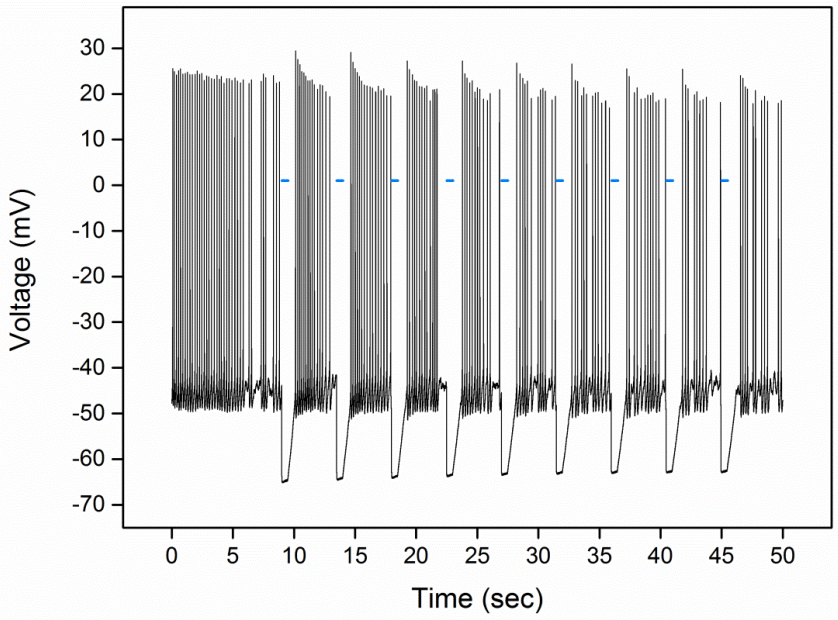

Figure 3.4-8 The amplitude of action potentials increased by light

In a typical neuron (DIV20) expressing GtACR1, a continuous current of 100 pA was injected to induce action potentials. The data were measured under low Cl^- concentration in the pipette and D-AP5 (25 µM), NBQX (10 µM), SR 95531 hydrobromide (20 µM) in the bath. Nine blue laser pulses were applied for inhibiting neural activity. Each pulse lasted for 500 milliseconds separated by a delay time of 4 seconds. In all blue light pulses, blue laser intensity was 0.21 W/mm^2.

Furthermore, I wanted to test whether the amplitude of hyperpolarization by GtACR1 has been changed by multiple activations because of the desensitization of GtACR1 (see: **Figure 3.4-3**). In order to avoid the effect from voltage-gated sodium current, before measurement a continuous current of 100 pA was injected into a typical cortical neuron expressing GtACR1 to arrive at the state of depolarization block. Most important, during the measurement this current was still injected into neurons in order to avoid the recovery of depolarization block through hyperpolarization induced by GtACR1 (see: **Figure 4.3-1**). As both **Figure 3.4-9** and **Fig. S 9** show, neural membrane potential was hyperpolarized by multiple light pulses, in which each pulse lasts 500 milliseconds with 4 seconds dark period in between. Most interesting, the amplitude of hyperpolarization decreased following multiple pulses. Also, I have tested two more neurons expressing GtACR1 and the same phenomenon was achieved (**Figure 3.4-9B)**. These data demonstrate in these GtACR1 expressing neuron, the amplitude of hyperpolarization can be declined by multiple pulses.

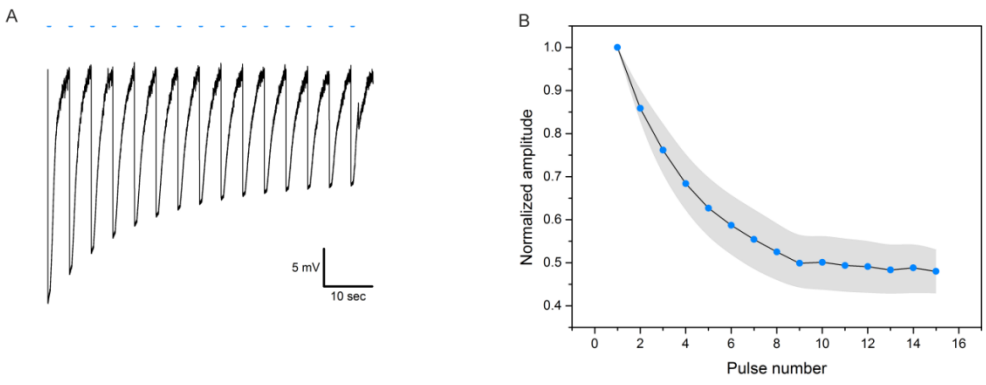

Figure 3.4-9 Amplitude of hyperpolarization decrease during multiple pulses

A) To arrive at depolarization block before measurement and during measurement, the continuous current of 100 pA was injected into a cortical neuron expressing GtACR1, resulting in a membrane potential of -35 mV. Neural membrane potential was hyperpolarized by multiple light pulses, which each lasted 500 milliseconds followed by 4 seconds of light off. Most interesting, the amplitude of hyperpolarization decrease following multiple pulses. In all light pulses, blue laser intensity was 0.21 W/mm^2. B) The amplitude of hyperpolarization was decreased by multiple laser applications. The data are mean values ± SEM (*n* = 3 cells, DIV 17), gray area indicates SEM.

4 Discussion and outlook

This chapter aims to the discussion and outlook on optogenetic tools in primary rat cortical neurons. My work consists of two parts - one is about ChR2opt, other one is regarding two new optogenetic tools in primary rat cortical neurons. Here, the outcomes of the study are revisited and deeply expanded.

4.1 Light-induced excitation-ChR2opt

In this section, the discussion on ChR2opt was presented, separated by two subsections. The subsection **4.1.1** is regarding using rAAV6 and hSyn promoter to achieve high-efficiency transduction and neuron-specific expression of ChR2opt; the other subsection **4.1.2** is discussing the application of ChR2opt on optical controlling of neuronal network.

4.1.1 High-efficiency transduction and neuron-specific expression

Recombinant AAV vectors are promising tools for gene delivery both, *in vitro* and *in vivo*. Multiple naturally occurring serotypes have been demonstrated to target cells in different tissues and organs, including the brain (Aschauer et al., 2013); (Schultz and Chamberlain, 2008). The transduction efficiency of cells or tissue strongly depends on the AAV serotype and its binding partners on the cell surface (Cearley and Wolfe, 2006). In this work, we have examined the transduction efficiency of different rAAV serotypes in rat primary cortical-glial mixed cultures and found that rAAV6 is best suited to gain high-efficiency transduction rates.

The ability to transfer a target gene into a specific cell type is an essential aspect of biomedical research. The specific expression of ChR2opt in this work would be useful for the field of optogenetics. The human synapsin 1 promoter confers neuron-specific transgene expression (Kügler et al., 2003). Our data have shown that the incidence of ChR2 or RFP expression was dramatically decreased in glial cells using the hSyn promoter (**Figure 3.1-3B**). In contrast, the commonly used CMV promoter led to gene expression in neuronal as well as glial cells (**Figure 3.1-2**). In addition, we observed more action potentials and even multiple action potentials in response to one light pulse in neurons that had been transduced with rAAV6-hSyn-ChR2opt rather than rAAV6-CMV-ChR2opt.

It has been described that the strength of depolarization and the delay time between two action potentials that result from ChR2 stimulation depend on the expression level of the Channelrhodopsin expression level (Lin et al., 2013). In order to elicit sufficient

photocurrent for depolarizing a neuron, the expression time of ChR2opt may play a significant role for achieving the higher expression level. Expression of the mKate tag fused to ChR2opt was already visible three days after transduction of cortical neurons. However, a longer expression time clearly improved detection of fluorescent tag. We observed convincing expression levels at 7DPT that is DIV15 (**Figure 3.1-2**) and laser stimulation of neurons synthesizing ChR2opt reproducibly resulted in the generation of action potentials. From our data, 7 days of ChR2opt's expression is best for the successful optical control of neuronal activity.

We found that ChR2opt is able to generate action potentials by illuminating the axon with a pulse of blue light. The illuminated area of the axon is smaller than the total laser spot area, which was about 450 μm^2. In contrast, light stimuli delivered to the cell's soma cover an area that has approximately the same size as the laser spot. Our data support the notion that neuronal activity can be evoked by blue light from almost any area of single, ChR2opt-expressing neurons. This implies that optical control of neuronal activity at the single cell level is possible when ChR2opt is employed.

When stimulating different locations in one single neuron, response times targeting axons/dendrites shown significant differences compared to targeting soma (**Figure 3.1-5C**). We calculated the speeds of action potential from stimulated site to soma, that are in the range of 18 - 44 µm/ms. The differences maybe come from the propagation of the action potential that need a few milliseconds in the same neuron.

When multiple spikes were elicited by a single light stimulation, we found the amplitude of the first spike was larger than that of the second one (**Figure 3.1-6D**). The reduction in AP amplitude may indicate depolarization block due to overly large photocurrents as shown by Berndt et al. using the transgene hSyn-ChR2(T159C) (Berndt et al., 2011). The persistent photocurrent during the first spike may prevent recovery of all the voltage-gated sodium channels from inactivation, which only could be achieved by hyperpolarization for several milliseconds (Bendahhou, 2012). This might imply that if the photocurrent of Channelrhodopsin is too large, it could completely block depolarization so that neuronal activity is silenced. Slow acting Channelrhodopsin variants, such as reported by Nagel et al. (2005) and Lin (2011) may allow this feature to be employed for a dual stimulation and inhibition system with a single light source.

In summary, we established high-efficiency transduction and neuron-specific expression of ChR2opt mediated by the rAAV6 serotype and the hSyn promoter. Using this strategy allowed us to successfully manipulate neuronal activity with single cell selectivity and good temporal accuracy after blue light activation of ChR2opt. We demonstrated rAAV6

as a suitable vector for transferring a gene into primary cortical neurons *in vitro*. To improve the efficiency and specificity of expression, we invoked the hSyn promoter to restrict gene expression to neurons. Notably, we could more effectively control neuronal activity with the hSyn-driven than the CMV-driven ChR2opt expression. Also, additional action potentials were generated when stimulating ChR2opt transduced neurons with longer blue laser light. The rAAV6 with hSyn promoter driven constructs provides a useful tool for specifically manipulating neuronal activity.

4.1.2 Optical control neuronal network using ChR2opt

The connectivity between brain neurons is very important for brain function. These neurons can contact through electrical signals, which involve in neurotransmitters release through synapses between the presynaptic and postsynaptic neurons. In the section **3.2**, optical control of the connectivity of neuronal network *in vitro* was performed, including the random and patterned networks.

In the random network (**Figure 3.2-1**), one optogenetic tool, ChR2opt, expressed very well in those neurons and the patched neuron can be activated by stimulating its neurite and the distant neurons. However, the random distribution of neurons severely hinders the next further analysis such as the distance between the stimulating site and the recorded site, the direction of the signal propagation. Neuron patterning can provide a simple neuronal network with less connections (Offenhäusser et al., 2007), which can be used to extract more information about the connectivity of these network.

On the X-shape pattern, the amplitude of spikes in the single patterned neuron gradually decreased as **Figure 3.2-5** depicted and 10% of laser pulses have not elicited action potentials (data not shown), which indicate the voltage-gated sodium channels of this patterned neuron slowly blocked by multiple laser stimulations as discussed in **4.1.1**.

Moreover, neurons were often at the not-node cross (see: patched neurons in the **Figure 3.2-5** and **Figure 3.2-6**), which implied neurons preferred to seed there with 4 connection other than the node cross with 8 connections. The connectivity analysis of the patterned network with X-shape can provide the information that how strong they connect between the pairs of neurons. In **Figure 3.2-6A**, neuron 2 or 3 at the edge of the pattern has 5 connections with other distant neurons. However, neuron 4 and 5 seeded on the same node where has 8 possible connections with other nodes, which maybe imply these two neurons have competed for connecting other neurons. The current (**Figure 3.2-6C**) and voltage traces (**Figure 3.2-6E**) show the patched neuron 1 has weak signaling when stimulating neuron 4 or 5. It is possible that the numbers of synapse between neuron 4 or

5 and the patched neuron 1 are less than other studied pairs of neurons in this network. Therefore, the numbers of the possible connections in the X-shape pattern would seriously affect the connectivity of neuronal network. However, how many defined connections and the distances between two neurons are still challenging.

In my work, single-cell optogenetic control of neuronal activity has been performed with the branch patterns (see: **Figure 3.2-7**). Most important, ChR2opt packed with AAV6 can successfully elicit action potentials at the single cell level when a small laser spot stimulates any area of a single neuron (**Figure 3.2-8** and **Figure 3.2-9**). That implies that the small laser spot would activate the neuron of interest without the influence on other neurons if ChR2opt packed with AAV6 is used *in vivo* with tightly packed cells.

Having investigated the optogenetic control at the single cell level in the branch pattern, the propagating time of the action potential and the average speed were also analyzed. In the branch pattern, it is very easy to measure the distance between the recorded site and the stimulated site since this pattern has a defined and clear structure for neuron patterning (see: **Figure 3.2-7**). The propagating speed of action potentials is in the range from 65 µm to 205 µm per millisecond (**Figure 3.2-12B**). Also as depicted in **Figure 3.2-12B**, the travelling time of action potential shows positive correlation with the distance between the recorded site and the stimulated site. In terms of cable theory (Goldwyn and Rinzel, 2016) , a cylindrical tube is considered as a model for a dendrite or axon process. The wall of the tube will be a high resistance membrane and the inside of the tube will be low resistance axoplasm. The time of propagation depends on the length of the tube. Therefore, our data can be explained by cable theory.

In summary, to achieve and confirm optical control neural activity with the single cell level, two branch patterns with defined structure were successfully employed. Based on this patterning technology, ChR2opt packed with AAV6 was used to effectively elicit action potentials only stimulating the small area of axons or dendrites. These results provide the strongly evidences on the optogentic control neuronal activity with single cell level.

4.2 New optogenetic tools

This section aims to discuss two new optogenetic tools in primary rat cortical neurons. In the subsection **4.2.1**, the outcomes of ChR2-XXL were discussed in two aspects – depolarization block and neurotransmission; in the subsection **4.2.2**, using blue laser illumination to inhibit neural activity by GtACR1 was revisited.

4.2.1 Depolarization block and neurotransmission induced by ChR2-XXL

In my work, stable depolarization block was achieved with ChR2-XXL in primary rat cortical neuron. Moreover, just exposure to white light for 10 minutes is enough to make neurons arrive at block state. From my results, ChR2-XXL could be used as a well tool to block pain fibers in future.

It has been demonstrated that compared with control neurons, ChR2-XXL positive neurons need more injected currents to hold membrane at -70 mV (**Figure 3.3-2A**). I have investigated currents required for holding potential at -70 mV in two populations of neurons, both at DIV7-10 and at DIV13-17, which stand for two types of excitable states (**Figure 3.3-2A**). Compared with control neurons, both neurons need more injected currents that indicate the membrane potential of these neurons were changed to more depolarization state than control neurons (**Figure 3.3-2B**). These results imply that ChR2-XXL channels had changed the membrane potential of neurons during exposure to white light due to cation influx through them.

Injecting sustained input current of increasing strength neurons eventually stop firing, entering a depolarization block, which can protect neurons from excessive spiking activity (Bianchi et al., 2012). It has been described depolarization block was induced by stimulating ChR2-XXL expressing primary rat cortical neurons at different culture days (**Figure 3.3-5**). The condition is making these neurons exposure to white light for 10 minutes without any current injection. All voltage traces (**Figure 3.3-5**) show voltage decrease happened in the beginning of measurement before laser stimulation, which indicates ChR2-XXL channels still opened but slowly closed as the original paper of ChR2-XXL demonstrated that ChR2-XXL has long open state (Dawydow et al., 2014). Together with other two features - large photocurrent and high light sensitivity, they can account for depolarization block phenomenon. White light with low intensity is able to keep ChR2-XXL channels open that can induce the influx of cation ions. In the beginning of this influx event, the membrane depolarization would be happened; After 10 minutes to white light, from my results (**Figure 3.3-5**), firing action potentials does not show any more by laser stimulation. Moreover, it is difficulty to recover this state by hyperpolarization at lower holding voltage, less than -170 mV (**Figure 3.3-3**). Our result support ChR2-XXL will be a potential ability to block highly excitable neurons in some disorders like schizophrenia with a hyperdopaminergic state (Valenti et al., 2011). When ChR2-XXL resulting in firing action potentials of ChR2-XXL expressing neurons is desired, red foil can be used (Dawydow et al., 2014) to avoid white light that can make ChR2-XXL expressing neurons enter into depolarization block state (**Figure 3.3-5**).

Neurotransmission plays a very role in the communication of brain cells through electrical activity. The first paper published ChR2-XXL (Dawydow et al., 2014) shows it promoted neurotransmitter release through optical control in the larval *Drosophila* neuromuscular junction (NMJ). They did not test in mammalian neurons. I designed this experiment (**Figure 3.3-6**) to investigate how photocurrent of ChR2-XXL shaped neurotransmitter release. Obviously, neurotransmission can be induced in primary rat cortical neurons *in vitro.* Very interesting thing is that long spiking of the postsynaptic neurons can persist after the end of stimulus (**Figure 3.3-7** and **Figure 3.3-8**). This phenomenon reflects that ChR2-XXL has long open-state lifetime. In addition, as depicted in **Figure 3.3-8**, the amplitude of action potentials declined during stimulus by light. After light off for around 20 seconds from **Figure 3.3-8D**, the amplitude of action potential slowly went back to near normal value as spontaneous action spike (see the first spike in **Figure 3.3-8D**). This phenomenon implies that synaptic inputs elicited by the large and sustained photocurrent of ChR2-XXL have blocked the recovery some light-gated sodium channels from inactivation, resulting in the declined action potentials.

What a very interesting thing is the frequency of spikes from the postsynaptic neurons, which evoked by stimulus at the presynaptic neurons, shows oscillation and decline (**Figure 3.3-9**). In the presynaptic terminals, calcium influx triggers exocytosis of neurotransmitter-containing synaptic vesicles (Neher and Sakaba, 2008). I hypothesize that oscillation maybe is associated with ChR2-XXL that can induce rhythmic patterns of calcium influx in the ChR2-XXL positive presynaptic neuron. Then, oscillation of calcium influx can result in oscillation of excitatory postsynaptic currents (EPSCs) that can evoke action potentials at the postsynaptic neurons. The photocurrent of ChR2-XXL shows a decay process (Dawydow et al., 2014), which can account for the decline of the frequency of action potentials. These data likely implies EPSCs evoked by light shows the decay process after starting to stimulate by laser. Our results strongly support the powerful ability of ChR2-XXL when it is expressed in primary rat cortical neurons.

The peripheral neuropathic pain, originates in the peripheral nerve fibers, most commonly in the arms and legs (Slavin, 2008) (Torrance et al., 2006). Scientists of neural engineering are seeking the improved approaches that can be used to block pain fibers selectively and reversibly to alleviate episodes of debilitating chronic pain. In summary, stable depolarization block has been successfully induced in ChR2-XXL expressing neurons, which may be useful for blocking pain fibers to treat peripheral neuropathic pain, and our data support ChR2-XXL will be a potential ability to block highly excitable neurons in some disorders like schizophrenia.

4.2.2 Photoinhibition of neuronal activity by GtACR1

The study of natural anion channelrhodopsins (ACRs) provides the potential approach to achieve the rapid and efficient suppression of neuronal activity by hyperpolarization (Govorunova et al., 2015) (Sineshchekov et al., 2015) (Sineshchekov et al., 2016). Most important, using the less-than-1000th lower light, hyperpolarizing photocurrents of ACRs were equal to the maximal currents of archaerhodopsin-3 (Arch) that is a proton pump for spike suppression. In the section **3.4** of this thesis, I have functionally validated the hyperpolarization of GtACR1 expressing neurons by light pulses. Using blue laser, the inhibition of neuronal firing- induced by pulsed current and spontaneous activity can be effectively achieved from young to old neurons *in vitro*. My work provides more evidence that GtACR1 can work well in neurons.

ACRs are significant different compared with cation channelrhodopsins (CCRs), not only the selectivity filter as well as the structural basis of channel gating (Sineshchekov et al., 2016). Channel closing of GtACR1 involves two mechanisms: (1) Fast closing is induced by a reversible L⇔M conversion. Glu-68 accounts for this transition. (2) Slow closing parallels irreversible depletion of the M-like and, hence, L-like state. Cys-102 plays an important role in this process. Based on these molecular mechanisms of these ACRs' function (Sineshchekov et al., 2015) (Sineshchekov et al., 2016) (Yi et al., 2016), GtACR1 variants by mutation will facilitate their application in the field of neuroscience, even *in vivo*.

GtACR1 can generate large outward current that effectively inhibits neuronal activity. In general, the expression level determinates the effectiveness of GtACR1. In my work, electrofection approach was applied to deliver GtACR1 DNA carried CMV promoter to primary rat cortical neuron. Therefore, the old GtACR1 expressing neurons such as DIV20 should generate the largest outward current to suppress neuronal activity. However, as depicted in **Figure 3.4-5A**, the currents with light from DIV8 shows the limitation as ones from DIV17 or DIV20. Moreover, the current of neurons at DIV14 that expressed GtACR1 for two weeks is less than the current of neurons at DIV8. Maybe the reasons is that CMV promoter is only stable in neurons of particular types (Wickersham and Callaway, 2007), not associated with GtACR1 channel itself since **Fig. S 6** shows during neuronal development the normalized currents with light are not significant different. In addition, the rAAV6 with hSyn promoter driven system studied by us (see: **3.1**) would eliminate this issue in primary rat cortical neurons.

After had investigated the IE relationship of GtACR1 during neural development, the reversal potentials for GtACR1 were depicted in **Figure 3.4-6**. This data implies the chloride concentration was decreasing during neural development, which is similar phenomenon as described in Prof. Yehezkel Ben-Ari's review paper (Ben-Ari, 2002). In this review, he had mentioned that they have shown that E_{Cl} decreases with age during the postnatal period in the rodent hippocampus. This implies that using laser illumination on GtACR1, chloride ions can flux into or out of neurons, which is determined by the age of neurons. Together with my results, it will facilitate the application of GtACR1 in the mature neurons.

The hyperpolarization by GtACR1 can recover the voltage-gated channels in neurons (**Figure 3.4-8**). However, by multiple illuminations, the frequency of action potentials shows the decreasing phenomenon (**Figure 3.4-8** and **Fig. S 8**). That may be a continuous current of 100 pA injected to induce action potentials result in generating more slow calcium-activated potassium outward currents for preventing over-exciting (Faber and Sah, 2003) (Zhu et al., 2016).

In summary, my work provides the strongly evidence for GtACR1 to inhibit neuronal activity including spontaneous activity and will facilitate the application of these natural anion channelrhodopsins. Most important, ACRs provides the potential approach to achieve the rapid and efficient suppression of neuronal activity by hyperpolarization. It means that the investigation of ACRs *in vivo* will come in near future.

4.3 Outlook

This work has achieved two main aims: (1) successfully established a useful tool for specifically manipulating neuronal activity with ChR2opt using rAAV transduction; (2) functionally validated two new powerful tools--ChR2-XXL and GtACR1 in primary rat cortical neurons. These achievements offer many opportunities for further investigations and improving the application of these tools. In the subsection **4.3.1**, the possibility to recover depolarization block is proposed through one typical result. In the subsection **4.3.2**, to improve the recording efficiency, the genetically encoded voltage sensor that is spectrally compatible with optogenetic actuators is foreseen. In the subsection **4.3.3**, stimulating neurons with light and gold is described when genetic modification is not desired for some fields.

4.3.1 Recovery from depolarization block by light

Hyperpolarization for a few milliseconds can recover the depolarization blocked neurons so that they enter an active state (Bendahhou, 2012). I supposed that GtACR1 could recover the depolarization block using laser pulses. One typical trial was done as depicted in **Figure 4.3-1**. Following the light illumination, the black trace shows the membrane potential was shifting to normal resting potential at the sixth illumination in the first round. Moreover, spiking behavior was seen after this illumination. In the second round (red trace in **Figure 4.3-1**), spiking was obtained many times. This result demonstrates that GtACR1 can be used to recover the depolarization block in primary rat cortical neuron using blue light pulses. Based on this trial, the deep investigations and more analysis are needed, which would provide a promising application for the field of neuroscience.

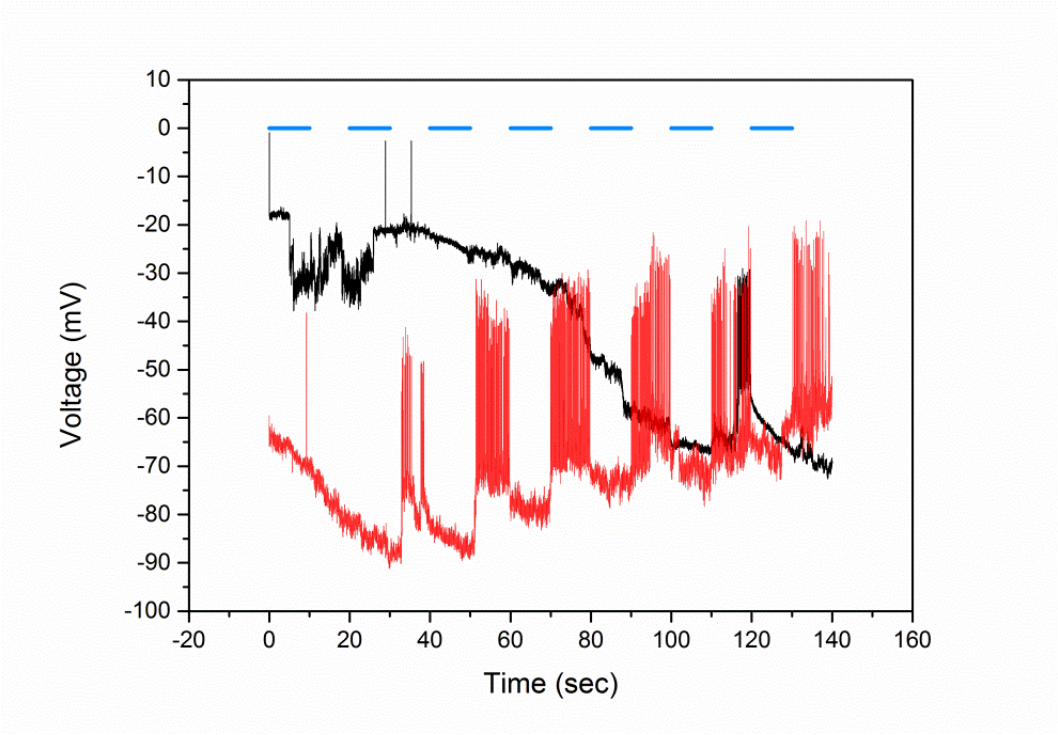

Figure 4.3-1 Recovery from depolarization block using GtACR1

In a typical neuron expressing GtACR1, a continuous current of 100 pA was injected to induce the depolarization block before the measurement. The measurement without any current injection includes two rounds separated by 95 seconds (black: first round, red: second round), each has 7 light stimuluses of 10 seconds. In the end of measurement, spiking was shown. In all light pulses, blue laser intensity was 0.21 W/mm^2.

4.3.2 Compatible with genetically encoded voltage sensor

In my work, two powerful tools have been investigated using whole cell patch clamp, which was spent a lot of time for fulfilling all measurements. So the high-speed recording approach with large-scale is needed. A genetically encoded voltage sensor provides one possibility for large-scale recording of neuronal electrical signals (St-Pierre et al., 2014) (Gong, 2015) (Gong et al., 2015) (Yang et al., 2016), which can be used for decoding neural circuits. How these optogenetic actuators and sensors work together is still unclear.

Prof. St-Pierre and his colleagues have developed Accelerated Sensor of Action Potentials 1 (ASAP1) (St-Pierre et al., 2014). It shown on and off kinetics of ~2 ms, reliably monitored single action potentials and subthreshold potential changes, and tracked spike trains of up to 200 Hz. He also developed ASAP2f (Yang et al., 2016), which is more adapted for fast two-photon microscopy, given its larger signal amplitude, and its slower off kinetics for allowing one to get more photons per action potential. As listed in **Table 4.3-1**, ASAP1 and ASAP2f can be excited with blue light, which will be spectrally compatible with red-activatable ChR (ReaChR) (Lin et al., 2013) for activating activity or red-shifted cruxhalorhodopsin (Jaws) (Chuong et al., 2014) and *Ps*ACR1 (Wietek et al., 2016) for photoinhibition. Moreover, in order to monitor neuronal activity induced by optogenetic tools such as ChR2-XXL that is activated by blue light, the red-shifted voltage sensor (VSFP3s) (Perron et al., 2009) can be employed. This is a good chance to develop a useful approach, which is able to simultaneously record and activate or inhibit neurons.

Voltage sensor (**light**)	Actuator (**light**)
ASAP1 (St-Pierre et al., 2014) or ASAP2f (Yang et al., 2016) (**blue light**)	ReaChR (Lin et al., 2013) (**red-activatable**) Jaws (Chuong et al., 2014) or *Ps*ACR1 (Wietek et al., 2016) (**red-shifted**)
VSFP3s (Perron et al., 2009) (**red-shifted**)	ChR2-XXL (Dawydow et al., 2014) (**blue light**)

Table 4.3-1 Optogenetic actuators spectrally compatible with genetically encoded voltage sensors

4.3.3 Stimulating neurons with light and gold

Optogenetic control of neuronal activity involves in genetic manipulation on cells, which is very promising technology for neuroscientists to decode neural circuits associated with specific behaviors, as well as neurological disorders. However, when translating this technology for biomedical applications, people are very afraid to apply genetics in human tissues such as the brain exposed to some virus. In 2015, scientists developed one new technology that can excite action potentials without genetic modification (Carvalho-de-Souza et al., 2015). Gold nanorods (AuNRs) can be targeted to neurons for firing action potentials using a modified scorpion neurotoxin. Using this technology, a light is used to heat these nanoparticles, which changes the capacitance of the membrane, resulting in the excitation of neurons. Based on this new technology, a specific approach for only eliciting cortical neurons can be addressed through searching for the specific biological ligands of brain cortex. It would be useful for medical applications because of unmodified neurons for humans.

5 Summary

The discovery of Channelrhodopsins (ChRs) allows their application in the field of neuroscience, so called optogenetics, for exciting or inhibiting neuronal activity. Nowadays optogenetics technology is very promising for decoding neuronal circuits associated with specific behaviors, as well as neurological disorders. However, many questions still need to be addressed, such as the lack of cell type-specific gene transfer methods for ChRs delivery or powerful and more efficient optogenetic tools.

In the first part of my thesis, recombinant adeno-associated virus (rAAV) serotypes are screened for their ability to transfer genes to neurons. rAAV6 was identified as the most efficient serotype for transduction of cortical-glial mixed cultures. First, we used the constitutively active cytomegalovirus (CMV) promoter to drive gene expression of the Channelrhodopsin 2 variant ChR2opt. The protein was detected in neurons as well as in glia cells. After exchanging the CMV promoter for the human synapsin (hSyn) promoter, ChR2opt expression was restricted to neurons. Notably, using blue light illumination, I could control electrical activity in primary cortical neurons expressing ChR2opt and succeeded in triggering action potentials by ChR2opt stimulation. Using this strategy, I was able to register responses at the single cell level with high temporal accuracy.

Based on the system of rAAV6-hSyn-ChR2opt investigated in the first part, the second part successfully achieved optical control of neuronal networks with both random and patterned connectivity *in vitro*. In both networks, optogenetic mapping of cortical microcircuits was performed. Most important, using two kinds of branched patterns with defined structure, optical control of neural activity at the single cell level was successfully achieved. Only stimulating the small area of axons or dendrites was sufficient to effectively elicit action potentials in the branched patterns. These results provide the next steps in increasing the resolution of optical control of neuronal activity.

In the third part of my thesis, one novel powerful tool with super light-sensitivity, long open-state and large photocurrent, termed ChR2-XXL, was employed in primary rat cortical neurons *in vitro*. Its two important features have been confirmed in neurons with whole cell patch clamp together with blue laser illumination. On the one hand, stable depolarization block could be achieved in ChR2-XXL expressing neurons; on the other hand, neurotransmission can be successfully induced when stimulating the presynaptic neurons that expressed ChR2-XXL.

The last part addressed a naturally occurring anion channelrhodopsin (GtACR1) in primary rat cortical neurons. Light-gated chloride conduction of GtACR1 was verified in primary cortical neurons. Subsequently, the efficient photosuppression of neuronal action potentials, including electrically stimulated and spontaneous activity, was performed using blue laser illumination. In addition, my work implies that the chloride concentration in neurons decreases during neural development. This work provides strong evidence that GtACR1 can not only inhibit neuronal signals, including spontaneous activity, but may also be used to manipulate Cl^- based cell maturation systems.

In summary, my work offers strong evidence to support two main aims. First, rAAV6 with hSyn promoter driven constructs provides a useful tool for specifically manipulating neuronal activity and mapping microcircuits. Employing this system to express ChR2opt, allowed both random and patterned networks to be manipulated with specificity of stimulation down to single neurites. Second, new tools have been validated for use in neurons. ChR2-XXL is able to generate stable depolarization block and shape powerful neurotransmission. Also, ACRs provide a method to achieve the rapid and efficient suppression of neuronal activity by hyperpolarization. These new tools, and the optimized method of gene transfer are promising candidates for *in vivo* applications of optogenetic control.

6 Zusammenfassung

Die Entdeckung des Channelrhodopsins (ChRs) erlaubt davon Einsatz in den Neurowissenschaft, an der so gennanten Optogenetics. Die Aktivität von Nervenzellen kann hierbei stimuliert oder gedämpft werden. Aktuell wird Optogenetics eingesetzt, um neuronale Schaltkreise, die mit spezifischem Verhalten oder neurologish erkrankheiten verbunden sind, zu erforschen. Jedoch sind noch viele Fragestellungen offen, z.B. wie ChR2 Gene in spezifische Zelltypen eingebracht werden können, und ob weiter Proteine als stärkere oder effizientere Optogeneticwerkzeuge eingesetzt werden können.

Im ersten Teil meiner Arbeit werden rekombinante adeno-assoziertes Viren (rAAV) in verschiedene Serotypen für ihre Transduktionfähigkeit in Neuronen getestet. rAAV6 wurde dabei als der effizienteste Serotyp zur Transduktion von Kulturen mit kortikalen und glial Zellen identifiziert. Zuerst wurde der konstitutive aktive Cytomegalovirus (CMV) Promotor benutzt ChR2opt (eine Variante von Channelrhodopsin 2) Genexpression zu betreiben. Das Protein konnte sowohl in Neuronen als auch in Gliazellen nachgewiesen werden. Anschließend wurde der CMV-Promotor gegen den humanen Synapsin (hSyn) Promotor ausgetauscht, um ChR2opt Expression auf Neuronen zu beschränken. Bemerkenswert ist, dass ich durch die Verwendung von blauem Licht die elektrische Aktivität in ChR2opt exprimierenden, primären kortikalen Neuronen steuern und erfolgreich Aktionspotentiale durch ChR2opt Stimulation induzieren konnte. Aktionspotentiale wurden dabei in rAAV transduzierten Zellen schneller ausgelöst als zuvor in transfizierten Zellen berichtet. Mit dieser Strategie habe ich die Aktivität auf der Einzelzellebene mit hoher Zeitauflösung kontrolliert.

Mit Benutzung dieses rAAV6-hSyn-ChR2opt, der ihn zweitem Teil diese Thesis erklärt wird gelang ervolkreiche Steuerung von zufällig und gemusterten neuronalen Netzwerken *in vitro*. In beide Netzwerken waren kortikal Microschaltkreisen optogenetisch erforscht. Die Benutzung von zwei verschiedenen verzweigtes Muster, erlaubt die optische Steurerung der neuronalen Aktivität auf Ebene der Einzelzelle. Auf die verzweigt Muster, Lichtstimulation über nur eine kleine Membranfläche von ein Axon oder Dendrit stärk genug war Aktionpotentialen zu auslösen. Diese Ergebniss sind die nächste Schritten für höhre Auflösung der neuronale Aktivitäts Steuerung.

Der dritte Teil meiner Thesis zeigt ein neues, mächtiges, optogenetisches Protein (ChR2-XXL), in primär kortikalen Neuronen der Ratte *in vitro* mit sehr höher Lichtempfindlichkeit, langer Kanal Öffnungsdynamik, und starkem induziertem Lichtstrom. Zwei wichtige Eigenschaften wurden durch Ganzzellenpatchclamp und Beleuchtung mit blauen

Laserlicht in Neuronen bestätigt; auf der einen Seite, daß Neuronen mit ChR2-XXL durch dauerhafte Depolarization blockiert werden, auf der anderen Seite daß Neurotransmission erfolgreich induziert wurde, wenn die präsynaptische Zelle mit ChR2-XXL stimuliert wurde.

Der letzte Teil meiner Arbeit erklärt die Benutzung eines Anion Channelrhodopsins aus Algae (GtACR1) in primär kortikalen Neuronen der Ratte. Es wurde bestätigt, daß GtACR1 auch in primären Neuronen als ein lichtsteuerbarer Chlorkanal funktioniert. Damit wurde neuronale Aktivität, z.B. elektrisch stimuliert, und spontane Aktionspotentiale durch Blaulichtbeleuchtung unterdrückt. Darüber hinaus zeigt meine Arbeit dass die Konzentration von Cl^- während neuronaler Entwicklung fällt. Dieser Beweis zeigt, dass GtACR1 möglicherweise nicht nur ein Weg ist neuronale Aktionspotentiale zu minimieren, auch diese von spontaner Netzwerkaktivität, sondern auch benutzt werden könnte Cl^- bassierte Entwicklungsprozesse zu manipulieren.

Zusammengefaßt ist meine Arbeit der Grundstein für zwei Themen. Erstens, das rAAV6 verpackte und mit hSyn Promoter getriebene Genekonstrukt ist ein wertvolles System für die Auswertung Zellularmikroschaltkreise und die Steuerung der neuronalen Aktivität. Wenn dieses System ChR2opt Produktion betreibt, erlaubt es die Manipulation von zufälligen und gemusterten Netzwerken mit Genauigkeit bis zu einzelnen Neuriten. Zweites, neue Proteine wurden für ihre Benutzung in Neuronen validiert. ChR2-XXL konnte stabil eine Depolarizationsperre generieren und Neurotransmission ändern. Auch ACRs sind ein System für schnelle und effiziente Unterdrückung von Neuronalaktivität durch Hyperpolarization. Diese neuen optogenetischen Proteine, und der durch rAAV optimiert Genlieferungsmethode sind attraktive Systeme für zukünftige optogenetische Beeinflussung *in vivo*.

Acknowledgments

Prof. Dr. Andreas Offenhäusser, I really appreciate you for giving me this good opportunity to study Optogenetics. You offered me the good scientific environment and excellent guidance during my PhD study. Many thanks for all your nice ideas on my projects. Specially, I would like to mention one of your supports that I attended the 2014 conference on 'Channelrhodopsin et al. – Optogenetic Tools and Applications'. In that conference, I learnt a lot and knew Prof. Dr. Georg Nagel for the cooperation.

Dr. Vanessa Maybeck, you are my best advisor so far. Except for many of your useful discussions and comments on my work, your ideas were really inspiring and help me a lot. In addition, I want to thank for your corrections on my papers and thesis.

Dr. Wienke Lange, I want to appreciate you for your instructions on the methods such as neurons culture, which is the core technology for my project, and your good work that is the footstone for parts of my work.

Prof. Dr. Georg Nagel and **Dr. Shiqiang Gao**, I want to thank you very much for all plasmids you offered. Because of you, I learnt a lot on optogenetic tools and made my work look more enriched.

Prof. Dr. Arnd Baumann, I want to thank you and your members for all your comments and nice ideas on the heterologous expression in neurons. In addition, your work on AAV production is very important for my work. Thanks a lot!

Prof. Dr. Frank Müller, many thanks for your detailed responses on electrophysiology questions I asked and your useful suggestions on my work in our optogenetics meetings.

Prof. Dr. Marc Spehr, I very much thank you for being my second supervisor and your precious time for reviewing my thesis.

Dr. Liping Du, I want to appreciate your nice printing work for neuron patterning. Most important, your branch patterns play an important role in my work on optogenetic at the single cell level.

Wenfang Li, I would like to appreciate you for your discussions and your helps on the electrofection skill, synaptic input blocking measurement and the maintenance of laser setup.

Dr. Philipp Rinklin and **La Chen**, I want to thank you for your Matlab programing skills, which is very useful for the analysis of my data.

Bettina Breuer and **Rita Fricke**, I want to thank you very much for your excellent assistance on the preparation of primary rat cortical neurons and the orders for my projects. Without you, my work would be not possible.

Jonas Albers and **Dr. Geng Zhu**, thank you for your skills on patch clamp, which is the basic technology I employed during my PhD study.

Martin Gocyla, I want to thank you very much for your helps on German language and all your ideas on my project. I like to talk with you in the train during my commute.

Dr. Francesca Santoro and **Pengcheng Zhang**, you were my office mates. Thank you for all of your helps and conversations.

Prof. Yi Zhang and other Chinese fellows, I am thankful for your good communications on the future dream and career.

I want to thank all the members in ICS-8/PGI-8 for the nice work atmosphere and help. I was happy to work in Germany because of you. Thank you very much!

Appendix

A1. Findpeaks script with MATLAB to analyze action potentials

A1-1. wden function to filter the raw data

```
function [yDen,yDrift,yMean]= den_wav(y)
% k=5;
% y=data(isfinite(data(:,k)),k); % Discard NaN elements
% t=data(isfinite(data(:,k)),1);
yMean=mean(y);
ySig=y-yMean;
% De-noise noisy signal using soft heuristic SURE thresholding and scaled noise option
yDen = wden(ySig,'heursure','s','mln',5,'bior6.8')+yMean;
yDrift=wden(ySig,'sqtwolog','s','one',8,'bior6.8')+yMean; %
% figure(4);
% yPulse=yDen-yDrift+yMean;
% plot(t,y,'b',t,yDen,'g',t,yDrift,'c',t,yPulse,'r');
% ylabel('Signal (V)');xlabel('Time (s)');title('Denoise by wavelet method');
% legend('Original signal','Filted signal','Backgroud drift','Pulse signal + Mean');
% grid on;
End
```

A1-2. Pulse analysis

```
%%% Pulse analysis for single file. 12/6/2014
%Get files to analyze.
[filename pathname]=uigetfile(...
    '*.asc',...
    'MultiSelect','on',...
    'Select input file');
%If a single file was selected assign its filename string to a cell array
%for referencing.
if ischar(filename)==1
    dummy=filename;
    clear filename;
    filename{1}=dummy;
end
%Run processing for each file.
for filenumber = 1:size(filename,2)
    %Merge filename and pathname to single string.
    file=fullfile(pathname, filename{filenumber});
    data=importdata(file, '\t');
    lev_on=0.30;
    lev_halfL=0.5;
    lev_halfR=0.5;
    lev_beforeH=0.25;
    lev_off=0;
```

```
MinPulseHeight=35; % Min pulse height in voltage as V/mV

MinPulseTime=10;   % Min pulse width in time as s/ms

response=zeros((size(data,2)-1)*size(data,1),16); %second dimension: Block number, pulse number; SigMean, Peak amplitude;...

% pulse-on time,pulse-on value;lev_halfL time,lev_halfL value;peak time, peak value;...

% lev_halfR time,lev_halfR value;lev_beforeH time,lev_beforeH value;pulse-off time, pulse-off value;

SigDen=zeros(size(data,1),size(data,2)); % initial denoised signals

SigDen(:,1)=data(:,1); % copy time column to SigDen

SigDrift=SigDen;   % initial backgroud drift signals

SigMean=zeros(size(data,2)); % initial mean value of signals

Ts=(data(2,1)-data(1,1)); Fs=1/Ts; % Get the sample time and frequency

for i=2:size(data,2)     % start

    SigLen=size(data(isfinite(data(:,i)),i),1); % get the effective length of signal

     % Before seaching pulses, filter the raw data


[SigDen(1:SigLen,i),SigDrift(1:SigLen,i),SigMean(i)]=den_wav(data(isfinite(data(:,i)),i));

    Sig=SigDen(:,i)-SigMean(i);   % substract background part

     %Find APs that exceed 'minpeakheight' and are more than 'minpeakdistance' apart.


[pks,locs]=findpeaks(Sig,'minpeakheight',MinPulseHeight,'minpeakdistance',ceil(MinPulseTime/Ts));

    if numel(locs)==0; continue; end

    for j=1:size(locs,2) % start to get information about peak, pulse-on and pulse-off and so on

        response((i-2)*size(data,1)+locs(j),1)=i-1;             % Block number
```

```
response((i-2)*size(data,1)+locs(j),2)=j;                % pulse number
response((i-2)*size(data,1)+locs(j),3)=SigMean(i);        % SigMean
response((i-2)*size(data,1)+locs(j),4)=Sig(locs(j));      % Peak amplitude
response((i-2)*size(data,1)+locs(j),9)=data(locs(j),1);   % Get the peak time and height
response((i-2)*size(data,1)+locs(j),10)=SigDen(locs(j),i);
k=locs(j);lev_on_value=Sig(k)*lev_on; % Initial the seach of pulse-on
while  sign(Sig(k)-lev_on_value) == sign(Sig(k-1)-lev_on_value)
    % the searchs go beyond the effective range
     if (j==1 && k-1==1)||((j>1)&& (k-1<=locs(j-1))); break; end
     k = k-1;
end
if  (j==1 && k-1==1)||((j>1)&& (k-1<=locs(j-1)));  % fail to get the pulse-on
    response((i-2)*size(data,1)+locs(j),5)=NaN;
    response((i-2)*size(data,1)+locs(j),6)=NaN;
else   % Get the pulse-on
    response((i-2)*size(data,1)+locs(j),5)=data(k,1)-Ts*(Sig(k)-lev_on_value)/(Sig(k)-Sig(k-1));
    response((i-2)*size(data,1)+locs(j),6)=lev_on_value+SigMean(i);
end
k=locs(j);lev_halfL_value=Sig(k)*lev_halfL; % Initial the seach of lev_halfL
while  sign(Sig(k)-lev_halfL_value) == sign(Sig(k-1)-lev_halfL_value)
    % the searchs go beyond the effective range
     if (j==1 && k-1==1)||((j>1)&& (k-1<=locs(j-1))); break; end
     k = k-1;
```

```
        end
        if  (j==1 && k-1==1)||((j>1)&& (k-1<=locs(j-1)));  % fail to get the lev_halfL
            response((i-2)*size(data,1)+locs(j),7)=NaN;
            response((i-2)*size(data,1)+locs(j),8)=NaN;
        else   % Get the lev_halfL
            response((i-2)*size(data,1)+locs(j),7)=data(k,1)-Ts*(Sig(k)-
lev_halfL_value)/(Sig(k)-Sig(k-1));
            response((i-2)*size(data,1)+locs(j),8)=lev_halfL_value+SigMean(i);
        end
        k=locs(j);lev_halfR_value=Sig(locs(j))*lev_halfR;  % Initial the seach of lev_halfR
        while sign(Sig(k)-lev_halfR_value) == sign(Sig(k-1)-lev_halfR_value)
            % the searchs go beyond the effective range
            if (j==(size(locs,2)) && k+1==SigLen)||((j+1<=(size(locs,2))&&
(k+1>=locs(j+1)))); break; end
            k = k+1;
        end
        if (j==(size(locs,2)) && k+1==SigLen)||((j+1<=(size(locs,2))&& (k+1>=locs(j+1)))); %
fail to get the lev_halfR
            response((i-2)*size(data,1)+locs(j),11)=NaN;
            response((i-2)*size(data,1)+locs(j),12)=NaN;
        else % Get the lev_halfR
            response((i-2)*size(data,1)+locs(j),11)=data(k,1)+Ts*(Sig(k)-
lev_halfR_value)/(Sig(k)-Sig(k+1));
            response((i-2)*size(data,1)+locs(j),12)=lev_halfR_value+SigMean(i);
        end
```

```
k=locs(j);lev_beforeH_value=Sig(locs(j))*lev_beforeH;    % Initial the seach of lev_beforeH

while sign(Sig(k)-lev_beforeH_value) == sign(Sig(k-1)-lev_beforeH_value)

    % the searchs go beyond the effective range

    if (j==(size(locs,2)) && k+1==SigLen)||((j+1<=(size(locs,2))&& (k+1>=locs(j+1)))); break; end

    k = k+1;

end

if (j==(size(locs,2)) && k+1==SigLen)||((j+1<=(size(locs,2))&& (k+1>=locs(j+1)))); % fail to get the lev_beforeH

    response((i-2)*size(data,1)+locs(j),13)=NaN;

    response((i-2)*size(data,1)+locs(j),14)=NaN;

else % Get the lev_beforeH

    response((i-2)*size(data,1)+locs(j),13)=data(k,1)+Ts*(Sig(k)-lev_beforeH_value)/(Sig(k)-Sig(k+1));

    response((i-2)*size(data,1)+locs(j),14)=lev_beforeH_value+SigMean(i);

end

k=locs(j);lev_off_value=Sig(locs(j))*lev_off;  % Initial the seach of pulse-off

while sign(Sig(k)-lev_off_value) == sign(Sig(k-1)-lev_off_value)

    % the searchs go beyond the effective range

    if (j==(size(locs,2)) && k+1==SigLen)||((j+1<=(size(locs,2))&& (k+1>=locs(j+1)))); break; end

    k = k+1;

end

if (j==(size(locs,2)) && k+1==SigLen)||((j+1<=(size(locs,2))&& (k+1>=locs(j+1)))); % fail to get the pulse-off
```

```
                response((i-2)*size(data,1)+locs(j),15)=NaN;
                response((i-2)*size(data,1)+locs(j),16)=NaN;
            else % Get the pulse-off
                response((i-2)*size(data,1)+locs(j),15)=data(k,1)+Ts*(Sig(k)-
lev_off_value)/(Sig(k)-Sig(k+1));
                response((i-2)*size(data,1)+locs(j),16)=lev_off_value+SigMean(i);
            end
        end
    end
end
 % All effective peak value
    AllrespEfta=response(response(:,1)~=0,:);
 % All the first or second and third peak value
    AllrespEfta1=response(response(:,2)==1,:);
    AllrespEfta2=response(response(:,2)==2,:);
    AllrespEfta3=response(response(:,2)==3,:);
    AllrespEfta4=response(response(:,2)==4,:);
    AllrespEfta5=response(response(:,2)==5,:);
    AllrespEfta6=response(response(:,2)==6,:);
    AllrespEfta7=response(response(:,2)==7,:);
 % As an example, just plot one signal of results
   i=6;
   respEft=response(response(:,1)==i-1,:);
   figure(5);
```

```
   plot(data(1:SigLen,1),data(1:SigLen,i),'b',data(1:SigLen,1),SigDen(1:SigLen,i),'r',...

   respEft(:,5),respEft(:,6),'g*', respEft(:,7),respEft(:,8),'b*',respEft(:,9),respEft(:,10),'m*',...

   respEft(:,11),respEft(:,12),'b*',respEft(:,13),respEft(:,14),'c*',
respEft(:,15),respEft(:,16),'r*');

   legend('Original signal','Filted signal');

   grid on;
```

A2. Supplementary Data

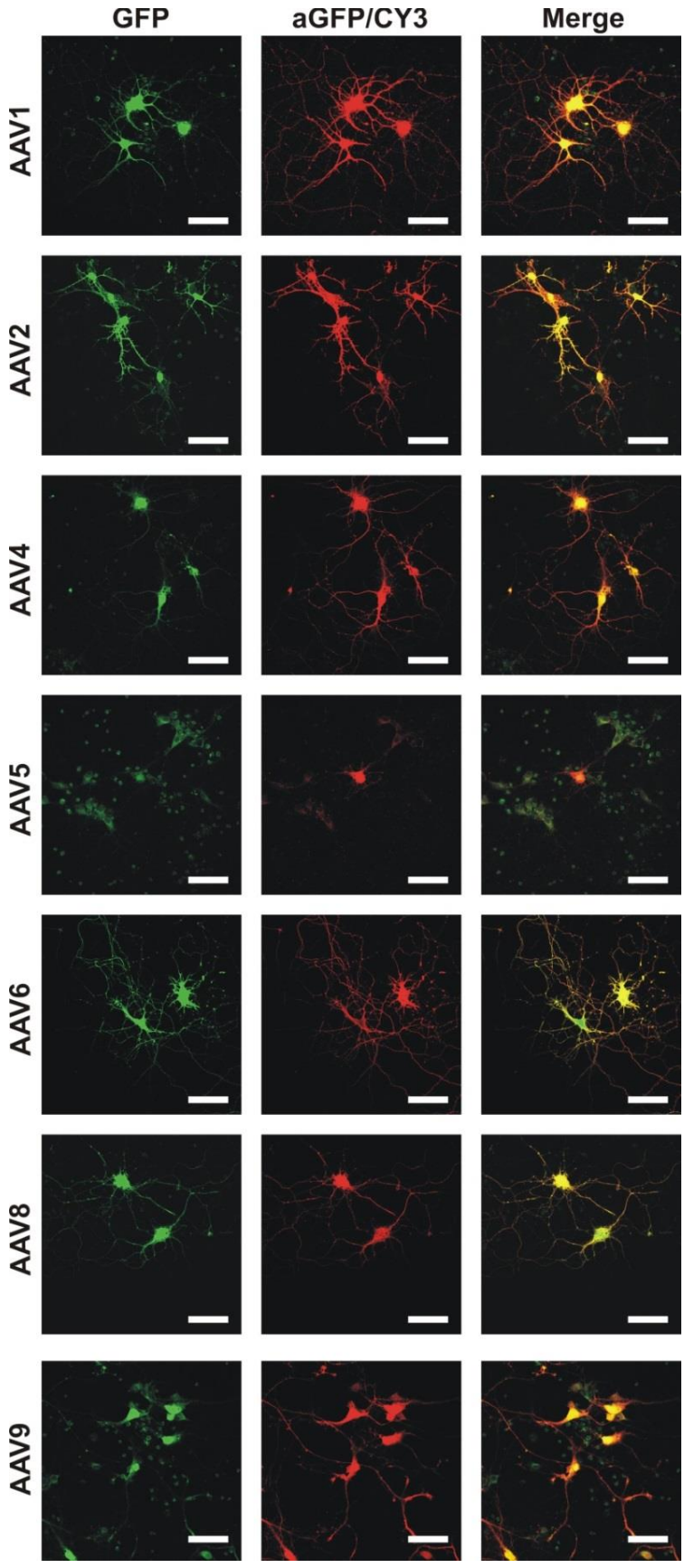

Fig. S 1 Transduction efficiency of different rAAV serotypes

Transduction efficiency of rAAV serotypes 1, 2, 4, 5, 6, 8 and 9 on primary cortical-glial mixed cultures transduced on DIV8 (fixed on DIV17, virus titer 10^9 (rAAV5) or 10^{10} (all other rAAVs)). Images in the first column show eGFP autofluorescence in transduced cells, images in the second column show cells stained with anti-GFP antibodies (red). Merged images are depicted in the third column. Scale bar is 50 µm.

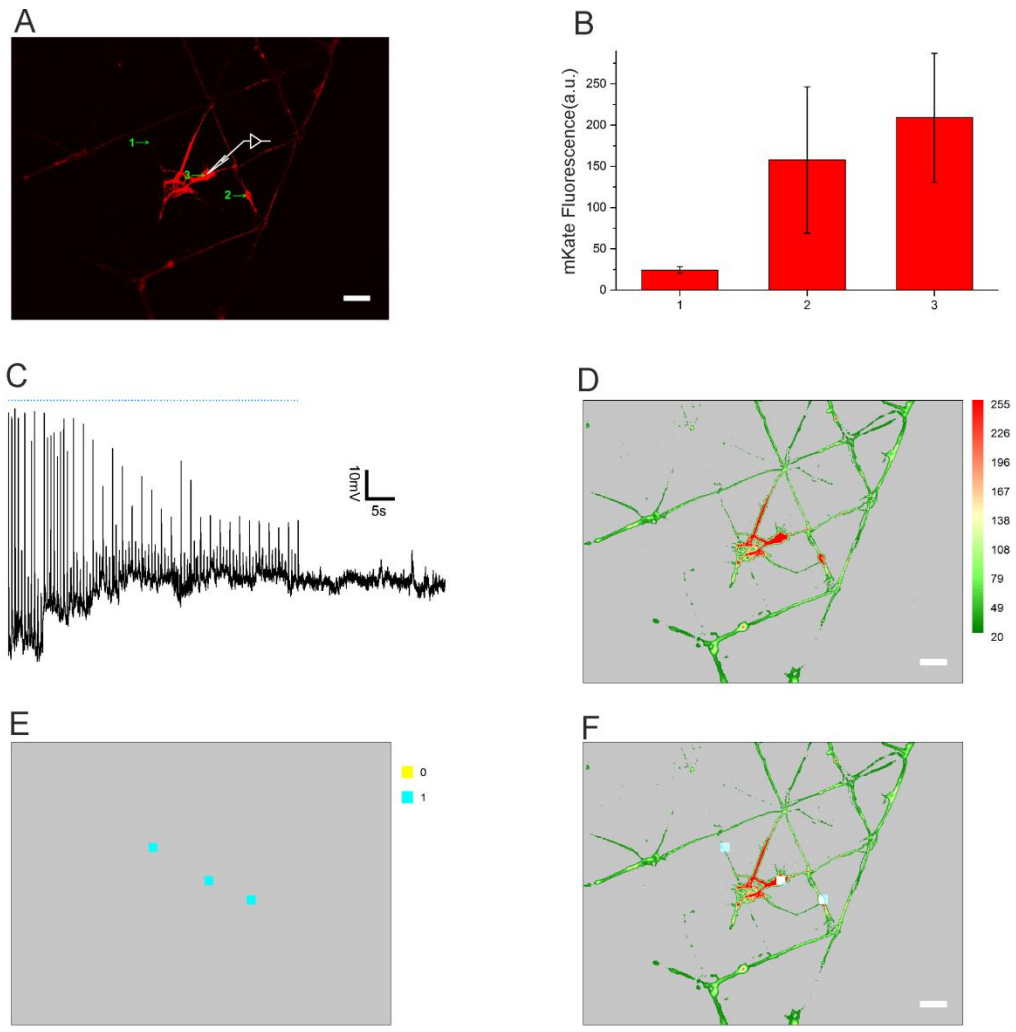

Fig. S 2 Mapping microcircuit of a small patterned neural network

A) A typical patterned neural network with X-shape shows mKate fluorescence. The numbered sites were stimulated sites with blue laser. The laser spot diameter was adjusted to about 24 μm, resulting in a laser intensity of approximately 1.74 W/mm^2. White pipette indicates the neuron, which patch clamp was employed to measure neural activity. Scale bar represents 50 μm. B) The intensity of mKate fluorescence at the inside of these numbered laser spots (the laser spot diameter was adjusted to about 24 μm) was shown. Data are means value ± SEM; blue dash indicates SEM. C) Voltage traces show evoked action potentials by a 50 milliseconds pulse (blue bar) of blue laser at 3 sites, repeated 30 rounds. D) The map of mKate fluorescence in the studied neural network was drew. The right side of this figure is the scale bar of fluorescent intensity. White bar at the right bottom represents 50 μm. E) The evoked action potentials of patched neuron was mapping. Yellow indicates no any evoked action potential; cyan indicates one elicited action potential by light. F) The microcircuit of one patterned neural network was mapping with figure D and E.

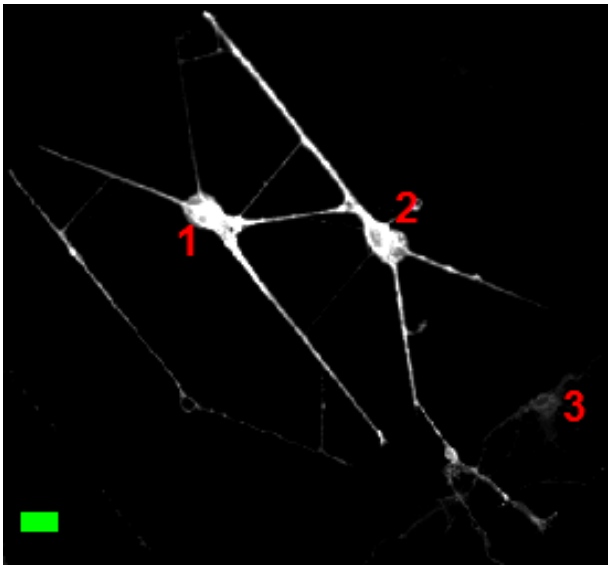

Fig. S 3 Strong mKate fluorescence of a patterned neural network expressing ChR2opt

The rAAV6 construct harboring the hSyn promoter to promote expression of ChR2opt was transduced into patterned neurons at DIV3. Numbers indicates three positions of laser stimulation. This picture was taken at DIV9, scale bar (green) represents 20 μm.

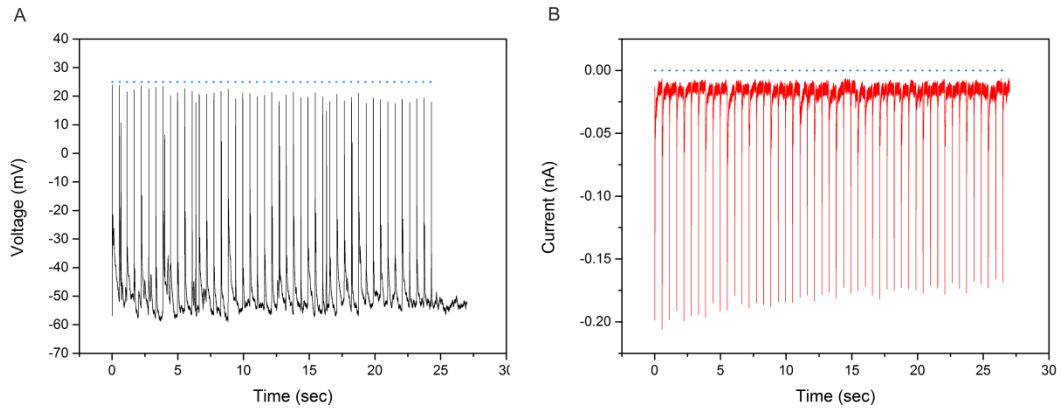

Fig. S 4 Voltage and current traces of patterned neural network with optogenetic

A typical patterned neural network (see: **Fig. S 3**) was measured with whole cell patch clamp combining with 473 nm laser stimulation. In this network, neurons numbered 1 and 2 are a pair of patterned neuron, neuron numbered 3 located unpatterned area, which connected to neuron 2 that was clamped. The stimulating order of one round is from site 1 to site 3, running 10 rounds. The laser spot diameter was adjusted to about 24 µm, resulting in a laser intensity of approximately 1.74 W/mm^2. Without any current injection, action potentials (A) were fired at each laser stimulus. Also, currents (B) were measured with voltage clamp with holding potential at - 50 mV.

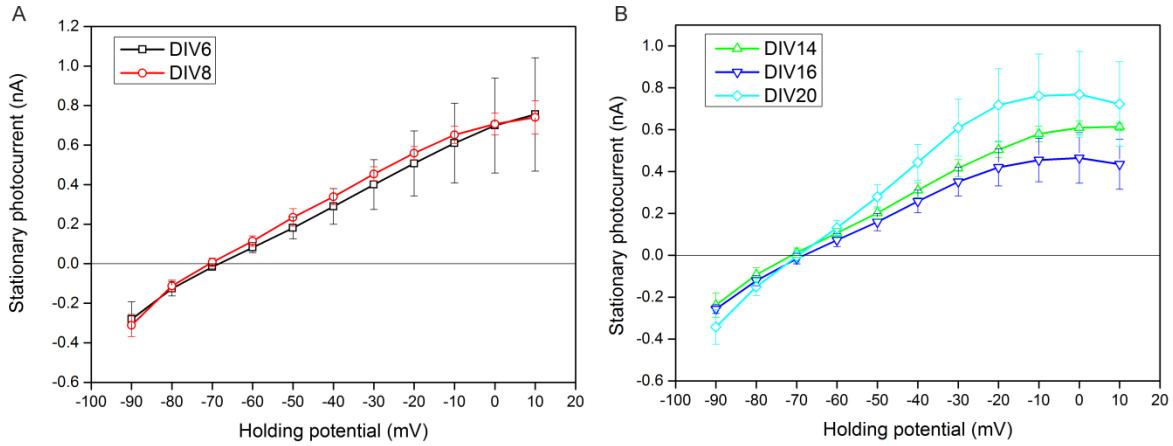

Fig. S 5 IE relationship for GtACR1 in primary rat cortical neurons under synaptic input blocking condition

A) IE relationship for GtACR1 in primary rat cortical neurons of both DIV6 and DIV8. B) IE relationship for GtACR1 in primary rat cortical neurons of DIV14, DIV16 and DIV20. All data were measured under low Cl^- concentration in the pipette and D-AP5

(25 µM), NBQX (10 µM), SR 95531 hydrobromide (20 µM) in the bath. The data (mean values ± SEM; n= 4 neurons in Figure A) or 3 neurons in Figure B)) were corrected by subtraction, with current values of the last 50 milliseconds without light was subtracted from current values of last 50 milliseconds with light.

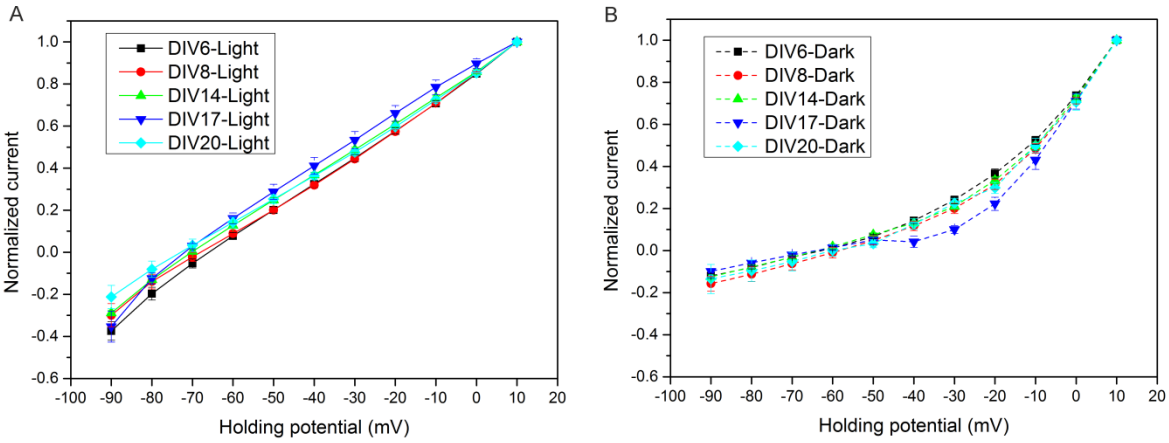

Fig. S 6 Normalized current of GtACR1-expressing neurons under light and dark

A) Normalized current of GtACR1-expressing neurons under light, whose raw data was normalized by the mean current of the last 50 milliseconds at 10 mV with voltage clamp each neuron. B) Normalized current of GtACR1-expressing neurons without light, whose raw data was normalized by the mean current of the last 50 milliseconds at 10 mV with voltage clamp each neuron. The data indicate mean values ± SEM (n= 3 to 5 neurons).

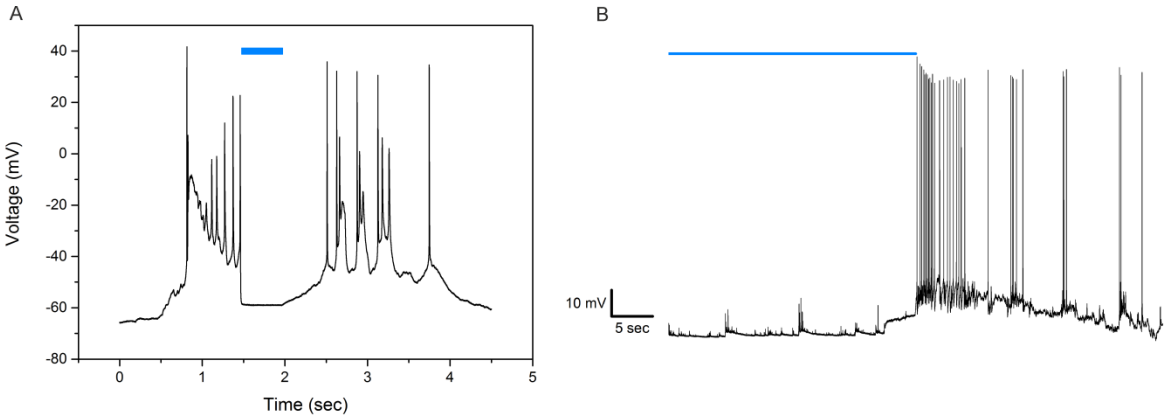

Fig. S 7 Photoinhibition of spontaneous activity

A) Photoinhibition of spontaneous activity from one GtACR1-expressing neuron of DIV20 without any current injection. The pulses of blue laser last 0.5 seconds. B) Photoinhibition of spontaneous activity from other different GtACR1-expressing neuron of DIV20 without

any current injection. The pulse of blue laser lasted 30 seconds. In all measurements, blue laser intensity was 0.21 W/mm^2. Blue bars indicate laser on.

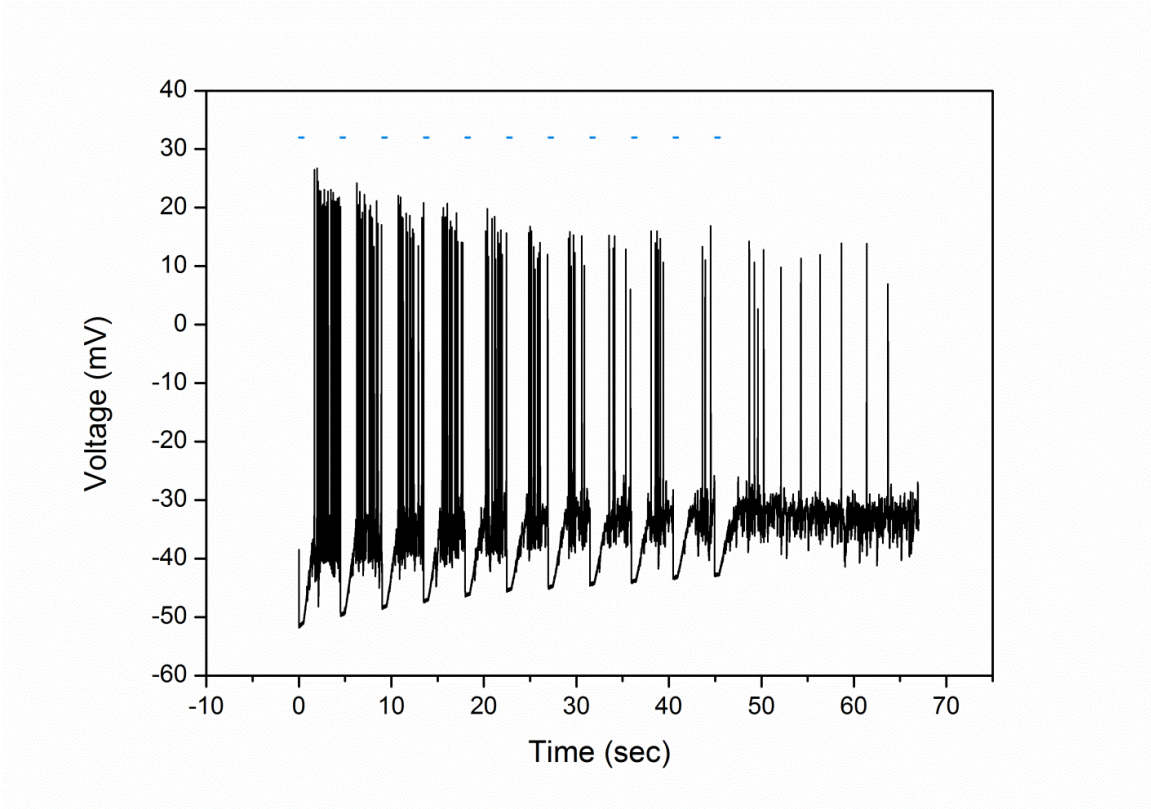

Fig. S 8 Spiking frequency decline after multiple illumination

In a typical neuron expressing GtACR1, 100 pA was applied to generate continuous action potential activity. 10 laser pulses of 500 milliseconds with 4 seconds delay time were used to make neural membrane potential hyperpolarize. Blue laser intensity was 0.21 W/mm^2.

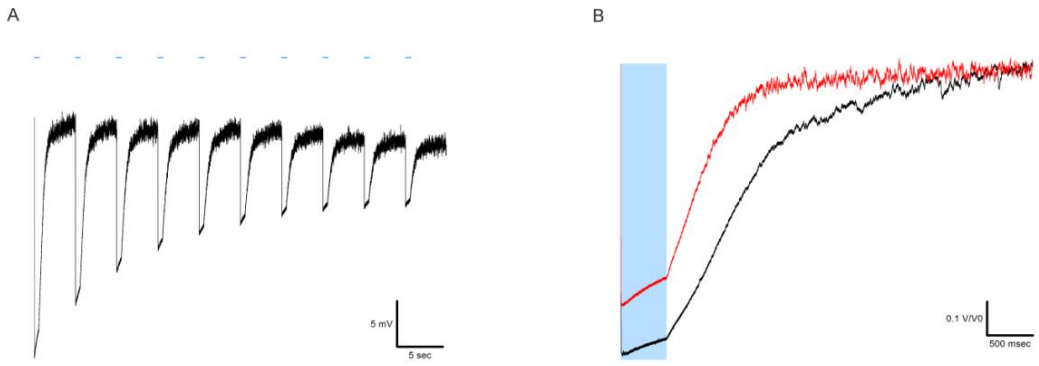

Fig. S 9 The comparison of recovery traces at two representative neurons

A) Using blue light to multiple stimulate GtACR1-expressing neurons, the amplitude of hyperpolarization on neural membrane gradually declined. Light intensity was 0.21 W/mm^2. Each stimulus was implemented with a light on of 500 milliseconds and a light off for 4 seconds. Blue bar indicates blue laser on. To obtain depolarization block, 100 pA of continuous current was injected into neuron by current clamp. B) At two representative neurons, the shape of recovery traces (after laser pulses) shows different. Compared with red trace extracted from the first stimulus in **Fig. S 9A**, black trace extracted from the first stimulus in **Figure 3.4-9A** shows the recovery of membrane potential is more slower. Blue area indicates blue light illumination.

Bibliography

Abilez, O.J., Wong, J., Prakash, R., Deisseroth, K., Zarins, C.K., and Kuhl, E. (2011). Multiscale Computational Models for Optogenetic Control of Cardiac Function. Biophys. J. *101*, 1326–1334.

Albers, J., Toma, K., and Offenhäusser, A. (2015). Engineering connectivity by multiscale micropatterning of individual populations of neurons. Biotechnol. J. *10*, 332–338.

Arenkiel, B.R., Peca, J., Davison, I.G., Feliciano, C., Deisseroth, K., Augustine, G.J., Ehlers, M.D., and Feng, G. (2007). In vivo light-induced activation of neural circuitry in transgenic mice expressing channelrhodopsin-2. Neuron *54*, 205–218.

Aschauer, D.F., Kreuz, S., and Rumpel, S. (2013). Analysis of transduction efficiency, tropism and axonal transport of AAV serotypes 1, 2, 5, 6, 8 and 9 in the mouse brain. PLoS One *8*, e76310.

Asokan, A., Schaffer, D. V, and Jude Samulski, R. (2012). The AAV Vector Toolkit: Poised at the Clinical Crossroads. Mol Ther *20*, 699–708.

Asrican, B., Augustine, G.J., Berglund, K., Chen, S., Chow, N., Deisseroth, K., Feng, G., Gloss, B., Hira, R., Hoffmann, C., et al. (2013). Next-generation transgenic mice for optogenetic analysis of neural circuits. Front. Neural Circuits *7*, 160.

Atchison, R.W., Casto, B.C., and Hammon, W.M. (1965). Adenovirus-Associated Defective Virus Particles. Science (80-.). *149*, 754–755.

Augustine, G., Chen, S., Gill, H., Hoffmann, C., Katarya, M., Kim, J., Kudolo, J., Lee, L.M., Lee, H., Lo, S.Q., et al. (2013). High-speed optogenetic circuit mapping. Proc. SPIE 8586, Optogenetics Opt. Methods Cell. Control *8586*, 858603–858603 – 7.

Avermann, M., Tomm, C., Mateo, C., Gerstner, W., and Petersen, C.C.H. (2012). Microcircuits of excitatory and inhibitory neurons in layer 2/3 of mouse barrel cortex. J. Neurophysiol. *107*, 3116–3134.

Ben-Ari, Y. (2002). Excitatory actions of gaba during development: the nature of the nurture. Nat Rev Neurosci *3*, 728–739.

Bendahhou, S. (2012). Keeping hyperactive voltage-gated sodium channels in silent mode. J. Physiol. *590*, 2543–2544.

Berndt, A., Yizhar, O., Gunaydin, L. a, Hegemann, P., and Deisseroth, K. (2009). Bi-stable neural state switches. Nat. Neurosci. *12*, 229–234.

Berndt, A., Schoenenberger, P., Mattis, J., Tye, K.M., Deisseroth, K., Hegemann, P., and Oertner, T.G. (2011). High-efficiency channelrhodopsins for fast neuronal stimulation at low light levels. Proc. Natl. Acad. Sci. U. S. A. *108*, 7595–7600.

Berndt, A., Lee, S.Y., Ramakrishnan, C., and Deisseroth, K. (2014). Structure-guided transformation of channelrhodopsin into a light-activated chloride channel. Science *344*, 420–424.

Bianchi, D., Marasco, A., Limongiello, A., Marchetti, C., Marie, H., Tirozzi, B., and Migliore, M. (2012). On the mechanisms underlying the depolarization block in the spiking dynamics of CA1 pyramidal neurons. J. Comput. Neurosci. *33*, 207–225.

Blacklow, N.R., Hoggan, M.D., Kapikian, A.Z., Austin, J.B., and Rowe, W.P. (1968). Epidemiology of adenovirus-associated virus infection in a nursery population. Am. J. Epidemiol. *88*, 368–378.

Boyden, E.S. (2011). A history of optogenetics: the development of tools for controlling brain circuits with light. F1000 Biol. Rep. *3*, 11.

Boyden, E.S., Zhang, F., Bamberg, E., Nagel, G., and Deisseroth, K. (2005). Millisecond-timescale, genetically targeted optical control of neural activity. Nat. Neurosci. *8*, 1263–1268.

Bregestovski, P., Waseem, T., and Mukhtarov, M. (2009). Genetically Encoded Optical Sensors for Monitoring of Intracellular Chloride and Chloride-Selective Channel Activity. Front. Mol. Neurosci. *2*, 15.

Brewer, G.J., Torricelli, J.R., Evege, E.K., and Price, P.J. (1993). Optimized survival of hippocampal neurons in B27-supplemented neurobasal™, a new serum-free medium combination. J. Neurosci. Res. *35*, 567–576.

Buchen, L. (2010). Neuroscience: Illuminating the brain. Nature *464*, 26–28.

Carvalho-de-Souza, J.L., Treger, J.S., Dang, B., Kent, S.B.H., Pepperberg, D.R., and Bezanilla, F. (2015). Photosensitivity of Neurons Enabled by Cell-Targeted Gold Nanoparticles. Neuron *86*, 207–217.

Cearley, C.N., and Wolfe, J.H. (2006). Transduction characteristics of adeno-associated virus vectors expressing cap serotypes 7, 8, 9, and Rh10 in the mouse brain. Mol. Ther. *13*, 528–537.

Chen, C., and Okayama, H. (1987). High-efficiency transformation of mammalian cells by plasmid DNA. Mol. Cell. Biol. *7*, 2745–2752.

Chuong, A.S., Miri, M.L., Busskamp, V., Matthews, G.A.C., Acker, L.C., Sorensen, A.T., Young, A., Klapoetke, N.C., Henninger, M.A., Kodandaramaiah, S.B., et al. (2014). Noninvasive optical inhibition with a red-shifted microbial rhodopsin. Nat Neurosci *17*, 1123–1129.

Crick, F.H. (1979). Thinking about the brain. Sci. Am. *241*, 219–232.

Cutsuridis, V., Wennekers, T., Graham, B.P., Vida, I., and Taylor, J.G. (2009). Microcircuits - Their structure, dynamics and role for brain function. Neural Networks *22*, 1037–1038.

Dawydow, A., Gueta, R., Ljaschenko, D., Ullrich, S., Hermann, M., Ehmann, N., Gao, S., Fiala, A., Langenhan, T., Nagel, G., et al. (2014). Channelrhodopsin-2-XXL, a powerful optogenetic tool for low-light applications. Proc. Natl. Acad. Sci. 2–7.

Deisseroth, K., Feng, G., Majewska, A.K., Miesenböck, G., Ting, A., and Schnitzer, M.J. (2006). Next-Generation Optical Technologies for Illuminating Genetically Targeted Brain Circuits. J. Neurosci. *26* , 10380–10386.

Desai, M., Kahn, I., Knoblich, U., Bernstein, J., Atallah, H., Yang, a, Kopell, N., Buckner, R.L., Graybiel, a M., Moore, C.I., et al. (2011). Mapping brain networks in awake mice using combined optical neural control and fMRI. J. Neurophysiol. *105*, 1393–1405.

Dugué, G.P., Akemann, W., and Knöpfel, T. (2012). A comprehensive concept of optogenetics. Prog. Brain Res. *196*, 1–28.

During, M. (1997). Adeno-associated virus as a gene delivery system. Adv. Drug Deliv. Rev. *27*, 83–94.

Faber, E.S.L., and Sah, P. (2003). Calcium-Activated Potassium Channels: Multiple Contributions to Neuronal Function. Neurosci. *9* , 181–194.

Fricke, R., Zentis, P.D., Rajappa, L.T., Hofmann, B., Banzet, M., Offenhäusser, A., and Meffert, S.H. (2011). Axon guidance of rat cortical neurons by microcontact printed gradients. Biomaterials *32*, 2070–2076.

Girod, a, Ried, M., Wobus, C., Lahm, H., Leike, K., Kleinschmidt, J., Deléage, G., and Hallek, M. (1999). Genetic capsid modifications allow efficient re-targeting of adeno-associated virus type 2. Nat. Med. *5*, 1052–1056.

Goldwyn, J.H., and Rinzel, J. (2016). Neuronal coupling by endogenous electric fields: Cable theory and applications to coincidence detector neurons in the auditory brainstem. J. Neurophysiol.

Gong, Y. (2015). The evolving capabilities of rhodopsin-based genetically encoded voltage indicators. Curr. Opin. Chem. Biol. *27*, 84–89.

Gong, Y., Huang, C., Li, J.Z., Grewe, B.F., Zhang, Y., Eismann, S., and Schnitzer, M.J. (2015). High-speed recording of neural spikes in awake mice and flies with a fluorescent voltage sensor. Sci. *350* , 1361–1366.

Govorunova, E.G., Sineshchekov, O.A., Janz, R., Liu, X., and Spudich, J.L. (2015). Natural light-gated anion channels: A family of microbial rhodopsins for advanced optogenetics. Sci. *349* , 647–650.

Gunaydin, L. a, Yizhar, O., Berndt, A., Sohal, V.S., Deisseroth, K., and Hegemann, P. (2010). Ultrafast optogenetic control. Nat. Neurosci. *13*, 387–392.

Hamm, A., Krott, N., Breibach, I., Blindt, R., Bosserhoff, A.K., and Ph, D. (2002). Efficient Transfection Method for Primary Cells. Tissue Eng. *8*, 235–245.

Hegemann, P., and Moglich, A. (2011). Channelrhodopsin engineering and exploration of new optogenetic tools. Nat Meth *8*, 39–42.

Hegemann, P., and Nagel, G. (2013). From channelrhodopsins to optogenetics. EMBO Mol. Med. *5*, 173–176.

Hernandez, Y.J., Wang, J., Kearns, W.G., Loiler, S., Poirier, A., and Flotte, T.R. (1999). Latent Adeno-Associated Virus Infection Elicits Humoral but Not Cell-Mediated Immune Responses in a Nonhuman Primate Model. J. Virol. *73* , 8549–8558.

Holmes, D. (2012). Is neurology ready to see the light? Lancet Neurol. *11*, 663–664.

Hooks, B.M., Lin, J.Y., Guo, C., and Svoboda, K. (2015). Dual-Channel Circuit Mapping Reveals Sensorimotor Convergence in the Primary Motor Cortex. J. Neurosci. *35*, 4418–4426.

Howard, D.B., Powers, K., Wang, Y., and Harvey, B.K. (2008). Tropism and toxicity of adeno-associated viral vector serotypes 1,2,5,6,7,8,9 in rat neurons and glia in vitro. Virology *372*, 24–34.

Huber, D., Petreanu, L., Ghitani, N., Ranade, S., Hromádka, T., Mainen, Z., and Svoboda, K. (2008). Sparse optical microstimulation in barrel cortex drives learned behaviour in freely moving mice. Nature *451*, 61–64.

Ishizuka, T., Kakuda, M., Araki, R., and Yawo, H. (2006). Kinetic evaluation of photosensitivity in genetically engineered neurons expressing green algae light-gated channels. Neurosci. Res. *54*, 85–94.

Jansen, V., Alvarez, L., Balbach, M., Strünker, T., Hegemann, P., Kaupp, U.B., and Wachten, D. (2015). Controlling fertilization and cAMP signaling in sperm by optogenetics. Elife *4*, 1–15.

Jin, L., Lange, W., Kempmann, A., Maybeck, V., Günther, A., Gruteser, N., Baumann, A., and Offenhäusser, A. (2016). High-efficiency transduction and specific expression of ChR2opt for optogenetic manipulation of primary cortical neurons mediated by recombinant adeno-associated viruses. J. Biotechnol. *233*, 171–180.

Karra, D., and Dahm, R. (2010). Transfection techniques for neuronal cells. J. Neurosci. *30*, 6171–6177.

Konermann, S., Brigham, M.D., Trevino, A.E., Hsu, P.D., Heidenreich, M., Cong, L., Platt, R.J., Scott, D. a, Church, G.M., and Zhang, F. (2013). Optical control of mammalian endogenous transcription and epigenetic states. Nature *500*, 472–476.

Kozak, M. (1991). Structural Features in Eukaryotic mRNAs That Modulate the. J. Biol. Chem. *266*, 19867–19870.

Kügler, S., Kilic, E., and Bähr, M. (2003). Human synapsin 1 gene promoter confers highly neuron-specific long-term transgene expression from an adenoviral vector in the adult rat brain depending on the transduced area. Gene Ther. *10*, 337–347.

Kumar, A., Biebuyck, H.A., and Whitesides, G.M. (1994). Patterning Self-Assembled Monolayers: Applications in Materials Science. Langmuir *10*, 1498–1511.

Lange, W., Jin, L., Maybeck, V., Meisenberg, A., Baumann, A., and Offenhäusser, A. (2014). Recombinant Adeno-associated virus (rAAV) -mediated transduction and optogenetic manipulation of cortical neurons in vitro. Proc. SPIE 8928, Opt. Tech. Neurosurgery, Neurophotonics, Optogenetics, 89282S.

Li, W., Xu, Z., Huang, J., Lin, X., Luo, R., Chen, C.-H., and Shi, P. (2014). NeuroArray: A Universal Interface for Patterning and Interrogating Neural Circuitry with Single Cell Resolution. Sci. Rep. *4*, 4784.

Li, X., Gutierrez, D. V, Hanson, M.G., Han, J., Mark, M.D., Chiel, H., Hegemann, P., Landmesser, L.T., and Herlitze, S. (2005). Fast noninvasive activation and inhibition of neural and network activity by vertebrate rhodopsin and green algae channelrhodopsin. Proc. Natl. Acad. Sci. U. S. A. *102*, 17816–17821.

Liewald, J.F., Brauner, M., Stephens, G.J., Bouhours, M., Schultheis, C., Zhen, M., and Gottschalk, A. (2008). Optogenetic analysis of synaptic function. Nat. Methods *5*, 895–902.

Lim, D.H., LeDue, J., Mohajerani, M.H., Vanni, M.P., and Murphy, T.H. (2013). Optogenetic approaches for functional mouse brain mapping. Front. Neurosci.

Lin, J.Y., Knutsen, P.M., Muller, A., Kleinfeld, D., and Tsien, R.Y. (2013). ReaChR: a red-shifted variant of channelrhodopsin enables deep transcranial optogenetic excitation. Nat. Neurosci. *16*, 1499–1508.

Madisen, L., Mao, T., Koch, H., Zhuo, J., Berenyi, A., Fujisawa, S., Hsu, Y.-W. a, Garcia, A.J., Gu, X., Zanella, S., et al. (2012). A toolbox of Cre-dependent optogenetic transgenic mice for light-induced activation and silencing. Nat. Neurosci. *15*, 793–802.

Mancuso, J.J., Kim, J., Lee, S., Tsuda, S., Chow, N.B.H., and Augustine, G.J. (2011). Optogenetic probing of functional brain circuitry. Exp. Physiol. *96*, 26–33.

Marconi, E., Nieus, T., Maccione, A., Valente, P., Simi, A., Messa, M., Dante, S., Baldelli, P., Berdondini, L., and Benfenati, F. (2012). Emergent Functional Properties of Neuronal Networks with Controlled Topology. PLoS One *7*, e34648.

Martinez, C.Y., and Hollenbeck, P.J. (2003). Transfection of Primary Central and Peripheral Nervous System Neurons by Electroporation. Methods Cell Biol. *71*, 339–351.

McCarty, D.M. (2008). Self-complementary AAV Vectors; Advances and Applications. Mol. Ther. *16*, 1648–1656.

Mourzina, Y., Kaliaguine, D., Schulte, P., and Offenhäusser, A. (2006a). Patterning chemical stimulation of reconstructed neuronal networks. Anal. Chim. Acta *575*, 281–289.

Mourzina, Y., Steffen, A., Kaliaguine, D., Wolfrum, B., Schulte, P., Böcker-Meffert, S., and Offenhäusser, A. (2006b). Spatially resolved non-invasive chemical stimulation for modulation of signalling in reconstructed neuronal networks. J. R. Soc. Interface *3*, 333–343.

Nagel, G., Ollig, D., Fuhrmann, M., Kateriya, S., Musti, A.M., Bamberg, E., and Hegemann, P. (2002). Channelrhodopsin-1: a light-gated proton channel in green algae. Science *296*, 2395–2398.

Nagel, G., Szellas, T., Huhn, W., Kateriya, S., Adeishvili, N., Berthold, P., Ollig, D., Hegemann, P., and Bamberg, E. (2003a). Channelrhodopsin-2, a directly light-gated cation-selective membrane channel. Proc. Natl. Acad. Sci. *100* , 13940–13945.

Nagel, G., Szellas, T., Huhn, W., Kateriya, S., Adeishvili, N., Berthold, P., Ollig, D., Hegemann, P., and Bamberg, E. (2003b). Channelrhodopsin-2, a directly light-gated cation-selective membrane channel. Proc Natl Acad Sci U S A. *100*, 13940–13945.

Nagel, G., Szellas, T., Kateriya, S., Adeishvili, N., Hegemann, P., and Bamberg, E. (2005a). Channelrhodopsins: directly light-gated cation channels. Biochem. Soc. Trans. *33*, 863–866.

Nagel, G., Brauner, M., Liewald, J.F., Adeishvili, N., Bamberg, E., and Gottschalk, A. (2005b). Light activation of channelrhodopsin-2 in excitable cells of Caenorhabditis elegans triggers rapid behavioral responses. Curr. Biol. *15*, 2279–2284.

Neher, E., and Sakaba, T. (2008). Multiple Roles of Calcium Ions in the Regulation of Neurotransmitter Release. Neuron *59*, 861–872.

Offenhäusser, A., Bocker-Meffert, S., Decker, T., Helpenstein, R., Gasteier, P., Groll, J., Moller, M., Reska, A., Schafer, S., Schulte, P., et al. (2007). Microcontact printing of proteins for neuronal cell guidance. Soft Matter *3*, 290.

Peralvárez-Marín, A., and Garriga, P. (2016). Optogenetics Comes of Age: Novel Inhibitory Light-Gated Anionic Channels Allow Efficient Silencing of Neural Function. ChemBioChem *17*, 204–206.

Perron, A., Mutoh, H., Launey, T., and Knöpfel, T. (2009). Red-Shifted Voltage-Sensitive Fluorescent Proteins. Chem. Biol. *16*, 1268–1277.

Petreanu, L., Huber, D., Sobczyk, A., and Svoboda, K. (2007). Channelrhodopsin-2-assisted circuit mapping of long-range callosal projections. Nat. Neurosci. *10*, 663–668.

Ramirez, S., Tonegawa, S., and Liu, X. (2013). Identification and optogenetic manipulation of memory engrams in the hippocampus. Front. Behav. Neurosci. *7*, 226.

Rosas, L.E., Grieves, J.L., Zaraspe, K., La Perle, K.M.D., Fu, H., and McCarty, D.M. (2012). Patterns of scAAV Vector Insertion Associated With Oncogenic Events in a Mouse Model for Genotoxicity. Mol Ther *20*, 2098–2110.

Samulski, R.J., and Muzyczka, N. (2014). AAV-Mediated Gene Therapy for Research and Therapeutic Purposes. Annu. Rev. Virol. *1*, 427–451.

Sandoz, G., and Levitz, J. (2013). Optogenetic techniques for the study of native potassium channels. Front. Mol. Neurosci. *6*, 6.

Sassen, M., and Zimmermann, M. (1973). Differential blocking of myelinated nerve fibres by transient depolarization. Pflügers Arch. *341*, 179–195.

Schultz, B.R., and Chamberlain, J.S. (2008). Recombinant adeno-associated virus transduction and integration. Mol. Ther. *16*, 1189–1199.

Shcherbo, D., Merzlyak, E.M., Chepurnykh, T. V, Fradkov, A.F., Ermakova, G. V, Solovieva, E. a, Lukyanov, K. a, Bogdanova, E. a, Zaraisky, A.G., Lukyanov, S., et al. (2007). Bright far-red fluorescent protein for whole-body imaging. Nat. Methods *4*, 741–746.

Siegel, R.M., and Callaway, E.M. (2004). Francis Crick's Legacy for Neuroscience: Between the α and the Ω. PLoS Biol *2*, e419.

Sineshchekov, O.A., Govorunova, E.G., Li, H., and Spudich, J.L. (2015). Gating mechanisms of a natural anion channelrhodopsin. Proc. Natl. Acad. Sci. *112* , 14236–14241.

Sineshchekov, O.A., Li, H., Govorunova, E.G., and Spudich, J.L. (2016). Photochemical reaction cycle transitions during anion channelrhodopsin gating. 1–8.

Slavin, K. (2008). Peripheral nerve stimulation for neuropathic pain. Neurotherapeutics *5*, 100–106.

Sonntag, F., Schmidt, K., and Kleinschmidt, J.A. (2010). A viral assembly factor promotes AAV2 capsid formation in the nucleolus. Proc. Natl. Acad. Sci. *107* , 10220–10225.

Sprössler, C., Scholl, M., Denyer, M.C., Krause, M., Nakajima, K., Maelicke, A., Knoll, W., and Offenhäusser, A. (2001). Model network architectures in vitro on extracellular recording systems using microcontact printing. Synth. Met. *117*, 281–283.

Srivastava, A., Lusby, E.W., and Berns, K.I. (1983). Nucleotide sequence and organization of the adeno-associated virus 2 genome. J. Virol. *45*, 555–564.

St-Pierre, F., Marshall, J.D., Yang, Y., Gong, Y., Schnitzer, M.J., and Lin, M.Z. (2014). High-fidelity optical reporting of neuronal electrical activity with an ultrafast fluorescent voltage sensor. Nat Neurosci *17*, 884–889.

Tabor, J.J., Salis, H., Simpson, Z.B., Chevalier, A.A., Levskaya, A., Marcotte, E.M., Voigt, C.A., and Ellington, A.D. (2009). A Synthetic Genetic Edge Detection Program. Cell *137*, 1272–1281.

Tabor, J.J., Levskaya, A., and Voigt, C.A. (2011). Multichromatic control of gene expression in Escherichia coli. J. Mol. Biol. *405*, 315–324.

Torrance, N., Smith, B.H., Bennett, M.I., and Lee, A.J. (2006). The Epidemiology of Chronic Pain of Predominantly Neuropathic Origin. Results From a General Population Survey. J. Pain *7*, 281–289.

Valenti, O., Cifelli, P., Gill, K.M., and Grace, A. a (2011). Antipsychotic drugs rapidly induce dopamine neuron depolarization block in a developmental rat model of schizophrenia. J. Neurosci. *31*, 12330–12338.

Vogt, N. (2015). Neuroscience: Algae are the best engineers of optogenetic inhibitors. Nat Meth *12*, 806–807.

Vogt, a K., Brewer, G.J., and Offenhäusser, a (2005a). Connectivity patterns in neuronal networks of experimentally defined geometry. Tissue Eng. *11*, 1757–1767.

Vogt, A.K., Lauer, L., Knoll, W., and Offenhäusser, A. (2003). Micropatterned Substrates for the Growth of Functional Neuronal Networks of Defined Geometry. Biotechnol. Prog. *19*, 1562–1568.

Vogt, A.K., Wrobel, G., Meyer, W., Knoll, W., and Offenhäusser, A. (2005b). Synaptic plasticity in micropatterned neuronal networks. Biomaterials *26*, 2549–2557.

Wang, H., Peca, J., Matsuzaki, M., Matsuzaki, K., Noguchi, J., Qiu, L., Wang, D., Zhang, F., Boyden, E., Deisseroth, K., et al. (2007). High-speed mapping of synaptic connectivity using photostimulation in Channelrhodopsin-2 transgenic mice. Proc. Natl. Acad. Sci. U. S. A. *104*, 8143–8148.

Watanabe, S.Y., Albsoul-Younes, A.M., Kawano, T., Itoh, H., Kaziro, Y., Nakajima, S., and Nakajima, Y. (1999). Calcium phosphate-mediated transfection of primary cultured brain neurons using GFP expression as a marker: application for single neuron electrophysiology. Neurosci. Res. *33*, 71–78.

Wickersham, I.R., and Callaway, E.M. (2007). Suitability of hCMV for viral gene expression in the brain. Nat Meth *4*, 379.

Wietek, J., Wiegert, J.S., Adeishvili, N., Schneider, F., Watanabe, H., Tsunoda, S.P., Vogt, A., Elstner, M., Oertner, T.G., and Hegemann, P. (2014). Conversion of channelrhodopsin into a light-gated chloride channel. Science *344*, 409–412.

Wietek, J., Beltramo, R., Scanziani, M., Hegemann, P., Oertner, T.G., and Simon Wiegert, J. (2015). An improved chloride-conducting channelrhodopsin for light-induced inhibition of neuronal activity in vivo. Sci. Rep. *5*, 14807.

Wietek, J., Broser, M., Krause, B.S., and Hegemann, P. (2016). Identification of a Natural Green Light Absorbing Chloride Conducting Channelrhodopsin from Proteomonas sulcata. J. Biol. Chem. *291* , 4121–4127.

Wilkinson, G.W.G., and Akrigg, A. (1992). Constitutive and enhanced expression from the CMV major IE promoter in a defective adenovirus vector. Nucleic Acids Res. *20*, 2233–2239.

Xiao, X., Li, J., and Samulski, R.J. (1998). Production of high-titer recombinant adeno-associated virus vectors in the absence of helper adenovirus. J. Virol. *72*, 2224–2232.

Yang, H.H., St-Pierre, F., Sun, X., Ding, X., Lin, M.Z., and Clandinin, T.R. (2016). Subcellular Imaging of Voltage and Calcium Signals Reveals Neural Processing In Vivo. Cell *166*, 245–257.

Yi, A., Mamaeva, N. V, Li, H., Spudich, J.L., and Rothschild, K.J. (2016). Resonance Raman Study of an Anion Channelrhodopsin: Effects of Mutations Near the Retinylidene Schiff Base. Biochemistry.

Yizhar, O., Fenno, L.E., Davidson, T.J., Mogri, M., and Deisseroth, K. (2011a). Optogenetics in neural systems. Neuron *71*, 9–34.

Yizhar, O., Fenno, L.E., Prigge, M., Schneider, F., Davidson, T.J., O'Shea, D.J., Sohal, V.S., Goshen, I., Finkelstein, J., Paz, J.T., et al. (2011b). Neocortical excitation/inhibition balance in information processing and social dysfunction. Nature *477*, 171–178.

Zeitelhofer, M., Vessey, J.P., Thomas, S., Kiebler, M., and Dahm, R. (2009). Transfection of Cultured Primary Neurons via Nucleofection. In Current Protocols in Neuroscience, (John Wiley & Sons, Inc.),.

Zemelman, B. V, Lee, G.A., Ng, M., and Miesenböck, G. (2002). Selective Photostimulation of Genetically ChARGed Neurons. Neuron *33*, 15–22.

Zhang, F., Wang, L.-P., Boyden, E.S., and Deisseroth, K. (2006). Channelrhodopsin-2 and optical control of excitable cells. Nat. Methods *3*, 785–792.

Zhu, G., Du, L., Jin, L., and Offenhäusser, A. (2016). Effects of Morphology Constraint on Electrophysiological Properties of Cortical Neurons. Sci. Rep. *6*, 23086.

Declaration of Originality

I declare that this dissertation is an original work that has not been submitted for any other degree or title, at any higher education institution. I declare that this dissertation represents my own work and all work which is not my own has been cited as such.

Ich versichere eidesstattlich, dass ich diesen Promotionsantrag erstmalig einreiche und keine früheren Versuche einer Promotion unternommen habe. Ich erkläre eidesstattlich, dass ich die Dissertation selbständig verfasst und alle in Anspruch genommenen Hilfen in der Dissertation angegeben habe. Ich erkläre, dass durch die Veröffentlichung als Dissertation der RWTH Aachen bestehende Schutzrechte - inbesondere Urheberschutzrechte - nicht verletzt werden.

Lei Jin

Jülich, April 15, 2016